

การเตรียมไดเอสเทอร์โดยใช้ตัวเร่งปฏิกิริยาชนิดกรดที่มีรูปอนุขนาดกลาง

นายประเสริฐ เรืองยศสกุล

วิทยานิพนธ์นี้เป็นส่วนหนึ่งของการศึกษาตามหลักสูตรปริญญาวิทยาศาสตรมหาบัณฑิต

สาขาวิชาเคมี ภาควิชาเคมี

คณะวิทยาศาสตร์ จุฬาลงกรณ์มหาวิทยาลัย

ปีการศึกษา 2554

ลิขสิทธิ์ของจุฬาลงกรณ์มหาวิทยาลัย

บทคัดย่อและแฟ้มข้อมูลฉบับเต็มของวิทยานิพนธ์ตั้งแต่ปีการศึกษา 2554 ที่ให้บริการในคลังปัญญาจุฬาฯ (CUIR)

เป็นแฟ้มข้อมูลของนิสิตเจ้าของวิทยานิพนธ์ที่ส่งผ่านทางบัณฑิตวิทยาลัย

The abstract and full text of theses from the academic year 2011 in Chulalongkorn University Intellectual Repository (CUIR) are the thesis authors' files submitted through the Graduate School.

PREPARATION OF DIESTERS USING ACIDIC
MESOPOROUS CATALYSTS

Mr. Prasert Ruangyotsakul

A Thesis Submitted in Partial Fulfillment of the Requirements
for the Degree of Master of Science Program in Chemistry

Department of Chemistry

Faculty of Science

Chulalongkorn University

Academic Year 2011

Copyright of Chulalongkorn University

Thesis Title PREPARATION OF DIESTERS USING ACIDIC
 MESOPOROUS CATALYSTS
By Mr. Prasert Ruangyotsakul
Field of Study Chemistry
Thesis Advisor Duangamol Tungasmita, Ph.D.

Accepted by the Faculty of Science, Chulalongkorn University in Partial
Fulfillment of the Requirements for the Master's Degree

.....Dean of the Faculty of Science
(Professor Supot Hannongbua, Dr. rer. nat.)

THESIS COMMITTEE

.....Chairman
(Assistant Professor Warinthorn Chavasiri, Ph.D.)

.....Thesis Advisor
(Duangamol Tungasmita, Ph.D.)

.....Examiner
(Associate Professor Nuanphun Chantarasiri, Ph.D.)

.....External Examiner
(Suchada Butnark, Ph.D.)

ประเสริฐ เรืองยศสกุล : การเตรียมไดเอสเทอร์โดยใช้ตัวเร่งปฏิกิริยาชนิดกรดที่มีรูพรุนขนาดกลาง (PREPARATION OF DIESTERS USING ACIDIC MESOPOROUS CATALYSTS) อ.ที่ปรึกษาวิทยานิพนธ์หลัก: อ. ดร. ดวงกมล ตุงคะสมิต, 141 หน้า

ได้สังเคราะห์ตัวเร่งปฏิกิริยาเอสปีเอ-15 และเอฟเอสเอ็ม-16 ที่มีหมู่ไพโรฟิลซิลโฟนิก เอริลซิลโฟนิก หรืออะลูมิเนียมด้วยวิธีทางความร้อน จากนั้นตรวจสอบลักษณะเฉพาะของวัสดุที่สังเคราะห์ได้ด้วยเทคนิคการเลี้ยวเบนของรังสีเอกซ์ เทคนิคการดูดซับไนโตรเจน กล้องจุลทรรศน์อิเล็กตรอนแบบส่องกราด การวิเคราะห์ปริมาณซิลเฟออร์ และการคายแอมโมเนียด้วยการเพิ่มอุณหภูมิแบบตั้งโปรแกรม ทำการเปรียบเทียบประสิทธิภาพของตัวเร่งปฏิกิริยาที่สังเคราะห์ พบว่าเอฟเอสเอ็ม-16 ที่มีหมู่ไพโรฟิลซิลโฟนิกเป็นตัวเร่งปฏิกิริยาที่มีประสิทธิภาพสูงสุด ทดสอบประสิทธิภาพความว่องไวของเอฟเอสเอ็ม-16 ที่มีหมู่ไพโรฟิลซิลโฟนิกด้วยปฏิกิริยาการเตรียมเอสเทอร์ฟิเคชันของกรดแอดิพิกกับ 2-เอทิลเฮกซานอล ภาวะที่เหมาะสมในการเตรียมสารหล่อลื่นคือ ปริมาณตัวเร่งปฏิกิริยา 3% โดยน้ำหนักสารตั้งต้น ที่อุณหภูมิ 100 องศาเซลเซียส เป็นเวลา 5 ชั่วโมง ด้วยอัตราเร็วในการกวน 150 รอบต่อนาที อัตราส่วนโดยโมลระหว่าง 2-เอทิล เฮกซานอลต่อกรดแอดิพิกเท่ากับ 2 สารละลายหลังปฏิกิริยาให้ปริมาณ 2-เอทิลเฮกซิลเอสเทอร์สูงสุดที่ 96.2% จำเพาะต่อไดเอสเทอร์ 86.0% และจำเพาะต่อโมโนเอสเทอร์ 14.0% การเพิ่มอัตราส่วนโดยโมลของ 2-เอทิลเฮกซานอลต่อกรดแอดิพิก ช่วยเพิ่มผลได้และความเลือกจำเพาะต่อไดเอสเทอร์ ขนาดของกรดไดคาร์บอกซิลิกมีผลต่อผลได้เอสเทอร์อย่างมีนัยสำคัญ เมื่อจำนวนคาร์บอนในสายโซ่ของกรดไดคาร์บอกซิลิกเพิ่มขึ้น ผลได้ของไดเอสเทอร์และความเลือกจำเพาะต่อไดเอสเทอร์ลดลง เนื่องจากผลของความเกะกะที่เพิ่มขึ้น เอฟเอสเอ็ม-16 ที่มีหมู่ไพโรฟิลซิลโฟนิกถูกนำมาใช้สองครั้งเพื่อทดสอบการนำกลับมาใช้ใหม่ ซึ่งให้เห็นว่าเป็นตัวเร่งปฏิกิริยาสามารถนำกลับมาใช้ใหม่ได้โดยปราศจากการสูญเสียความสามารถในการเร่งปฏิกิริยาเมื่อใช้เฮกเซนล้างตัวเร่งปฏิกิริยา

ภาควิชา.....เคมี..... ลายมือชื่อนิสิต.....
 สาขาวิชา.....เคมี..... ลายมือชื่อ อ.ที่ปรึกษาวิทยานิพนธ์หลัก.....
 ปีการศึกษา....2554.....

5272406623: MAJOR CHEMISTRY

KEYWORDS: SBA-15 / FSM-16 / FSM-16-PrSO₃H / ADIPIC ACID / 2-ETHYL
HEXANOL / ESTERIFICATION / LUBRICATING OIL

PRASERT RUANGYOTSAKUL: PREPARATION OF DIESTERS USING
ACIDIC MESOPOROUS CATALYSTS. ADVISOR: DUANGAMOL
TUNGASMITA, Ph.D., 141 pp.

SBA-15 and FSM-16 catalysts, which contained propyl sulfonic, aryl sulfonic or aluminium, were synthesized by hydrothermal method. The synthesized materials were characterized by X-ray powder diffraction, nitrogen sorption analysis, scanning electron microscopy, sulfur elemental analysis and ammonia temperature programmed desorption techniques. When comparison between synthetic catalysts, the FSM-16-PrSO₃H was the best efficient catalyst. Catalytic performances of FSM-16-PrSO₃H were studied via esterification of adipic acid with 2-ethyl hexanol. The optimum condition on lubricating oil additive preparation was carried out over catalyst amount of 3%wt. of the reaction mixture at 100 °C for 5 hrs. with stirring speed 150 rpm. and molar ratio of alcohol to carboxylic acid as 2. The reaction mixtures exhibited highest 2-ethyl hexyl adipate esters yield as 96.2% with 86.0% of diester and 14.0% of monoester selectivities. An increasing in the 2-ethyl hexanol to adipic acid molar ratio resulted in an improvement of the diester yield and selectivity. The molecular size of diacid was significantly affected, when the number of carbon in the linear alkyl chain of dicarboxylic acid was increased, the diester yield and the diester selectivity were decreased due to the enhancement of steric effect. The FSM-16-PrSO₃H was used for two times to examine its reusability. It was indicated that the catalyst can be reused without losing catalytic activity when using hexane as washing agent.

Department:.....Chemistry.....

Student's Signature:

Field of Study:.....Chemistry.....

Advisor's Signature:

Academic Year:2011.....

ACKNOWLEDGEMENTS

The accomplishment of this thesis can be attributed to the extensive support and assistance from Dr. Duangamol Tungasmita, my thesis advisor. I would like to sincere gratitude to her for valuable advice, assistance, guidance and encouragement in this research as well as extraordinary experiences throughout the work.

I would like to thank sincerely my gratitude to the members of thesis committee consisting of Assistant Professor Warinthorn Chavasiri, Ph.D., Associate Professor Nuanphun Chantarasiri, Ph.D., and Suchada Butnark, Ph.D., the external examiner from PTT Research and Technology Institute for all of their comments and useful suggestion about this research.

I would like to gratefully thank Department of Chemistry, Faculty of Science, Chulalongkorn University for the valuable knowledge and experience. I would like to thank Thailand Japan Technology Transfer Project for supporting instruments. Moreover, I deeply appreciate PTT Research and Technology Institute and Center for Petroleum, Petrochemicals, and Advanced Materials for partial lab expense supporting.

Many thanks go in particular to the members of Materials Chemistry and Catalysis Research Unit and my friends for their sincere help and kindness. Finally, I deeply wish to thank my family for their entirely care and understanding during my graduate study.

CONTENTS

	Page
Abstract in Thai.....	iv
Abstract in English.....	v
Acknowledgements.....	vi
Contents.....	vii
List of Tables.....	xii
List of Figures.....	xiv
List of Schemes.....	xix
List of Abbreviations.....	xx
 CHAPTER	
I	
INTRODUCTIONS.....	1
1.1 Statement of problems.....	1
1.2 Literature reviews.....	2
1.2.1 Synthesis catalysts.....	2
1.2.2 Diester synthesis from diacid.....	3
1.2.3 Catalysts in esterification.....	4
1.3 Objectives.....	6
1.4 Scopes of work.....	6
II	
THEORY.....	7
2.1 Lubricating oil classification.....	7
2.1.1 Animal fat/ vegetable oil.....	7
2.1.2 Mineral oils.....	7
2.1.3 Synthetic lubricants.....	7
2.2 Synthetic ester lubricants.....	8
2.2.1 General features and product groups.....	9
2.2.2 Manufacture of ester lubricants.....	11
2.2.3 Physicochemical properties of ester lubricants.....	14
2.2.4 Application areas.....	21
2.3 Catalysts.....	23

CHAPTER	Page
2.4 Properties of industrial catalysts.....	24
2.5 Type of the catalysts.....	24
2.6 Acid catalyst for esterification.....	26
2.6.1 Brønsted acids.....	27
2.6.2 Lewis acids.....	28
2.6.3 Solid acids.....	31
2.7 Porous molecular sieves.....	35
2.8 Mesoporous materials.....	35
2.8.1 Classification of mesoporous materials.....	36
2.8.2 Synthesis schemes of mesoporous materials.....	37
2.8.2.1 The behavior of surfactant molecules in an aqueous solution.....	37
2.8.2.2 Interaction between inorganic species and surfactant micelles.....	38
2.8.2.3 Formation mechanism of mesoporous materials.....	40
2.8.3 Synthesis strategy of mesoporous material using block-copolymer as directing agent.....	42
2.9 SBA-15.....	44
2.9.1 Structure and properties of SBA-15	44
2.9.2 Synthesis of SBA-15 and formation mechanism.....	45
2.10 FSM-16.....	46
2.10.1 Structure and properties of FSM-16	46
2.10.2 Synthesis of FSM-16 and formation mechanism....	47
2.11 Step in a heterogeneous catalytic reaction.....	48
2.12 Modification of catalysts.....	49
2.12.1 Direct synthesis.....	49
2.12.2 Post synthesis.....	50
2.13 Characterization of materials.....	51
2.13.1 X-ray powder diffraction (XRD).....	51
2.13.2 Nitrogen adsorption-desorption technique.....	52
2.13.3 Scanning electron microscope (SEM).....	54
2.13.4 Temperature-programmed desorption of ammonia	55

CHAPTER	Page
III	
EXPERIMENTS	57
3.1 Instruments and apparatus.....	57
3.1.1 Oven and furnace.....	57
3.1.2 X-ray powder diffractometer (XRD).....	58
3.1.3 Nitrogen adsorption-desorption technique.....	58
3.1.4 Scanning electron microscope (SEM).....	58
3.1.5 Ammonia temperature-program desorption.....	58
3.1.6 Sulfur analyzer.....	58
3.1.7 Gas chromatograph (GC).....	59
3.1.8 Gas chromatograph-mass spectrometer (GC-MS)....	59
3.1.9 Nuclear magnetic resonance spectrometer (NMR)...	59
3.1.10 Parr reactor.....	59
3.2 Chemicals.....	60
3.2.1 Chemicals for synthesis catalysts.....	60
3.2.2 Chemicals for esterification.....	60
3.2.3 Chemical for reaction product analysis.....	61
3.3 Synthesis of mesoporous materials	61
3.3.1 Synthesis SBA-15 by hydrothermal method.....	61
3.3.2 Synthesis FSM-16 by hydrothermal method.....	62
3.4 Sulfonic functionalized mesoporous materials.....	64
3.5 Aluminium functionalized mesoporous materials.....	64
3.6 Acid-base titration.....	64
3.7 Procedure in lubricant preparation.....	65
3.8 Parameters affecting lubricant preparation.....	66
3.8.1 Effect of reaction time.....	66
3.8.2 Effect of temperature.....	66
3.8.3 Effect of catalytic amount.....	66
3.8.4 Effect of stirring speed.....	66
3.8.5 Effect of 2-ethyl hexanol to adipic acid molar ratio..	67
3.8.6 Effect of various catalysts.....	67
3.8.7 Effect of chain length of dicarboxylic acid.....	67

CHAPTER	Page
3.8.8 Effect of structure of alcohol.....	67
3.9 Recycle of catalysts.....	67
IV RESULTS AND DISCUSSION.....	69
4.1 Synthesis of SBA-15 catalysts.....	69
4.1.1 The physic-chemical properties of sulfonic functionalized SBA-15.....	69
4.1.1.1 XRD results.....	69
4.1.1.2 Sorption properties of sulfonic functionalized SBA-15.....	70
4.1.1.3 SEM images.....	72
4.1.1.4 Elemental analysis and acid-base titration....	73
4.1.2 The physic-chemical properties of aluminium functionalized SBA-15.....	73
4.1.2.1 XRD results.....	73
4.1.2.2 Sorption properties of Al-SBA-15.....	74
4.1.2.3 SEM images.....	77
4.1.2.4 Elemental analysis and acid-base titration....	78
4.2 Synthesis of FSM-16 catalysts.....	79
4.2.1 The physic-chemical properties of sulfonic functionalized FSM-16.....	80
4.2.1.1 XRD results.....	80
4.2.1.2 Sorption properties of sulfonic functionalized FSM-16.....	81
4.2.1.3 SEM images.....	83
4.2.1.4 Elemental analysis and acid-base titration....	84
4.2.2 The physic-chemical properties of aluminium functionalized FSM-16.....	84
4.2.2.1 XRD results.....	84
4.2.2.2 Sorption properties of Al-FSM-16.....	85
4.2.2.3 SEM images.....	88
4.2.2.4 Elemental analysis and acid-base titration....	89

CHAPTER	Page
4.3 Comparison of synthetic catalysts.....	90
4.3.1 Acidity.....	90
4.3.2 Hydrothermal stability.....	91
4.3.2.1 XRD results.....	91
4.3.2.2 Sorption properties of synthetic catalysts.....	92
4.3.2.3 SEM images.....	92
4.3.3 Acid leaching test.....	93
4.3.4 Initial rate, TON and TOF.....	94
4.4 Catalytic activities of FSM-16-PrSO ₃ H in lubricant preparation.....	95
4.4.1 Effect of reaction time.....	95
4.4.2 Effect of reaction temperature.....	96
4.4.3 Effect of catalytic amount.....	98
4.4.4 Effect of stirring speed.....	99
4.4.5 Effect of 2-ethyl hexanol to adipic acid molar ratio..	100
4.4.6 Effect of catalytic types.....	102
4.4.6.1 Homogeneous catalysts.....	102
4.4.6.2 Ion-exchange resins.....	102
4.4.6.3 Zeolites.....	104
4.4.6.4 Mesoporous materials.....	106
4.4.7 Effect of chain length of dicarboxylic acid.....	107
4.4.8 Effect of structure of alcohol.....	108
4.5 Catalyst reusability.....	109
4.5.1 Characterization of used catalysts.....	109
4.5.2 Activity of recycled FSM-16-PrSO ₃ H.....	111
4.5.3 Characterization of regenerated catalysts	113
4.5.4 Activity of regenerated FSM-16-PrSO ₃ H.....	114
V CONCLUSION.....	115
REFERENCES.....	117
APPENDIX.....	124
VITAE.....	141

LIST OF TABLES

Table	Page
2.1 Physical properties comparisons of important lubricants.....	8
2.2 The effect of specification on the performance of an ester lubricant.....	14
2.3 Guidelines on the compatibility of elastomers and plastics with esters....	19
2.4 Overview of physicochemical properties of ester lubricants.....	21
2.5 Comparison of homogeneous and heterogeneous catalysts.....	25
2.6 IUPAC classification of porous materials.....	35
2.7 Various synthesis conditions of hexagonal mesoporous materials and the types of interaction between templates and inorganic species.....	36
2.8 Properties of some hexagonal mesoporous materials.....	36
2.9 Example routes for interactions between the surfactant and the inorganic soluble species.....	39
2.10 Comparison of two well-known mesoporous materials, MCM-41 and SBA-15 in their characteristic properties.....	45
2.11 Comparison of two well-known mesoporous materials, MCM-41 and FSM-16 in their characteristic properties.....	47
2.12 Features of adsorption isotherms.....	54
3.1 Stoichiometric amounts of sodium aluminate in alumination of mesoporous materials with various Si/Al ratios.....	64
4.1 Textural properties of SBA-15 and sulfonic functionalized SBA-15.....	70
4.2 Sulfur analysis and acid value of sulfonic functionalized SBA-15.....	73
4.3 Textural properties of SBA-15 and Al-SBA-15 with various Si/Al ratios.....	77
4.4 Acid value of aluminium functionalized SBA-15.....	79
4.5 Textural properties of FSM-16 and sulfonic functionalized FSM-16.....	83
4.6 Sulfur analysis and acid value of sulfonic functionalized FSM-16.....	84
4.7 Textural properties of FSM-16 and Al-FSM-16 with various Si/Al ratios.....	88
4.8 Elemental analysis and acid value of aluminium functionalized FSM-16....	89
4.9 Acid value of synthetic catalysts.....	90

Table	Page
4.10 Textural properties of synthesized SBA-15-PrSO ₃ H and FSM-16-PrSO ₃ H with hydrothermal method before and after thermal stability test...	92
4.11 Leaching out of synthetic catalysts.....	93
4.12 Initial rate, TON and TOF of synthetic catalysts in esterification of adipic acid with 2-ethyl hexanol at 30 min.....	94
4.13 Effect of reaction time on ester yield and product distribution over FSM-16-PrSO ₃ H.....	95
4.14 Effect of reaction temperature on ester yield and product distribution over FSM-16-PrSO ₃ H.....	97
4.15 Effect of catalytic amount on ester yield and product distribution over FSM-16-PrSO ₃ H.....	98
4.16 Effect of stirring speed on ester yield and product distribution over FSM-16-PrSO ₃ H.....	100
4.17 Effect of 2-ethyl hexanol to adipic acid molar ratio on ester yield and product distribution over FSM-16-PrSO ₃ H.....	101
4.18 Effect of homogeneous catalysts on ester yield and product distribution..	102
4.19 Physicochemical and textural properties for ion-exchange resins.....	103
4.20 Effect of ion-exchange resins catalysts on ester yield and product distribution.....	103
4.21 Physicochemical and textural properties for zeolites.....	104
4.22 Effect of zeolite catalysts on ester yield and product distribution.....	105
4.23 Effect of mesoporous catalysts on ester yield and product distribution.....	106
4.24 Effect of 2-ethyl hexanol to adipic acid molar ratio on ester yield and product distribution over FSM-16-PrSO ₃ H.....	107
4.25 Effect of structure of alcohol on ester yield and product distribution over FSM-16-PrSO ₃ H.....	108
4.26 Molecular width and length calculation by Hyper Chem program.....	108
4.27 Textural properties of fresh and used FSM-16-PrSO ₃ H.....	110
4.28 Textural properties of fresh and regenerated FSM-16-PrSO ₃ H.....	114
A-1 Preparation of standard 2-ethyl hexyl mono adipate calibration solution...	128
A-2 Preparation of standard 2-ethyl hexyl di adipate calibration solution.....	128

LIST OF FIGURES

Figure	Page
2.1 Examples of aromatic esters.....	10
2.2 Chemical structure of diester.....	10
2.3 Chemical structure of polyol ester.....	11
2.4 Synthesis of ester lubricants.....	12
2.5 Thermal decomposition of (a) esters with β -hydrogens (<i>e.g.</i> dibasic acid esters) and (b) esters without β -hydrogens (<i>e.g.</i> polyol esters).....	17
2.6 The relationship between activation energy (E_a) and enthalpy (ΔH) of the reaction with and without a catalyst.....	23
2.7 Phase sequence of the surfactant-water binary system (a) spherical micelle, (b) rod-shaped micelle, (c) reverse micelle, (d) lamellar phase, and (e) hexagonal phase.....	37
2.8 Schematic representation of the different types of silica-surfactant interfaces. Dashed line corresponded to H-bonding interactions.....	40
2.9 Mechanism of mesoporous formation (a) LCT of MCM-41 formation, (b) Folding sheet formation of FSM-16 and (c) H-bonding interaction in HMS formation.....	41
2.10 Block copolymer used in mesostructured generation.....	42
2.11 (a) Schematic view of the (S^0H^+)(X^-I^-), S^0I^0 , and (S^0M^+)(X^-I^0) hybrid interphases (HIs) (b) Three possible structures of a HI composed by a nonionic polymer and an inorganic framework.....	44
2.12 Pore evolution upon thermal treatment, depending on pre-treatment and aging.....	45
2.13 formation mechanism of (a) silicate structure of disilicate ($H_2Si_2O_5$) and (b) structure of FSM-16 with surfactant.....	47
2.14 Steps in heterogenous catalysis.....	48
2.15 In-situ oxidation synthesis strategy for the preparation of sulfonic-acid-modified mesostructured materials.....	50
2.16 Post synthesis procedure for the preparation of sulfonic-acid-modified mesostructured materials.....	51
2.17 Diffraction of X-ray by regular planes of atoms.....	52
2.18 The IUPAC classification of adsorption isotherm.....	53

Figure	Page
3.1 The temperature program for the calcination of (a) SBA-15 and (b) FSM-16.....	57
3.2 The GC heating condition for monoester and diester analysis.....	59
3.3 The temperature program for esterification reaction.....	60
4.1 X-ray powder diffraction patterns of (a) SBA-15, (b) SBA-15-PrSO ₃ H and (c) SBA-15-ArSO ₃ H.....	69
4.2 N ₂ adsorption-desorption isotherm and BJH-pore size distribution of (a) SBA-15, (b) SBA-15-PrSO ₃ H and (c) SBA-15-ArSO ₃ H.....	71
4.3 SEM images of (a) SBA-15, (b) SBA-15-PrSO ₃ H and (c) SBA-15-ArSO ₃ H.....	72
4.4 X-ray powder diffraction patterns of calcined Al-SBA-15 with various Si/Al mole ratios in reactant mixture (a) SBA-15, (b) Al-SBA-15(10), (c) Al-SBA-15(25), (d) Al-SBA-15(50) and (e) Al-SBA-15(100).....	74
4.5 N ₂ adsorption-desorption isotherms of (a) Al-SBA-15(10), (b) Al-SBA-15(25), (c) Al-SBA-15(50) and (d) Al-SBA-15(100).....	75
4.6 BJH-Pore size distributions of (a) Al-SBA-15(10), (b) Al-SBA-15(25), (c) Al-SBA-15(50) and (d) Al-SBA-15(100).....	76
4.7 SEM images of (a) Al-SBA-15(10), (b) Al-SBA-15(25), (c) Al-SBA-15(50), and (d) Al-SBA-15(100).....	78
4.8 X-ray powder diffraction patterns of (a) reference kanemite by Wang <i>et al.</i> method and (b) synthesis kanemite.....	79
4.9 SEM images of kanemite at different magnifications (a) ×5000 and (b) ×10,000.....	80
4.10 X-ray powder diffraction patterns of (a) FSM-16, (b) FSM-16-PrSO ₃ H and (c) FSM-16-ArSO ₃ H.....	81
4.11 N ₂ adsorption-desorption isotherm and BJH-pore size distribution of (a) FSM-16, (b) FSM-16-PrSO ₃ H and (c) FSM-16-ArSO ₃ H.....	82
4.12 SEM images of (a) FSM-16, (b) FSM-16-PrSO ₃ H and (c) FSM-16-ArSO ₃ H.....	84
4.13 X-ray powder diffraction patterns of calcined Al-FSM-16 with various Si/Al mole ratios in reactant mixture (a) FSM-16, (b) Al-FSM-16(10), (c) Al-FSM-16(25), (d) Al-FSM-16(50) and (e) Al-FSM-16(100).....	85

Figure	Page
4.14 N ₂ adsorption-desorption isotherms of (a) Al-FSM-16(10), (b) Al-FSM-16(25), (c) Al-FSM-16(50) and (d) Al-FSM-16(100).....	86
4.15 BJH-Pore size distributions of (a) Al-FSM-16(10), (b) Al-FSM-16(25), (c) Al-FSM-16(50) and (d) Al-FSM-16(100).....	87
4.16 SEM images of (a) Al-FSM-16(10), (b) Al-FSM-16(25), (c) Al-FSM-16(50), and (d) Al-FSM-16(100).....	89
4.17 X-ray powder diffraction patterns of synthesized catalysts with hydrothermal method comparison with hydrothermal stability test (a) SBA-15-PrSO ₃ H and (b) FSM-16-PrSO ₃ H.....	91
4.18 SEM images of catalytic synthesis (a) before, (b) after hydrothermal stability test of SBA-15-PrSO ₃ H and (c) before, (d) after hydrothermal stability test of FSM-16-PrSO ₃ H.....	93
4.19 Ester yield and product selectivity over SBA-15-PrSO ₃ H and FSM-16-PrSO ₃ H.....	94
4.20 Influence of reaction time on the ester yield over FSM-16-PrSO ₃ H. Reaction conditions: 2-ethyl hexanol/adipic acid mole ratio as 2; reaction temperature 100°C; catalytic amount 3 wt.%; stirring speed 150 rpm. (Symbols: (■) monoester selectivity, (▲) diester selectivity and (◆) total ester yield).....	96
4.21 Influence of reaction temperature on the ester yield over FSM-16-PrSO ₃ H. Reaction conditions: 2-ethyl hexanol/adipic acid mole ratio as 2; reaction time 5 hrs.; catalytic amount 3 wt.%; stirring speed 150 rpm. (Symbols: (■) monoester selectivity, (▲) diester selectivity and (◆) total ester yield).....	97
4.22 Influence of catalytic amount on the ester yield over FSM-16-PrSO ₃ H. Reaction conditions: 2-ethyl hexanol/adipic acid mole ratio as 2; reaction time 5 hrs.; reaction temperature 100°C; stirring speed 150 rpm. (Symbols: (■) monoester selectivity, (▲) diester selectivity and (◆) total ester yield).....	99
4.23 Influence of stirring speed on the ester yield over FSM-16-PrSO ₃ H. Reaction conditions: 2-ethyl hexanol/adipic acid mole ratio as 2; reaction time 5 hrs.; reaction temperature 100°C; catalytic amount 3 wt.%. (Symbols: (■) monoester selectivity, (▲) diester selectivity and (◆) total ester yield).....	100

Figure	Page
4.24 Influence of 2 ethyl hexanol to adipic acid mole ratio on the ester yield over FSM-16-PrSO ₃ H. Reaction conditions: reaction time 5 hrs.; reaction temperature 100°C; catalytic amount 3 wt.%; stirring speed 150 rpm. (Symbols: (■) monoester selectivity, (▲) diester selectivity and (◆) total ester yield).....	101
4.25 Structures of zeolites (a) ZSM-5, (b) MCM-22 and (c) Beta zeolite.....	105
4.26 X-ray powder diffraction patterns of (a) fresh, (b) 1 st used hexane, (c) 2 nd used hexane, (d) 1 st used acetone, (e) 2 nd acetone, (f) 1 st used methanol and (g) 2 nd used methanol FSM-16-PrSO ₃ H.....	109
4.27 FSM-16-PrSO ₃ H deactivation following multiple reaction cycles of esterification of adipic acid with 2-ethyl hexanol at 100°C with solvent washing (a) hexane, (b) acetone and (c) methanol and drying between cycles.....	112
4.28 X-ray powder diffraction patterns of (a) fresh (b) 1 st used hexane, (c) 2 nd used hexane and (d) regenerated FSM-16-PrSO ₃ H.....	113
4.29 Activities of fresh and regenerated FSM-16-PrSO ₃ H using hexane as solvent washing.....	114
A-1 NH ₃ -TPD profile of (a) SBA-15-PrSO ₃ H and (b) SBA-15-ArSO ₃ H....	125
A-2 NH ₃ -TPD profile of (a) FSM-16-PrSO ₃ H and (b) FSM-16-ArSO ₃ H....	125
A-3 NH ₃ -TPD profile of (a) Al-SBA-15 ratio Si/Al=10, (b) Al-SBA-15 ratio Si/Al=25, (c) Al-SBA-15 ratio Si/Al=50 and (d) Al-SBA-15 ratio Si/Al=100.....	126
A-4 NH ₃ -TPD profile of (a) Al-FSM-16 ratio Si/Al=10, (b) Al- FSM-16 ratio Si/Al=25, (c) Al- FSM-16 ratio Si/Al=50 and (d) Al- FSM-16 ratio Si/Al=100.....	126
A-5 Calibration curve of (a) 2-ethyl hexyl mono adipate and (b) 2-ethyl hexyl di adipate.....	130
A-6 Calibration curve of (a) 2-ethyl hexyl mono azelate and (b) 2-ethyl hexyl di azelate.....	131
A-7 Calibration curve of (a) 2-ethyl hexyl mono sebacate and (b) 2-ethyl hexyl di sebacate.....	132
A-8 Calibration curve of (a) octyl mono adipate and (b) octyl di adipate.....	133
A-9 Calibration curve of (a) octyl mono azelate and (b) octyl di azelate.....	134
A-10 Calibration curve of (a) octyl mono sebacate and (b) octyl di sebacate...	135
A-11 GC chromatogram of 2-ethyl hexyl adipates product from esterification reaction.....	136
A-12 GC chromatogram of 2-ethyl hexyl azelates product from esterification reaction.....	137

Figure		Page
A-13	GC chromatogram of 2-ethyl hexyl sebacates product from esterification reaction.....	138
A-14	Mass spectrum of (a) 2-ethyl hexyl monoadipate and (b) 2-ethyl hexyl diadipate.....	139

LIST OF SCHEMES

Scheme		Page
3.1	Preparation diagram for SBA-15-Pr-SO ₃ H by hydrothermal method.	62
3.2	Preparation diagram for FSM-16-Pr-SO ₃ H by hydrothermal method.	63
3.3	Diagram for acid-base titration.....	65
3.4	Diagram for lubricating oil preparation and analysis.....	66
3.5	Regenerated catalyst preparation	68

LIST OF ABBREVIATIONS

Å	Angstrom
a.u.	Arbitrary unit
BET	Brunauer-Emmett-Teller
BJH	Barret, Joyner, and Halenda
°C	Degree Celsius
CMC	critical micelle concentration
CSPTMS	2-(4-chlorosulfonylphenyl)ethyltrimethoxysilane
GC	Gas chromatography
g	Gram (s)
hr	Hour (s)
MPTMS	(3-mercaptopropyl)trimethoxysilane
MS	Mass spectroscopy
µm	Micrometer (s)
ml	Milliliter (s)
min	Minute (s)
M	Molarity
nm	Nanometer (s)
%	Percentage
SEM	Scanning electron microscopy
TEOS	Tetraethyl orthosilicate
TOF	Turnover frequency
TON	Turnover number
XRD	X-ray diffraction

CHAPTER I

INTRODUCTION

1.1 Statement of Problems

Lubricant is very important substance since it is used in the most of mechanical parts in machines and engines. Approximately 85 % of fluids used as lubricants are petroleum-based mineral oils [1]. Because of their low biodegradability (lower than 30 %), mineral oils are not environmentally friendly. Moreover, the world petroleum resources are limited. In order to avoid the environmental problems arising from an increase in the consumption of lubricants in various kinds of application, the utilization of biodegradable lubricants has been encouraged [2]. Diester is one of the major classes of ester-based biodegradable lube oil. Due to their dumbbell-like structure, diesters have low pour points, high flash points, shear stability, good oxidation and thermal stability, and high viscosity index [3].

Conventionally, the synthesis of diesters is performed via an esterification of corresponding dicarboxylic acids with linear or branched C₆-C₁₀ alcohols. The most widely used catalysts for the esterification are sulfuric acid and organo sulfonic acids, e.g. *p*-C₇H₇-SO₃H. These catalysts actively promote the complete conversion of the diacids, giving the high yield of diesters since they possess high acidity and dissolve in the reaction mixture. However, at the end of the production process, a neutralisation step is necessary to stop the catalytic reaction after which a purification of the ester product can be attempted. Typically, washing with an alkali, such as sodium hydroxide solution, is applied to the neutralization, followed by another washing to remove the salt formed in the purification by which a large amount of wastewater is produced, representing a disadvantage of the conventional procedure. The washing step also changes any unreacted diacid component to salt in the discharge liquor. Moreover, some esters may be lost in the aqueous alkali phase, depending on the solubility of the esters in such a solution.

Recently, the application of heterogeneous acid catalysts to conventional esterification/transesterification for oleochemical syntheses has attracted considerable attention since the process can be simplified by using of a designed-column reactor

packed with the solid catalysts. Consequently, the need of subsequent steps for the catalyst separation and the product purification can be reduced [4-6]. A variety of materials have been used as solid acid catalysts, including clays [7], zeolites [8], heteropolyacids [9], cation-exchange resins [10], *etc.* More importantly, the most of heterogeneous catalysts themselves are recyclable, less toxic and non-corrosive. The migration from the strong soluble acids to strongly acidic solid for the synthesis of biolubricants via the corresponding esterification is our desirable goal. In this research, focus on heterogeneous catalysts SBA-15 and FSM-16 due to the distribution of pore size uniformity, high surface area and high thermal stability. Furthermore, it can be easily separated from product, reusability, environmental compatibility and non-toxicity.

The aim of this thesis is to synthesize SBA-15 and FSM-16 and enhance catalytic properties by grafting with aluminium group or sulfonic group for using in esterification of dicarboxylic acids (adipic acid, azelaic acid and sebacic acid) with alcohols (2-ethyl-1-hexanol and *n*-octanol). Effects of reaction time, reaction temperature, catalytic amount, molar ratio of dicarboxylic acid/alcohol and type of catalysts on the ester yield and selectivity were investigated.

1.2 Literature reviews

This topic will be explained into 3 parts, *i.e.* catalyst synthesis, diester synthesis from diacid and catalysts in esterification.

1.2.1 Catalyst synthesis

Stucky *et al.* [11] synthesized well-ordered hexagonal mesoporous silica structure (SBA-15) which was synthesized in acidic media. SBA-15 exhibited pore size from 50 to 300 angstroms pore volume fractions up to 0.85 and wall thickness of 31 to 64 angstroms. SBA-15 used a variety poly(alkylene oxide) triblock copolymers and addition of co-solvent organic molecules.

Because the SBA-15 contains less acidity. In 2005, Luo *et al.* [12] studied the increasing acidity of SBA-15 by grafting sulfonic acid group on the surface using post-synthesis method. The effects of time and amount of oxidizing agent were investigated. The modified material showed high acidity when oxidized with 30%

H₂O₂ for 24 hrs. Moreover, SBA-15-SO₃H exhibited a good long-range order, high specific surface area (*ca.* 600 m²/g) and uniform pore size (*ca.* 6 nm).

The Al-SBA-15 could be synthesized by incorporating aluminium into SBA-15 *via* direct synthesis and post synthesis. Yue *et al.* [13] studied Al-SBA-15 by direct synthesis and the resulting materials retain the hexagonal order and physical properties of purely siliceous SBA-15. The Al-SBA-15 catalysts exhibited higher catalytic activities in the cumene cracking reaction than Al-MCM-41.

In 2001, Wang *et al.* [14] synthesized highly ordered hexagonal mesoporous silica structure (FSM-16) from water glass using cetylpyridium bromide (CPBr) as template. FSM-16 exhibited surface area as 1246.3 m²/g along pore size distribution 3.0 nm., pore volume 1.0 cm³/g and wall thickness of 15 angstroms.

In 2008 Dhar *et al.* [15] synthesized highly active FSM-16 which was supported with molybdenum compared with SBA-15, HMS and SiO₂. The highest active (mmol.h⁻¹.g⁻¹) was obtained at 12% Mo catalysts supported on FSM-16.

1.2.2 Diester synthesis from diacid

Gryglewicz and Oko [16] studied the synthesis of new oligomeric esters of dicarboxylic acids, which can be excellent additives for improving properties of synthetic oils. This research carried out esterification of adipic acid and sebacic acid with 2-ethyl hexanol. The results showed that straight adipates and sebacates of 2-ethyl hexanol can be used as component of lubricating oils. In addition, these esters can reduce the pour point by a few degrees in comparison with the tested base oil. Moreover, the oligomeric ester exhibited higher viscosity index than base oil about 16 unit.

Mansoori and Sejidov [17] studied the production of mixed-synthetic diester base oils from the waste of electrochemical production of sebacic acid (mixtures of methyl esters of dicarboxylic acids, HOOC(CH₂)_nCOOH, n = 4, 6, 8). The mixtures of methyl esters of dicarboxylic acids are transesterified by pure alcohols and also different mixtures of aliphatic monohydric alcohols, C₆-C₁₀ of *iso*- and normal structure, in the presence of a new catalytic system (tetra-*n*-butyl orthotitanate, Ti(O-*n*-Bu)₄). The obtained mixed diester oils showed similar thermal properties and low pour point (minimum -70 °C), and improved viscosity temperature properties

compared with commercially available dioctyl sebacate (DOS) and dioctyl adipate (DOA) diester oils.

1.2.3 Catalysts in esterification

Liu *et al.* [18] studied the impact of carboxylic acid chain length on the kinetics of liquid-phase acid-catalyzed esterification. Using sulfuric acid and a commercial Nafion solid acid catalyst (SAC-13), initial kinetics were measured for the reactions of a series of linear chain carboxylic acids (acetic, propionic, butyric, hexanoic, and caprylic acid) with methanol at 60°C. It was found that reaction rate decreased as the number of carbons in the linear alkyl chain increased for both H₂SO₄ and SAC-13. This trend is discussed in terms of the polar and steric effects of the alpha-substituent to the carboxylic group and evaluated by a Taft-type correlation which was first proposed models that attempted to quantify polar, resonance and steric effects of substituents in chemical reactivity. Using a mechanistically based kinetic model, the reaction kinetic parameters of SAC-13 catalysis were determined and compared for different carboxylic acids. Moreover, important parameters, such as water deactivation, catalyst reusability, and regeneration, were also affected by the size of the carboxylic acid used. Using THF washing, the Nafion catalyst showed good reusability in the esterification of low-molecular-weight acids. However, the catalyst experienced continuous activity loss in consecutive reaction cycles using the larger caprylic acid. Catalyst deactivation was probably due to accumulation of the carboxylic acid molecules and/or intermediates in the Nafion resin. Such an accumulation may be caused by the irreversible adsorption of carboxylic acids on Brønsted sites and/or their entanglement with the polymeric chains of the Nafion. Effective regeneration is needed to improve the applicability of SAC-13 in the esterification of large FFAs.

Özbay *et al.* [19] studied the activities of Amberlyst-15 (A-15), Amberlyst-35 (A-35), Amberlyst-16 (A-16) and Dowex HCR-W2 resins in direct free fatty acids (FFA) esterification were examined in the temperature range of 50–60°C and the effect of catalytic amount (1-2 wt.%) on FFA conversion. FFA conversion increased with increasing reaction temperature and catalytic amount. Order of catalytic activities was found as A-15 > A-35 > A-16 > Dowex HCR-W2. This was related to

the size of average pore diameters and magnitude of BET surface area. The highest FFA conversion (45.7 %) was obtained over the strongest acidic macroreticular ion-exchange resin A-15 at 60 °C with 2 wt.% catalytic amount.

Rahman *et al.* [20] studied the enzymatic synthesis of methyl adipate via green esterification of adipic acid and methanol in hexane. Lipase from *Candida rugosa* immobilised onto various layered double hydroxides (LDHs) by a reproducible and simple method of physical adsorption was used as biocatalyst with promising result. Mg/Al-NO₃⁻, Zn/Al-NO₃⁻ and Ni/Al-NO₃⁻ of LDHs with molar ratio of M²⁺/M³⁺ = 4:1 were synthesized by co-precipitation method with continuous agitation. The percentages of protein loading on Mg/Al-NO₃⁻, Zn/Al-NO₃⁻ and Ni/Al-NO₃⁻ were 71%, 67% and 58%, respectively, due to the larger surface area, porosity and basal spacing of the supports. Parameter studies of reaction time, reaction temperature, water activity, thermostability, storage, leaching and reusability were optimised. The optimum conditions to produce adipate ester upto 80 % were reaction time; 2.5 h, temperature; 50°C, and water activity; 0.53, respectively.

Reddy *et al.* [21] studied the esterification of dicarboxylic acids with various alcohols and phenols in presence of metal exchanged montmorillonite clay catalyst (Mⁿ⁺-mont; Mn = Al³⁺, Fe³⁺, Cr³⁺, Zn²⁺, Mn²⁺, and Ni²⁺). Among the used catalysts, Al³⁺-mont was found to be the most effective, as it gave good to excellent yields of esters under mild reaction conditions. Moreover these catalysts can be regenerated and reused.

Nagaraju *et al.* [22] studied kinetic rate on esterification of acetic acid with *n*-propyl alcohol, *iso* propyl alcohol, *n*-butyl alcohol and *iso*-butyl alcohol over zeolite H β , HY and HZSM5 catalysts. The esterification reaction was carried out over 0.5 g of catalyst at 110°C for 1 hour with molar ratio of alcohol to acetic acid as 1. Order of catalytic activities was found as H β > HZSM5 > HY.

Sastre *et al.* [23] studied influence of the alkyl chain length of HO₃S-R-MCM-41 acid catalyst (R= different alkyl) on the esterification of glycerol with lauric acid and oleic acid. As compare to methyl, ethyl and mixture alkyl group, the HO₃S-ethyl-MCM-41 is the best catalyst which provided conversion more than 95%.

From previous literature reviews, only few researches were studied the ester lubricant synthesis over mesoporous material. Thus, this research will be studied

esterification of dicarboxylic acid with alcohol over grafting with aluminium group and sulfonic group on SBA-15 and FSM-16 as catalysts.

1.3 Objectives

The objectives of this research are:

1. To synthesis acidic porous heterogeneous catalysts.
2. To study reaction parameters base on ester yield and product selectivity in esterification of dicarboxylic acid with alcohol over heterogeneous catalysts.

1.4 Scopes of work

- 1.4.1 Synthesis SBA-15 and FSM-16 by hydrothermal methods.
- 1.4.2 Functionalized synthetic mesoporous silicon oxide with aluminium or sulfonic group.
- 1.4.3 Characterization all prepared catalysts.
- 1.4.4 Study reaction parameters of esterification conditions base on yield and selectivity of ester.
 - Reaction time 0.5-8 hrs.
 - Reaction temperature 80-120°C
 - Catalytic amount 0-10 wt.%
 - Molar ratio of alcohol to dicarboxylic acid mole ratio 1.0-5.0
 - Type of dicarboxylic acid Adipic acid ($C_6H_{10}O_4$), azelaic acid ($C_9H_{16}O_4$) and sebacic acid ($C_{10}H_{18}O_4$)
 - Type of alcohol 2-ethyl-1-hexanol and *n*-octanol
 - Type of catalysts
- 1.4.5 Study reusability and regeneration of catalysts.

CHAPTER II

THEORY

2.1 Lubricating oil classification

Lubricating oils are classified into three categories as following:

- Animal fat/vegetable oils
- Mineral oils
- Synthetic lubricants

2.1.1 Animal fat/vegetable oil

The animal fat/vegetable oils are not utilized for industrial bearing applications, due to acid formation after a short period of use. The acid is detrimental to the bearing surface performance. The natural fat and oils are generally reserved for cooking purposes.

2.1.2 Mineral oils

The majority of lubricating oil using these days is derived from refined crude petroleum. The refining method is either by the solvent refining process or by the hydrotreating process. Both processes consist of a number of stages designed to remove undesired components, such as aromatic hydrocarbons, acid components, organic sulfur compounds and wax. They were improved desirable properties, including viscosity index, pour point and stability. After refining, the oils are finished with a base stock oil to which additives are blended to enhance the lubricating performance. For example, molybdenum dialkylphosphorodithioates are added into the mineral oil to reduce oxidation property and foaming formation [24].

2.1.3 Synthetic lubricants

Synthetic lubricants are man-made chemicals designed to work under conditions where normal petroleum base oils would find limitations. They possess well-defined functional groups to serve specific applications. They are usually more consistent and uniform in structure than petroleum base stocks. For some types, the use of synthetic lubes has the following features.

- **Advantages**
 - No waxes are present at very low temperatures.
 - Petroleum-based oils have a temperature application limit of approximately 320°C, whereas synthetic lubes can also be used at much higher temperatures.
 - At higher temperatures, sludging and acid buildup are less apparent due to their improved oxidation stability.
 - Synthetics have a more stable viscosity index (VI) and can be relied upon to be a more stable lubricant over different temperature value.

- **Disadvantages**
 - Synthetics are much more expensive to purchase. Prices range from five times to mineral-based lubricant cost.
 - Many synthetics are not compatible with certain sealing materials and may require replacement of seal, hoses, and paint.

Table 2.1 Physical properties comparisons of important lubricants [25].

Property	Mineral Oil	Polyalphaolefin	Diester	Polyglycol
Viscosity characteristics (temperature)	Moderate	Good	Excellence	Good
V.I.	Moderate	Very good	Good	Very good
Low temperature pour point	Good	Very good	Very good	Good
Oxidation stability	Moderate	Very good	Good	Very good
Volatility	Moderate	Good	Very good	Good
Lubricating properties	Good	Good	Very good	Good
Mineral oil compatibility	-	Excellence	Good	Poor
Cost	Low	Medium	Medium	Medium

2.2 Synthetic ester lubricants

Although the development of the synthetic esters is relatively recent, the use of esters as lubricating fluids is as old as mankind technology. Before mineral oils became worldwide available as a co-products of the petroleum-based fuel industry,

lubricants were defined from animal fats and vegetable oils, which are either tri-esters of glycerine with different fatty acids, *e.g.* tallow and olive oil, or long chain monoesters of fatty acids with fatty alcohols, such as sperm whale oil.

The application of synthetic esters as high performance lubricating fluids was originally driven by an invention of gas turbine or jet engine for aviation. The aviation turbines are operated at higher temperatures than the formerly used piston engines and the jet aircrafts are capable of working at much higher altitudes. Consequently, the suitable lubricants for the aviation turbines are required to provide both very good stability at high temperatures and good cold flow properties. However, the mineral oils and other synthetic hydrocarbons could not deliver the combination of both properties, and diesters were adopted as the lubricant base fluids of choice for early aviation turbines. As the gas turbine technology developed, the operating temperature increased further, and diesters have been largely substituted by polyol esters, which possess even better thermal stability. Despite an intensive research into alternative functional fluids, the polyol esters remain the best choice for the aviation turbine lubrication.

In addition to their good properties at extreme temperatures, the synthetic esters have other desirable characteristics including good lubricity, high viscosity index, low volatility, and compatibility with base fluids and standard lubricant additives. The ester base fluids with a wide range of viscosities can be designed through flexibility of fundamental chemistry and a variety of raw materials. Other key properties, such as biodegradability, are also possibly controlled by a molecular design. Consequently, the synthetic esters have found many applications outside the aviation engines. The examples include automotive crankcase and gear oils, 2-stroke engine lubricants, metal cutting and rolling fluids, air compressor lubricants, and refrigeration compressor lubricants.

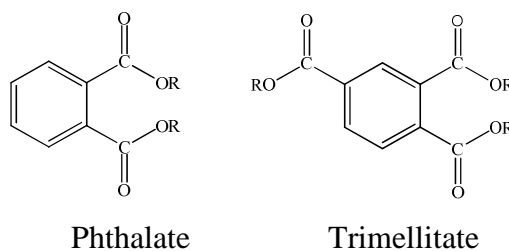
2.2.1 General features and product groups [26]

Ester is defined as a class of organic compounds containing the ester functional group. They are normally manufactured by esterification of carboxylic acids with alcohols, essentially in the presence of acid catalysts and techniques of water elimination.

The physicochemical properties of the product esters can be controlled via an appropriate selection of the raw materials used by which they are mainly dependent on molecular weight, number of ester groups per molecule, and degree of branching in the hydrocarbon chain. The ester linkages exhibit a high bond energy, resulting in a good heat resistance. Moreover, they usually have good oxidation stability and excellent viscosity index and volatility characteristics [27].

There are three main classes of the synthetic esters that are currently used as lube fluids: aromatic esters, aliphatic diesters and polyol esters.

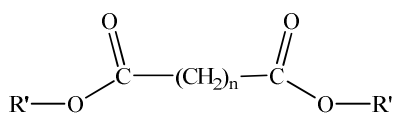
1. Aromatic esters, as shown in Figure 2.1, are produced by the reaction of aromatic di- or poly- acids or aromatic anhydrides, such as phthalic anhydride, trimellitic anhydride, or pyromellitic anhydride, with pure monoalcohols or mixture of monoalcohols.



R = C7-C10 linear or branched alkyl groups

Figure 2.1 Examples of aromatic esters.

2. Diesters (Figure 2.2) can be synthesized by esterifying linear diacid with monoalcohols or mixtures of monoalcohols.

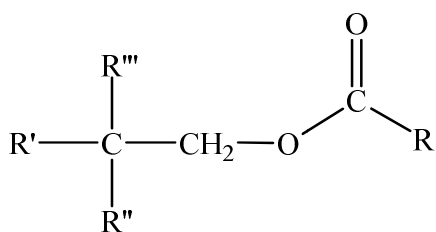


n = 4 – 10, R' = C7-C10 linear or branched alkyl groups

Figure 2.2 Chemical structure of diester.

3. As illustrated in Figure 2.3, polyol esters are esterified products of diols or polyols having a neopentyl structure, such as neopentyl glycol, trimethylol propane or pentaerythritol, and monoacids or mixtures of monoacids. Similarly, oligometric esters, generally known as complex esters, can be manufactured by the reaction of diols or polyols with di- or poly- acids/anhydrides to act as capping reagent. The variety of the starting reagent allows the preparation of lube compounds having

relatively high average molecular weights and viscosities when compared to diesters and polyol esters.



PE; pentaerythritol; $R' = R'' = R''' = \text{CH}_2\text{OCOR}$

TMP; Trimethylol propane;

$R' = R''' = \text{CH}_2\text{OCOR}$, $R'' = \text{Ethyl}$

NPG; Neopentyl glycol;

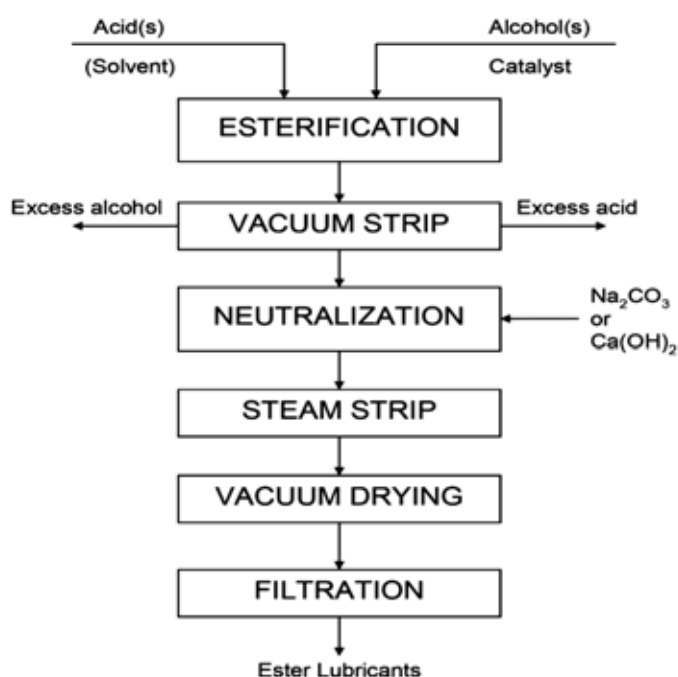
$R' = \text{CH}_2\text{OCOR}$, $R'' = R''' = \text{Methyl}$

$R = \text{C}_4\text{-C}_{17}$ linear or branched alkyl groups

Figure 2.3 Chemical structure of poly ester.

However, due to a distribution of molecular weights in the complex esters, their volatility characteristics are not as good as simple esters of the similar average molecular weights.

2.2.2 Manufacture of ester lubricants [28]



The manufacturing process of esters consists of three distinct stages; esterification, neutralization and filtration

Figure 2.4 Synthesis of ester lubricants.

A schematic of the manufacturing process is given in Figure 2.4. The production of esters is based on the following reaction: acid + alcohol = ester + water.

For diesters, the reaction can be driven to a high level of completion by using excess alcohol to remove the water of reaction. This usually takes several hours, during which the reaction is monitored by taking samples periodically for acid number determination. The use of an azeotroping agent such as xylene or toluene (to aid water removal) is optional. The acid and alcohol can be reacted directly or in the presence of a catalyst. Possible catalysts include: sulfuric acid, paratoluenesulfonic acid, tetraalkyl titanate, anhydrous sodium sulfate, phosphorous oxides and stannous octanoate.

After the ester has been formed, unreacted acid is neutralized by means of sodium carbonate or calcium hydroxide and removed by filtration. Typical reaction conditions for titanium catalysts are 230°C in vacuum; acid catalysts require milder conditions, since side reactions (*e.g.*, color formation) become prominent at higher temperatures. A significant amount of alcohol vaporizes along with the water and must be recovered. This is accomplished by condensing the reactor vapors and decanting the resulting two-phase liquid mixture. The alcohol is then refluxed and return to the reactor.

Polyol esters are made by reacting a polyhydric alcohol, such as neopentyl glycol (NPG), trimethylol propane (TMP), pentaerythritol (PE), or dipentaerythritol (diPE) with a monobasic acid to give a desired ester.

Polyol esters can also be made via a transesterification (alcoholysis) route. Here, monoesters (usually methyl) are transesterified with a neopentyl alcohol in the presence of a catalyst. Catalysts specifically designed to help the transesterification process are now available.

Variations in raw materials dominate a major influence on the final physical properties of the ester. For example, the monofunctional alcohols used to make monoesters, diesters, phthalates, trimellitates and pyromellitates are often mixtures of varying chain lengths, degrees of branching of isomers for example:

Isotridecanol, which is a mixture of branched carbon chain lengths C_{11} to C_{14} , rich in C_{13} alkyl caains.

Isodecanol, which is a mixture of branched carbon chain lengths C₉ to C₁₁, rich in C₁₀ alkyl caains.

The degree of branching, the chain length, and the ratio of isomers are highly dependent on the feedstock and catalyst used to make the alcohol. Batches of the same alcohol purchased from different companies or from different plants of same company can vary significantly. Therefore, the typical properties of a given ester may differ from supplier to supplier. Even if exactly the same raw materials are used, the processing specification is a major impact on the physical properties and the performance of ester. The following properties of the ester should be tightly controlled: residual unreacted acid, hydroxyl number (degree of esterification), residual unreacted alcohol, cross-contamination of other esters made on plant, residual catalyst and residual neutralizing agents.

Guidelines for the recommended levels of these ester properties are listed in Table 2.2. These are only guidelines and may need to be adjusted depending on the application of use.

Table 2.2 The effect of specification on the performance of an ester lubricant.

Property	Effects	Typical value
Total acid number	Hydrolytic stability Thermal stability Wear	< 0.1 mg KOH/g
Hydroxyl number	Hydrolytic stability Deposit formation Foaming Volatility Flash point	< 4 mg KOH/g
Iodine number	Thermal stability Color stability Deposit formation Low temperature flow	As low as possible
Water content	Hydrolytic stability	< 0.1 % w/w
Process residuals (<i>e.g.</i> catalyst, neutralizing agents, azeotrope, <i>etc.</i>)	Thermal stability Deposit formation Hydrolytic stability Foaming	< 5 ppm metals
Purity	All of the above	

2.2.3 Physicochemical properties of ester lubricants [29]

Mineral oil base stocks are derived from crude oil and consist of complex mixtures of long-chain hydrocarbons. Synthetic ester lubricants, on the other hand, are prepared from raw materials having uniform molecular structures. This uniformity yields well-defined properties that can be tailored for specific applications.

Many lubricant requirements are translated into specific properties of an oil measurable by conventional laboratory tests, *e.g.* viscosity, evaporation, flash point, etc. Other, more critical requirements are related to the chemical properties of the lubricant and many of these can be measured satisfactorily only by elaborate and

expensive apparatus specially developed to simulate performance. A wide variety of raw materials can be used for the preparation of ester-type base fluids and this affects a number of lubricant properties including: viscosity, flow properties, lubricity, thermal stability, hydrolytic stability, solvency, and biodegradability.

Viscosity; the viscosity of an ester lubricant can be altered by:

- increasing the molecular weight of the molecule by:
 - increasing the carbon chain length of the acid
 - increasing the carbon chain length of the alcohol
 - increasing the number of ester groups
- increasing the size or degree of branching
- including cyclic groups in the molecular backbone
- maximising dipolar interactions

One disadvantage of very long-chain molecules is their tendency to shear into smaller fragments under stress.

Flow properties; the viscosity index (VI) of an ester lubricant can be increased by:

- increasing the acid chain length
- increasing the alcohol chain length
- increasing the linearity of the molecule
- not using cyclic groups in the backbone, which lowers the VI even more than aliphatic branches
- by molecular configuration-viscosity indices of polyol esters tend to be lower than their diester analogues, from more compact configurations of the polyol molecules

The pour point of an ester lubricant can be decreased by:

- increasing branching
- positioning of the branch-branching in the centre of the molecule gives better pour points than branches near to the chain ends
- decreasing the acid chain length
- decreasing the internal symmetry of the molecule

From the above lists, there is a natural trade-off between viscosity index and pour point, *e.g.* by increasing the linearity of the ester, the viscosity index improves but the pour point increases. Esters made from mixtures of normal and branched acids with the same carbon number have viscosity indices between those of the normal and branched acid esters. But their pour points are lower than those esters formed separately from either branched or normal acids.

Lubricity; ester groups are polar and therefore affect the efficiency of anti-wear additives. When a base fluid is used which is too polar, the anti-wear additives will be adsorbed onto, and cover, the metal surfaces, giving higher wear characteristics. Consequently, although esters have superior lubricity properties compared to mineral oil, they are less efficient than anti-wear additives. Esters are classified in terms of polarity or non-polarity by the Van der Waal formula, Equation (2.1):

$$\text{Non-polarity index} = \frac{[\text{Total number of C atoms} \times \text{Molecular weight}]}{[\text{Number of carboxylic groups} \times 100]} \quad (2.1)$$

Generally, the higher the non-polarity index, the lower the affinity for the metal surface. Using the above formula it can be seen that as a general rule, increasing molecular weight improves overall lubricity. Esters terminated by normal acids or alcohols have better lubricities than those made from branched acids/alcohols, while esters made from mixed acids/alcohols have lubricities intermediate between esters of normal acids/alcohols and esters of branched acids/alcohols.

Thermal stability; the ester linkage is exceptionally stable; bond energy determinations predict that it is more thermally stable than the C–C bond. The thermal stability advantages of polyol esters compared to diesters is well documented and has been investigated on a number of occasions. The absence of hydrogen atoms on the β -carbon atom of the alcohol portion of an ester leads to superior thermal stability. The presence of the β -hydrogen atom enables a low-energy decomposition mechanism to operate via a six-membered cyclic intermediate producing acids and 1-alkenes, Figure 2.5 (a). When β -hydrogen atoms are replaced by alkyl groups, this mechanism cannot operate and decomposition occurs by a free radical mechanism. This type of decomposition requires more energy and can occur only at higher temperatures, as in Figure 2.5 (b).

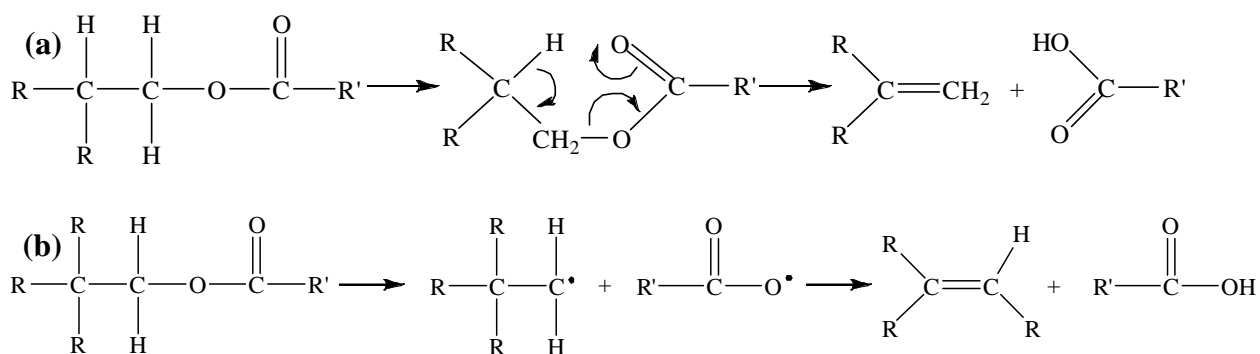
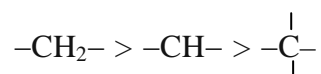


Figure 2.5 Thermal decomposition of (a) esters with β -hydrogens (*e.g.* dibasic acid esters) and (b) esters without β -hydrogens (*e.g.* polyol esters).

Primarily, the oxidative and thermal stabilities of polyol esters are dependent on:

- the absence of hydrogens on β -carbons, as stated above
- the number and type of hydrogens present in decreasing order of stability,



Thus, in general, linear acid esters are more stable than branched, and short-chain acids are more stable than long-chain acids,

- The stability of the alcohol used, which decreased in the following order of stability, PE > diPE > TMP > NPG.

One exception to the rule that branched acid esters give poorer stability than linear acids is the branched C9 acid 3,5,5-trimethylhexanoic acid. The weak tertiary hydrogen is sterically hindered and is more stable than would normally be expected. The structure has fewer secondary hydrogens than the linear form and is hence more stable. Esters made from normal acids generally have higher flash points than those made from branched acids. Increasing molecular weight increases flash points.

Hydrolytic stability; the hydrolytic stability of esters depends on two main features:

- processing parameters
- molecular geometry

If the final processing parameters of esters are not tightly controlled, they dominate a major effect on the hydrolytic stability of the esters, such as the following:

- their acid value – which must be <0.05 mg KOH/g
- the degree of esterification, $>98\%$
- the catalyst used during esterification and the level remaining in the ester after processing, as a low ash level

Molecular geometry effects will assert themselves. Molecular geometry affects hydrolytic stability in several ways. By sterically hindering the acid portion of the molecule, because hindrance on the alcohol portion has relatively little effect, hydrolysis can be slowed down. For this purpose, geminal di- branched acids such as neoheptanoic acids have been used. However, with these feedstocks there are penalties, namely very long reaction times to achieve complete esterification and also poor pour points. The length of the acid chain is also very important, for acids shorter than pentanoic tend not to be used owing to their corrosion. The hydrolytic stability of neopolyol esters can generally be regarded as superior to that of dibasic esters.

Solvency; this can be divided into compatibility with additives and other lubricants, and also elastomer compatibility.

- *Compatibility with additives and other lubricants:* esters are generally fully compatible with mineral oils, which gives them three major advantages. First, there are no contamination problems and therefore esters can be used in machinery that previously used mineral oil. In addition, they can be blended with mineral oil (semi-synthetics) to boost their performance. Second, most additive technology is based on mineral oil experience and this technology is usually directly applicable to esters. Third, esters can be blended with other synthetics such as polyalphaolefins, PAOs, giving them great flexibility, whilst blending with other oils gives unrivalled opportunities to balance the cost of a lubricant blend against its performance.
- *Elastomer compatibility:* elastomers contacting liquid lubricants undergo an interaction with liquid diffusing through the polymer network. There are

two possible kinds of interaction, chemical (rare) and physical. During physical interactions two different, and opposing, processes occur:

- 1) extraction of soluble components out of the elastomer, causing shrinkage.
- 2) adsorption of the lubricant by the elastomer, causing swelling. The degree of swelling of elastomeric materials depends on:
 - the size of the lubricant-the larger the lubricant, the smaller the degree of swelling.
 - the molecular dynamics of the lubricant-linear lubricants diffuse into elastomers quicker than branched or cyclic lubricants.
 - the closeness of the solubility parameters of the lubricant and the elastomer the ‘like-dissolves-like’ rule is followed.
 - the polarity of the lubricant – it is known that some elastomers are sensitive to polar ester lubricants. The non-polarity index can be used to model elastomeric seal swelling trends for specific ester types.

Several polar esters are well-known industrial plasticisers. Non-polar base stocks, such as PAOs, have a tendency to shrink and harden elastomers. By carefully balancing these compounds with esters, lubricants with neutral physical behaviour towards elastomeric materials can be formulated. Table 2.3 shows the compatibility of elastomers and plastics with ester lubricants.

Table 2.3 Guidelines on the compatibility of elastomers and plastics with esters.

Compatible	Not compatible
Viton	PVC
Teflon	Polystyrene and styrene (ABS)
Nylon	SBR Rubber
High nitrile (>33%)	Low nitrile (<33%)
Fluorosilicone	Neoprene
Polysulfide	Ethylene propylene copolymers, natural rubber, BUNA-s

Environmental aspects; increasing environmental awareness has raised water pollution to a major issue. The environment can become polluted in many ways, for example, oils and oil-containing effluents in water can have devastating consequences on fish stocks and other water fauna.

Ecotoxicity; Germany classifies materials according to their potential to pollute water, or ‘Wassergefährdungsklasse’ (WGK) with substances given a ranking of between 0 and 3, where:

WGK 0 Not water endangering

WGK 1 Slightly water endangering

WGK 2 Water endangering

WGK 3 Highly water endangering

The esters generally having the ranking given below showing that esters have a low environmental impact.

Polyols, polyoleates, C36 dimer esters, diesters WGK 0

Phthalates and trimellitates WGK 0–2

Biodegradability; the general biochemistry of microbial attack on esters is well known and has been thoroughly reviewed. The main steps of ester hydrolysis, β -oxidation of long-chain hydrocarbons and oxygenase attack on aromatic nuclei have been extensively investigated. The main structural features which slow or reduce microbial breakdown are the following:

- the position and degree of branching, which reduces β -oxidation
- the degree to which ester hydrolysis is inhibited
- the degree of saturation in the molecule
- increasing of the ester molecular weight

Table 2.4 Overview of physicochemical properties of ester lubricants.

	Diesters	Phthalates	Trimellitates	Polyols	Polyoleates
Viscosity at 40 °C	6-46	29-84	47-366	14-35	8-95
Viscosity at 100 °C	2-8	4-9	7-22	3-6	10-15
Viscosity index	90-170	40-90	60-120	120-130	130-180
Pour point (°C)	-70 to -40	-50 to -30	-55 to -25	-60 to -9	-40 to -5
Flash points	200/260	200/270	270/300	250/310	220/380
Thermal stability	Good	Very good	Very good	Excellent	Fair
Percentage					
biodegradable	75-100	46-88	0-69	90-100	80-100
Costs (PAO =1)	0.9-2.5	0.5-1.0	1.5-2.0	2.0-2.5	0.6-1.5

2.2.4 Application areas [29]

1. *Engine oils*; it is now widely accepted that synthesized fluids, such as polyalphaolefin/ester blends, offer a number of inherent performance advantages over conventional petroleum based oils for the formulation of modern automotive engine oils. Practical benefits which may derive from their use include improved cold starting, better fuel and oil economy, together with improved engine cleanliness, wear protection and viscosity retention during service. Fluid types used in the development of automotive crankcase oils, either commercialized or considered for commercialization, include polyalphaolefins (PAOs) – more correctly hydrogenated olefin oligomers, organic dibasic esters, polyolesters, alkylated aromatic hydrocarbons, and polyglycols. Experience from numerous laboratories of engine bench and vehicle test programs conducted over the last ten years has shown that a blend of PAO and an organic ester provides an excellent base fluid for the formulation of synthesized crankcase oils.

Low temperature viscosity is perhaps the single most important technical feature of a modern crankcase lubricant. Cold starts are a prime cause of engine wear which can be mitigated only by immediately effective lubricant circulation. Furthermore, motor vehicles are increasingly required to operate reliably in arctic conditions. Esters provide this essential low temperature fluidity and, because of their low volatility, do so without any sacrifice of lubricant efficiency at high operating or ambient temperatures. Low volatility is especially important in the context of the modern trend towards smaller sump capacities and longer oil change intervals.

2. *Two-stroke oils*; ester lubricants (such as C₃₆ dimer esters and polyoleates) offer a number of advantages over mineral oils as the lubricant component of two-stroke engine mixtures. First, the clean-burn characteristics result in less engine fouling with much reduced ring stick and lower levels of dirt built-up on ring grooves, skirts and undercrowns. Ignition performance and plug life are also enhanced. Second, due to their polar nature, esters are more efficient lubricants than mineral oils. Mineral oil has oil-fuel dilution ratios of 50:1 whereas esters can be used at 100:1 and even 150:1. This higher dilution factor results in reduced oil emissions which is a benefit in environmentally-sensitive applications such as marine outboard engines and chainsaw motors. Third, in some applications, such as engines used to power snowmobile-type vehicle, low temperature performance is important. In these applications, esters with low pour point (down to -56 °C) are very suitable.

Finally a 25 % decrease in the amount of PAH (polyaromatic hydro- carbons) in the exhaust emission of a two-stroke engine has been found when a carboxylic ester has been used in place of a mineral oil. PAHs have been found to be one of the major contributors to the carcinogenic nature of exhaust emissions. Esters can also be used to reduce the level of smoke emitted by the engine.

3. *Compressor oils*; this sector of the market covers a wide range of compressor types, used for a number of different gases. Diesters and phthalates have found their major application in air compressor lubricants, but are also used in compressors handling natural gas. In reciprocating compressors, where oils of rather higher viscosity are preferred, trimellitate esters can be used. Diesters and polyol esters may also be blended with PAOs for use in the various compressor types.

Diesters have inherently good oxidation resistance and low volatilities (3-10% according to viscosity) when compared to mineral oil. Coupled with their higher flash and auto-ignition temperatures, and low order of toxicity for vapor inhalation, ingestion and skin irritation, these properties make them considerably safer lubricants to use than mineral oil. Their low toxicity and high biodegradability can also lessen their environmental impact. Diesters generally have high viscosity indices, giving them a wide temperature range without the use of viscosity improvers. A further advantage of esters is their good thermal conductivity which allows them to conduct heat away from heat sources more effectively than mineral oils. Specific heat values

of 5-10% higher than mineral oils enable esters to ‘soak up’ heat and allow the compressor to operate at cooler temperatures.

In the past, lubricants produced from naphthenic and paraffinic mineral oils have been used in refrigerator compressor system. These oils were fully compatible with the traditional chlorofluorocarbons refrigerants and fully met system requirements. Because of chemical differences between CFCs and the new alternative refrigerants, tradition mineral oils are not capable of meeting these requirements. The main reason for this is that the hydrofluorocarbons are choosing replace CFCs.

4. *Aviation oil*; the bulk of aviation lubricant demand is for gas turbine lubricants for both military and civilian use. The requirements placed on jet engine oils, namely lubricating, oxidation and ageing stability, cannot be met by hydrocarbon oils. The first generation of oils (Type 1) was diesters but, over the last 25 years, these have slowly lost ground to the more expensive (Type 2) polyol esters. Some diesters are still used in less-demanding applications, *e.g.* for small private aircraft, turbo-prop engines, *etc.* Type 2 aviation gas turbine lubricants are produced to a viscosity of 5 cSt (at 100 °C). For some military applications, where operability at low temperatures is vital, the corresponding viscosity is reduced to 3 cSt.

2.3 Catalysts

A catalyst is a substance that increased the rate of a chemical reaction by reducing the activation energy (E_a) as shown in Figure 2.6. The highest peak position performing the highest energy refers to the transition state. In typically reaction, the energy required to enter the transition state is high, whereas the energy to transition state decreases in catalytic reaction. In addition, the catalyst may participate in multiple chemical transformations and is not consumed by the reaction.

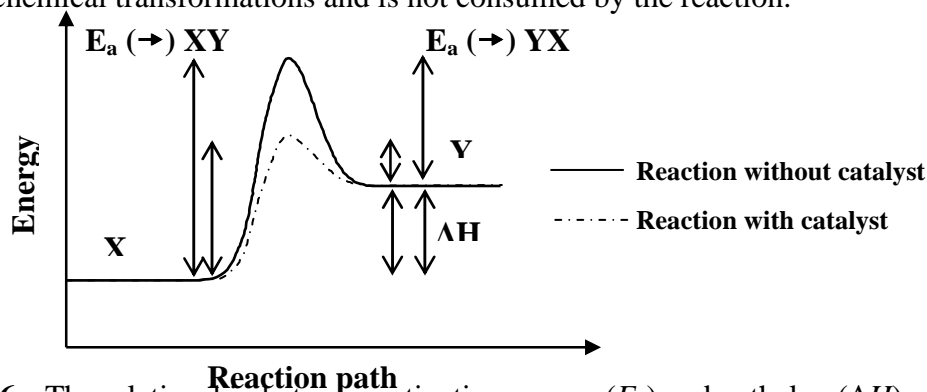


Figure 2.6 The relationship between activation energy (E_a) and enthalpy (ΔH) of the reaction with and without a catalyst [30].

2.4 Properties of industrial catalysts

In general, the suitable catalysts for industrial processes are considered mainly on the three properties [31]:

a) Activity is a measure of how fast one or more reactions proceed which can be defined in terms of kinetics. A high activity catalyst will be given high productivity when the less amount of the catalyst is utilized or the reaction is performed in mild operating condition, particularly temperature, which enhances selectivity and stability if the thermodynamic is more favorable. It is appropriate to measure reaction rates in the temperature that will be occurred in the reactor.

b) Selectivity of a reaction is the fraction of the starting material that is converted to the expected product. High selectivity catalyst produces high yield of a desired product, whereas undesirable competitive and consecutive reactions are suppressed. This means that the texture of the catalyst (in particular pore size and pore volume) should be improved toward reducing limitation by internal diffusion, which in case of consecutive reactions rapidly reduces selectivity.

c) Stability of a catalyst determines its lifetime in industrial processes. Catalyst stability is influenced by various factors such as decomposition, coking and poisoning. Catalyst deactivation can be followed by measuring activity or selectivity as a function of time. Deactivated catalysts can often be regenerated before they ultimately have to be replaced. The catalyst lifetime is a crucial importance for the economics of process.

Nowadays, the efficient use of raw materials and energy is of major importance, and it is preferable to optimize existing processes than to develop new ones. For various reasons, the target quantities should be given the following order of priority:

Selectivity > Stability > Activity

2.5 Type of the catalysts

Catalysts can be classified into two main types by the boundary of the catalyst and the reactant. Heterogeneous reaction, the catalyst is in a different phase from the reactants, whereas the catalyst in the same phase of reactant is called homogeneous reaction. Thus, the solid catalysts are identified as heterogeneous catalysts, and the liquid catalysts are specified as homogeneous catalysts when assume reactant is liquid.

Homogeneous catalyst has a higher degree of dispersion than heterogeneous catalyst only the surface atoms are active [31]. Summary of the advantage and disadvantage of two-type catalyst is presented in Table 2.5.

Table 2.5 Comparison of homogeneous and heterogeneous catalysts.

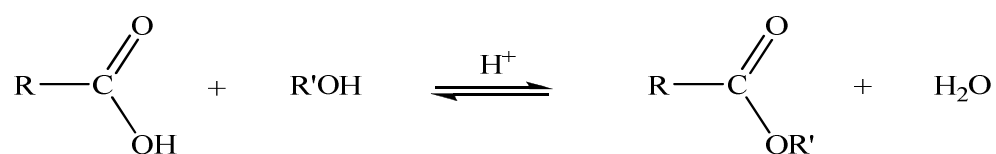
Consideration	Homogeneous catalyst	Heterogeneous catalyst
1. Active centers	All metal atoms	Only surface atoms
2. Concentration	Low	High
3. Selectivity	High	Low
4. Diffusion problems	Practically absent	Present (mass-transfer-controlled reaction)
5. Reaction conditions	Mild (50-200°C)	Severe (often >250°C)
6. Applicability	Limited	Wide
7. Activity loss	Irreversible reaction with product (cluster formation), poisoning	Sintering of the metal crystallites, poisoning
8. Structure/ Stoichiometry	Defined	Undefined
9. Modification possibility	High	Low
10. Thermal stability	Low	High
11. Catalyst separation	Sometimes laborious (chemical decomposition, distillation, extraction)	Fixed-bed: unnecessary Suspension: filtration
12. Catalyst recycling	Possible	Unnecessary (fixed-bed) or easy (suspension)
13. Cost of catalyst losses	High	Low

The major disadvantage of homogeneous catalyst is the difficulty of separating the catalyst from the product. Heterogeneous catalysts are either automatically removed in the process (*e.g.* vapor-phase reaction in fixed bed reactor) or separated by simple methods such as filtration or centrifugation. However, in more complicated

processes, distillation, liquid-liquid extraction and ion exchange are necessarily used in homogeneous catalyst case.

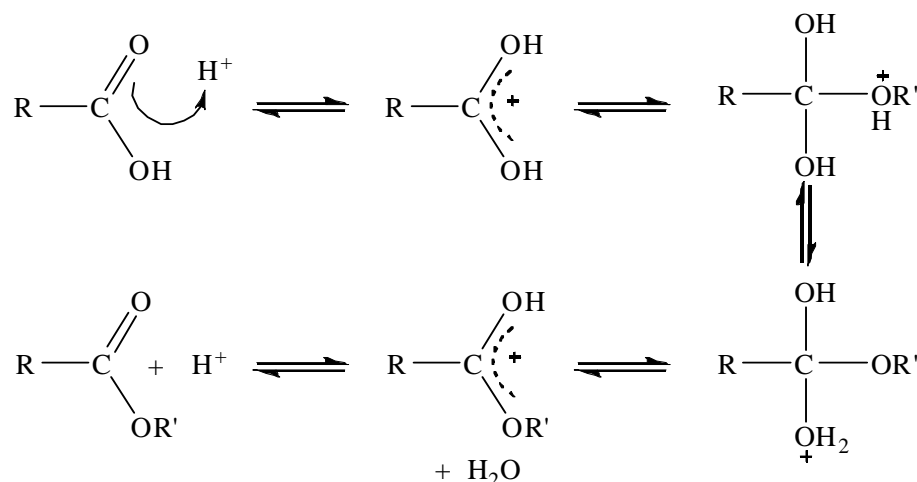
2.6 Acid catalyst for esterification [32]

The most usual method for the preparation of esters is the reaction of carboxylic acid and alcohol with elimination of water. Esterification is a reversible reaction, but is driven to completion by using of excess alcohol and removal of water as it forms by azeotroping agent, *e.g.* toluene.



The uncatalysed reaction is usually too slow to be useful. The acid and alcohol can be reacted thermally, usually in the presence of a catalyst in an esterification reactor. Possible catalysts include sulfuric, *p*-toluene sulfonic acid, tetra alkyl titanate, anhydrous sodium hydrogen sulfate, phosphorous oxides and stannous octanoate.

- Mechanism for reaction for acid catalyzed esterification [33]



Step 1: An acid/base reaction, protonation of the carbonyl makes it more electrophilic

Step 2: The alcohol O functions as the nucleophile attacking the electrophilic C in the C=O, with the electrons moving towards the oxonium ion, creating the tetrahedral intermediate.

Step 3: An acid/base reaction. Deprotonate the alcoholic oxygen.

Step 4: An acid/base reaction. Need to make an OH leave, it doesn't matter which one, so convert it into a good leaving group by protonation.

Step 5: Use the electrons of an adjacent oxygen to help "push out" the leaving group, a neutral water molecule.

Step 6: An acid/base reaction. Deprotonation of the oxonium ion reveals the carbonyl in the ester product.

2.6.1 Brønsted acids

Since acid catalysis is one of the most popular methods for esterification, numerous papers are available. When the substances are acid-resistant, the reaction is usually carried out in the presence of a Brønsted acid such as HCl, HBr, H₂SO₄, NaHSO₄, ClSO₃H, H₃PO₄, *etc.*

In case in which the acidity is not high enough to trigger the desired reaction, the acid is combined with an activator. Other ways to activate the acid catalysts are provided by the use of ultrasound and microwave. H₂SO₄-catalyzed esterification, which usually requires a long reaction time under refluxing conditions, is complete at room temperature in several hours on exposure to ultrasonic waves. Microwave irradiation accelerates the *p*-toluenesulfonic acid-catalyzed esterification, the reaction finishing within 10 min. Aqueous HCl is not employable for water-sensitive compounds. In such cases, dry HCl gas must be used, but generation of this is not operationally simple. Alternatively, generation of HCl under anhydrous conditions is conveniently feasible by addition of acetyl chloride to methanol or ethanol. Treatment of alcohol and carboxylic acid in the HCl solution obtained provides the desired ester. By this method, the concentration of HCl can be readily adjusted by changing the amount of acetyl chloride.

In situ generation of catalytic HCl is accessible photolytically. Photoirradiation of carboxylic acids in methanol containing CBr₄ furnishes the corresponding methyl esters. Interestingly, sp³ carbon-tethered carboxylic acids

undergo esterification smoothly under these conditions, while sp^2 or sp carbon-tethered carboxylic acids are not esterified. Similar photolytic esterification occurs in CCl_4 or $BrCCl_3$ in place of CBr_4 . It has been proposed that HCl generated by abstraction of an α -hydrogen of alcohol by Cl radical is the real catalytic species in this reaction.

Hydrophobic polystyrene-supported sulfonic acids catalyze reaction between carboxylic acid and alcohol in water. The catalysts are recovered and reused for further reactions. The acidity of strong acids is moderated by forming the corresponding ammonium salts. Diphenylammonium triflate is an efficient catalyst for mediation of condensation between alcohol and carboxylic acid in a 1:1 ratio [34]. The reaction usually affords greater than 90 % yields of esters simply on treatment of the reactants with 1 mol% of the catalyst in refluxing toluene. After the reaction is complete, the solvent is evaporated and column chromatography of the residue furnishes the esters. Pentafluorophenylammonium triflate is also a good esterification catalyst. The pentafluorophenyl group causes formation of a hydrophobic environment around the catalytic center, so that dehydration techniques are required. Use of bulky ammonium groups together with arenesulfonyl anion results in highly efficient esterification. Dimesitylammonium pentafluorobenzenesulfonate is one of the most useful catalysts, effecting condensation between carboxylic acid and alcohol in a 1:1 ratio without use of Dean-Stark apparatus.

Polyaniline salts with HCl, HNO_3 , H_2SO_4 , H_3PO_4 , p -tolSO₃H, etc. catalyze reactions between carboxylic acids and alcohols, and can be separated easily from the reaction mixture by filtration. Brønsted acidic ionic liquids function as dual solvents/catalysts for condensation between carboxylic acid and alcohol. Immobilized acidic ionic liquids can be recycled in catalysis for esterification. Acidic ionic liquids can catalyze reactions of carboxylic acids with alcohols in water.

2.6.2 Lewis acids

Lewis acids are another important class of acid catalyst. In general, they are milder than Brønsted acids and, more importantly, template effects are to be expected as they are sterically bulkier than a proton; the utilization of Lewis acids is therefore rapidly increasing. They are classified as follows, according to elements:

B	$\text{BF}_3 \cdot \text{OEt}_2$, BCl_3
Al	AlCl_3 , $\text{AlCl}_3/\text{ZnCl}_2$
Zn	ZnO , $\text{Zn}(\text{ClO}_4)_2 \cdot 6\text{H}_2\text{O}$
Sn	SnCl_2 , Bu_2SnO , Ph_2SnCl_2
Mn	$\text{Mn}(\text{OAc})_2 \cdot 2\text{H}_2\text{O}$
Fe	$\text{Fe}(\text{ClO}_4)_3$, $\text{Fe}_2(\text{SO}_4)_3 \cdot \text{H}_2\text{O}$, FeCl_3
Ni	$\text{NiCl}_2 \cdot 6\text{H}_2\text{O}$, <i>etc.</i>

- $\text{BF}_3 \cdot \text{OEt}_2$ is the oldest Lewis acid to have been employed as an esterification catalyst, since the $\text{BF}_3/\text{CH}_3\text{OH}$ complex had been known to be used for conversion of simple carboxylic acids to their methyl esters prior to GLC analysis.

- BCl_3 is also useful for esterification with primary alcohols, but yields are not so high with secondary and tertiary alcohols. The disadvantage of this method is the cleavage of coexisting methyl ether function. 3,4,5-Trifluorobenzeneboronic acid is claimed to be the most effective catalyst among boronic acids. Esterification takes place smoothly if heavy alcohols such as 1-butanol are employed. The reaction is presumed to proceed via a carboxylate intermediate.

- AlCl_3 is one of the most popular Lewis acids, but it is not employed in esterification because of its too strong acidity. However, polymer-supported AlCl_3 works as a milder catalyst for esterification although the yields are not always as high as those obtained by other methods. The advantage lies in the ease of separation of the catalyst by filtration. The Lewis acidity can be moderated in combination with a soft nucleophile, NaI , in CH_3CN . An equimolar mixture of acid and alcohol is smoothly converted into the desired ester under reflux, but the yield is not high in general (77 % at highest). Phenyl esters, which are otherwise rather difficult to prepare, can be obtained by reaction between aromatic or benzylic carboxylic acids with phenol in the presence of a catalytic amount of AlCl_3 and one equivalent of ZnCl_2 . The strong acidity of AlCl_3 is responsible for efficient esterification, while ZnCl_2 serves for dehydration of the reaction mixture. Treatment of pentaerythritol with oleic acid in the presence of ZnO as catalyst provides a triester. Production of commercially important *p*-hydroxybenzoic acid ester (paraben) from *p*-hydroxybenzaldehyde and alcohol is catalyzed by ZnCl_2 under microwave irradiation conditions. The microwave

irradiation is effective for esterification catalyzed by $\text{Zn}(\text{OTf})_2$. An equimolar mixture of carboxylic acid and alcohol is esterified, but yields are less than 90 %. Smooth esterification is catalyzed by $\text{Zn}(\text{ClO}_4)_2 \cdot 6\text{H}_2\text{O}$ in the presence of MgSO_4 as a dehydrating agent.

Methyl esterification is feasible by heating a MeOH solution of carboxylic acid in the presence of InCl_3 (20 mol%). The reaction proceeds at room temperature under sonication as well.

- Another popular Lewis acid, SnCl_4 , is also not usually employed in esterification, although the milder Lewis acid, SnCl_2 , can catalyze reaction between carboxylic acids and solvent PrOH. Organotin compounds work quite well, however, because the acidity is moderated by the replacement of chlorine with electron-donating alkyl groups.

High-yielding ester synthesis from an equimolar mixture of carboxylic acid and alcohol is accessible by the use of $\text{TiO}(\text{acac})_2$. The catalyst is water-tolerant and neutral to leave various functional groups intact. Alcohols are acetylated by heating at reflux with $\text{Mn}(\text{OAc})_3 \cdot 2\text{H}_2\text{O}$ in acetic acid. Fe (III) salts are also effective. $\text{Fe}(\text{ClO}_4)_3 \cdot 9\text{H}_2\text{O}$ promotes esterification of carboxylic acids in alcohol. The reaction proceeds at room temperature, but a stoichiometric amount of the salt is needed. A catalytic version is available with $\text{Fe}_2(\text{SO}_4)_3 \cdot n\text{H}_2\text{O}$ and FeCl_3 . Addition of a small amount of H_2SO_4 greatly increases the catalytic activity of $\text{Fe}_2(\text{SO}_4)_3 \cdot n\text{H}_2\text{O}$. Moreover, anhydrous $\text{Fe}_2(\text{SO}_4)_3$ is highly active for catalyzing acetylation of alcohols in acetic acid. $\text{FeCl}_3 \cdot 6\text{H}_2\text{O}$ effects esterification of an equimolar mixture of long-chain acids and alcohols in high yields. The reaction requires an excess amount of one reaction component in refluxing benzene or toluene. A similar outcome is obtained with $\text{NiCl}_2 \cdot 6\text{H}_2\text{O}$ catalyst.

- Cupric salts are another class of species that work as catalysts. $\text{CuCl}_2 \cdot n\text{H}_2\text{O}$ catalyzes conversion of carboxylic acids in methanol solvent at 130 °C, while $\text{Cu}(\text{NO}_3)_2 \cdot 3\text{H}_2\text{O}$ effects acetylation of alcohols in refluxing acetic acid. $\text{Cu}(\text{OTf})_2$ is used for acetylation of alcohols but to a somewhat limited extent. Cupric methanesulfonate ($\text{Cu}(\text{OMs})_2$) is also effective. Treatment of carboxylic acid with alcohol (1.1 equiv.) in the presence of 1 mol% of the catalyst in refluxing cyclohexane

affords the desired ester in excellent yield. $\text{MoO}(\text{acac})_2$ also catalyzes transformation of propanoic acid into esters in refluxing alcohols.

- $\text{Sc}(\text{OTf})_3$ can be employed as a catalyst for acylation of high-molecular weight polyethylene glycols. Polycondensation between aliphatic dicarboxylic acids and diols is also achievable with this catalyst to furnish polyesters.

- $\text{HfCl}_4 \cdot 2\text{THF}$ in the presence of 4A molecular sieves enables the use of equimolar amounts of alcohol and carboxylic acid to afford good to excellent yields of the desired esters. This commercially available catalyst is highly active (usually 0.1-0.2 mol% loading) and hydrolytically stable. Polycondensations of ω -hydroxy acids or between dicarboxylic acids and diols to furnish polyesters are also feasible. The selective esterification of primary alcohols in the presence of secondary alcohols or phenol can be achieved with this catalyst. Similar results are obtained with the zirconium analog. Unfortunately, however, these metal chlorides are moisture-sensitive. This drawback is overcome by the use of water-tolerant $\text{ZrOCl}_2 \cdot 8\text{H}_2\text{O}$ and $\text{HfOCl}_2 \cdot 8\text{H}_2\text{O}$. Combination of $\text{Zr}(\text{O}^i\text{Pr})_4$ with $\text{Fe}(\text{O}^i\text{Pr})_3$ exerts a synergistic effect, giving rise to increased catalytic activity as compared to the respective metal alkoxides alone. This combined catalyst is recovered by extraction with ionic liquid, so that recycling of the catalyst is feasible. Another method to recycle the catalyst is immobilization on *N*-(polystyrylbutyl)pyridinium triflylimide. The catalyst can be recycled at least 10 times with this technology. When a carboxylic acid is heated in alcohol with a catalytic amount of iodine, esterification takes place [35]. Primary, secondary, and even tertiary alcohols are employable, although the yields are rather low (56 %) in the last case. The reaction is tolerant of high amounts of water. It is claimed that the iodine works as a Lewis acid.

2.6.3 Solid acids

Various solid acids are utilized for esterification, although the substrates that can be employed suffer from considerable limitations due to the strong acidity. Nevertheless, solid acids have a great advantage in that they can be removed from the reaction mixture by filtration and thus applied to large - scale production.

- Nafion-H is the oldest solid acid to have been utilized as an esterification catalyst. When a mixture of carboxylic acid and alcohol is allowed to

flow over this catalyst at 95-125 °C, high yields of the corresponding esters are obtained with a contact time of 5 s. A batch reaction is also employable.

- Amberlyst 15; α -hydroxy esters and α -amino acids are successfully converted into the corresponding esters with this catalyst.

- Amberlite IR 120; various substrates with hydroxy and related functions, such as sugars, shikimic and quinic acids are esterified with this resin.

- Wolfatit KSP 200; esterification of chiral α -hydroxy carboxylic acids without racemization is feasible by heating in EtOH or MeOH/CHCl₃ in the presence of the ion-exchange resin Wolfatit KSP200. The products are useful intermediates for synthesis of the corresponding α -hydroxy aldehydes.

- Zeolite; the rare earth-exchanged RE H-Y zeolite is the best of the various zeolite catalysts. Heating of alcohol solutions of carboxylic acids in the presence of the freshly activated zeolite at 150°C provides good to excellent yields of esters. Zeolite catalysts for petroleum cracking are employable for synthesis of α -amino acid esters and phenyl benzoates.

- Mesoporous Silica has received extensive attention recently. Al-MCM-41 molecular sieves effect reactions between various acids and alcohols in the vapor phase: acetic acid/amyl alcohol, acetic acid/butyl alcohols, terephthalic acid/methanol, butyric acid/1-pentanol, etc. Microporous titanosilicate ETS-10 molecular sieves are also effective for esterification of long-chain carboxylic acids with alcohols. Sulfonic acid-functionalized mesoporous silicas are utilized for esterification of fatty acids with methanol and glycerol. Mesoporous MCM-41 and SBA-15 functionalized with perfluoroalkanesulfonic acid are more active for esterification of long-chain fatty acids with alcohols than Nafion/silica composite. Comparison of commercial solid acid catalysts is now available in some reports.

- Modification of silica and alumina; treatment of silica or alumina with ClSO₃H results in immobilization of sulfuric acid on the surface of silica or alumina, which catalyzes esterification of aryloxyacetic acid or aromatic carboxylic acid. Silica chloride obtained from silica and thionyl chloride effects esterification of amino acids. Sulfate-, phosphate-, and borate-modified silica, alumina and zirconia furnish benzyl acetate from acetic acid and benzyl alcohol concomitant with only a small amount of dibenzyl ether.

- $\text{Nb}_2\text{O}_5 \cdot n\text{H}_2\text{O}$; this catalyst is claimed to be more active than cation-exchange resin, $\text{SiO}_2 \cdot \text{AlO}_3$, and solid super acids. Interestingly, supermicroporous niobium oxide, synthesized using a nonionic block copolymer as a structural directing reagent, is employable for gas-phase esterification of acetic acid with ethanol.

- $\text{ZrO}_2 \cdot n\text{H}_2\text{O}$ and Mo-ZrO_2 ; hydrous ZrO_2 , which catalyzes reactions between carboxylic acids and alcohols, exhibits the following advantages: (i) the catalyst is easily prepared and stable in air and (ii) the reaction does not require water-free conditions. The catalytic activity is further improved by use of Mo-ZrO_2 mixed oxide, because electron-deficient sites are formed by introduction of Mo cations into the lattice of the solid ZrO_2 .

- Strongly Acidic Carbon Materials; Graphite bisulfate, which can be prepared by electrolysis of 98 % H_2SO_4 with a graphite anode, brings about reaction between alcohol and carboxylic acid in a 1:1 ratio at room temperature. The yields are usually over 90 %. Sulfonation of incompletely carbonized D-glucose results in amorphous carbon consisting of small polycyclic carbon sheets with high density of SO_3H groups [36]. This carbon material exhibits remarkable catalytic performance for esterification of higher fatty acids. Poly(vinyl alcohol) membranes crosslinked with sulfosuccinic acid catalyze esterification of acetic acid with isoamyl alcohol.

- Natural Montmorillonite; another intercalation compound, natural montmorillonite, is useful for selective acylation of various functionalized primary and secondary alcohols.

- Metal-Exchanged Montmorillonite and Bentonite; montmorillonites enwrapped with various metal cations such as Na^+ , Al^{3+} , Fe^{3+} , Cr^{3+} , Zn^{2+} , Mn^{2+} , Ni^{2+} , Ti^{4+} are active catalysts for esterification. Acid-activated bentonite catalyzes reactions between various carboxylic acids and alcohols.

- Phosphorus oxides; phosphorus pentoxide can be used for dehydration between carboxylic acid and alcohol. Heating a mixture of alcohol, carboxylic acid, and P_4O_{10} is the simplest treatment. In addition to intermolecular esterification, lactonization is also achievable. This procedure is modified by initial treatment of P_4O_{10} with alcohol to furnish an equimolar mixture of mono- and dialkylphosphates.

- Inorganic Sn- or Ti- Based Solid Acids; amorphous M (IV) tungstates (M = Sn, Ti) are useful for synthesis of dioctyl phthalate. Methyl ester synthesis from

octanoic acid is feasible with a ceramic acid obtained by impregnating $\text{SnO}_2 \cdot \text{H}_2\text{O}$ and $(\text{NH}_4)_6(\text{H}_2\text{W}_{12}\text{O}_{40})$ followed by calcination. Solid superacid of sulfated tin oxide, $\text{SO}_4^{2-}/\text{SnO}_2$, is a highly active catalyst for condensation between acids and alcohols. Similarly, titanium superacid, $\text{SO}_4^{2-}/\text{SnO}_2$, is capable of esterifying chemically labile mandelic acid.

- Heteropolyacids; various bromoacetates are obtained by treatment of bromoacetic acids with alcohols in the presence of 12-tungstophosphoric acid, $\text{H}_3\text{PO}_4\text{W}_{12} \cdot \text{H}_2\text{O}$. Its partially substituted Cs and K salts are also useful catalysts for esterification. The corresponding ammonium salt catalyzes selective reactions between aliphatic carboxylic acids and alcohols in the presence of aromatic carboxylic acids. $\text{H}_{14}[\text{NaP}_5\text{W}_{30}\text{O}_{110}]$ can be employed for esterification of salicylic acid with aliphatic and benzylic alcohols. Cobalt-containing polyoxometalate, $\text{K}_5\text{CoW}_{12}\text{O}_{40} \cdot 3\text{H}_2\text{O}$, is suitable for esterification of mandelic acid.

- Acid Catalysts on Inorganic Solid Support; heteropoly acids often leak out of catalyst supports, because these acids are extraordinary soluble in water and several organic solvents. $\text{H}_3\text{PW}_{12}\text{O}_{40}$ can be immobilized onto hydrous zirconia, which catalyzes reactions between glacial acetic acid and cyclohexanol and between acetic acid and isoamyl alcohol. $\text{H}_4\text{SiW}_{12}\text{O}_{40}$ on hydrous zirconia brings about esterification of primary and secondary alcohols with C1-C3 carboxylic acids. Zirconia is also employable to support WO_3 , which catalyzes esterification of palmitic acid with methanol. Porous zirconium phosphate is also employable to support WO_3 . Silica gel is employable for supporting various acid catalysts: P_2O_5 ; $\text{H}_3\text{PMO}_{12}\text{O}_{40}$; $\text{H}_3\text{PW}_{12}\text{O}_{40}$. All of these supported catalysts are effective for esterification. Grinding $\text{Fe}(\text{ClO}_4)_3(\text{ROH})_6/\text{SiO}_2$ with an equimolar amount of carboxylic acid provides esters. This protocol is operationally simple, but requires a stoichiometric amount of the promoter. Aliphatic carboxylic acids are esterified preferentially over aromatic ones at room temperature with the aid of NaHSO_4 supported on silica gel. $\text{Hf}[\text{N}(\text{SO}_2\text{C}_8\text{F}_{17})_4]$ supported on fluorosulfonated silica gel efficiently catalyzes esterification of methacrylic acid with methanol. Supporting $\text{ZrOCl}_2 \cdot 8\text{H}_2\text{O}$ on mesoporous silica MCM-41 enhances the catalytic activity for esterification of C10-C18 normal acid with alcohols. 12-Phosphotungstic acid and its cesium salts supported on a dealuminated Y zeolite catalyze reaction between 1-butanol and acetic acid in high

yield. $\text{H}_3\text{PW}_{12}\text{O}_{40}$ can be supported on neutral alumina, catalyzing esterification of aliphatic carboxylic acids with primary and secondary alcohols. Activated carbon can tightly immobilize or entrap a certain amount of the acids. With $\text{H}_4\text{SiW}_{12}\text{O}_{40}$ entrapped in carbon, vapor-phase esterification of acetic acid with ethanol can be conducted efficiently. Zirconium sulfate supported on activated carbon exhibits higher activity for esterification of oleic acid with 1-butanol. Acid Catalysts on Organic Solid Support; heteropolyacids supported on ion-exchange resin accelerate the rates of reaction between lactic acid and ethanol. Polyaniline-supported acid catalysts are effective for esterification of carboxylic acids with alcohols. Triphenylphosphine ditriflate anchored onto cross-linked polystyrene is useful for ester synthesis from functionally substituted carboxylic acids and alcohols.

2.7 Porous molecular sieves

Molecular sieves are porous materials that exhibit selective adsorption properties which can be classified on the IUPAC definitions into three main types depending on their pore sizes that are microporous materials, mesoporous materials, and macroporous materials. Properties and examples of these materials are shown in Table 2.6.

Table 2.6 IUPAC classification of porous materials.

Type of porous molecular sieve	Pore size (Å)	Examples
Microporous materials	< 20	Zeolites, Activated carbon
Mesoporous materials	20 – 500	M41s, SBA-15, Pillared clays
Macroporous materials	> 500	Glasses

2.8 Mesoporous materials

Mesoporous materials are a type of molecular sieves, such as silicas or transitional aluminas or modified layered materials such as pillared clays and silicates. Mesoporous silica has uniform pore sizes from 20 to 500 Å and has found great utility as catalysts and sorption media because of the regular arrays of uniform channels. Larger surface area is desired for enhancing of the efficient in the reactions [37].

2.8.1 Classification of mesoporous materials

Mesoporous materials can be classified by different synthetic methods. By varying different types of templates used and pH of gel, synthesizing hexagonal mesoporous materials can be obtained. The interaction of various types of template with inorganic species for assembling these materials are different as summarized in Table 2.7, together with the condition typically employed for a synthesis [37-39].

Table 2.7 Various synthesis conditions of hexagonal mesoporous materials and the types of interaction between templates and inorganic species.

Materials	Template	Assembly	Solution
MCM-41	Quaternary ammonium salt	Electrostatic	base or acid
FSM-16	Quaternary ammonium salt	Electrostatic	base
SBA-15	Amphiphilic triblock copolymer	H- bonding	acid (pH<2)
HMS	Primary amine	H- bonding	neutral

MCM-41 and FSM-16 can be synthesized using quaternary ammonium salt as a template. In case of SBA-15, amphiphilic triblock copolymer can be modified as a template and must be synthesized in acidic condition of hydrochloric acid. On the other hand, HMS can be prepared in neutral and environmentally benign condition using primary amine as a template. Although these materials have the same hexagonal structure, some properties are different as shown in Table 2.8.

Table 2.8 Properties of some hexagonal mesoporous materials.

Material	Pore size (Å)	Wall thickness (nm)	BET specific surface area (m ² /g)	Framework structure
MCM-41	15-100	1	>1000	Honey comb
FSM-16	15-32	-	680-1000	Folded sheet
SBA-15	46-300	3-6	630-1000	Rope-like
HMS	29-41	1-2	640-1000	Wormhole

2.8.2 Synthesis schemes of mesoporous materials

Crystalline molecular sieves are generally obtained by hydrothermal crystallization. The reaction gel, usually, contains cations (*e.g.* Si^{4+} for silicate materials, Al^{3+} for aluminate materials) to form the framework; anionic species (*e.g.* OH^- and F^-); organic template and solvent (generally water). Typically, the nature of template can be considered into two parts that are hydrophobic tail on the alkyl chain side and hydrophilic head on the other side. The examples of templates used are primary, secondary tertiary and quaternary amines, alcohols, crown or linear ethers, and as well as polymers. An understanding of how organic molecules interact with each other and with the inorganic frameworks would increase the ability to design rational routes to molecular sieve materials. The organic templates are frequently occluded in the pores of the synthesized material, contributing to the stability of mineral backbone.

2.8.2.1 The behavior of surfactant molecules in an aqueous solution

In a simple binary system of water-surfactant, surfactant molecules can aggregate to form micelles in various types at a particular concentration. The shapes of micelle depend on the concentrations as shown in Figure 2.7.

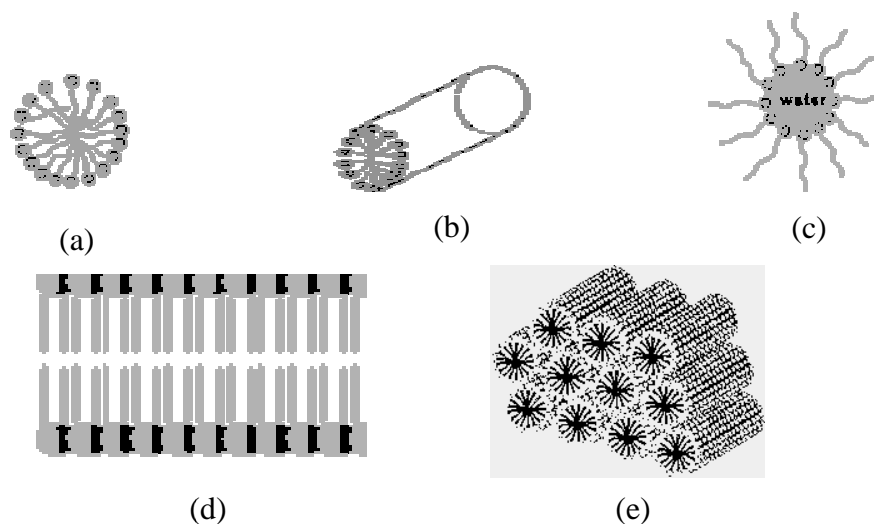


Figure 2.7 Phase sequence of the surfactant-water binary system (a) spherical micelle, (b) rod-shaped micelle, (c) reverse micelle, (d) lamellar phase, and (e) hexagonal phase [40].

At low concentration, they energetically exist as isolated molecules. With increasing concentration, surfactant molecules aggregate together to form isotropic spherical and rod shaped micelles by directing the hydrophobic tails inside and turning the hydrophilic heads outside in order to decrease the system entropy. The initial concentration threshold at which those molecules aggregate to form isotropic micelle is called critical micelle concentration (CMC). The CMC determines thermodynamic stability of the micelles. When the concentration is continuously increased, the micellar shape changes from sphere or rod shapes to hexagonal, lamellar, and inverse micelles. The particular phase present in a surfactant aqueous solution depends not only on the concentrations but also on the nature of surfactant molecules such as its length of the hydrophobic carbon chain, hydrophilic head group, and counter ion. Besides the ionic strength, pH value, and temperature including other additives are the factors determining the shape of micelles.

2.8.2.2 Interaction between inorganic species and surfactant micelles

A number of models have been proposed to explain the formation of mesoporous materials and to provide a rational basis for synthesis routes [40]. On the common level, these models are predicted upon the presence of surfactants in a solution to direct the formation of inorganic mesostructure from stabilized inorganic precursors. The type of interaction between the surfactant and the inorganic species is significantly different depending on the various synthesis routes as shown in Table 2.9

Table 2.9 Example routes for interactions between the surfactant and the inorganic soluble species.

Surfactant type	Inorganic type	Interaction type	Example materials
Cationic (S^+)	I^-	S^+I^-	MCM-41, MCM-48
	I^+X^-	S^+XI^+	SBA-1, SBA-2, zinc phosphate
	I^0F^-	S^+FI^0	silica
Anionic (S^-)	I^+	S^-I^+	Al, Mg, Mn, Ga
	IM^+	$S^-M^+I^-$	alumina, zinc oxide
Neutral S^0 or N^0	I^0	S^0I^0 or N^0I^0	HMS, MSU-X, aluminum oxide
	I^+X^-	S^0XI^+	SBA-15

Where S^x or N^x : surfactant with charge of X

I^x : inorganic species with charge of X

X^- : halogenide anions

F^- : fluoride anion

M^{n+} : with charge of X

Using ionic surfactant (S^+ and S^-), the hydrophilic head mainly binds with inorganic species through electrostatic interactions. There are two possible formation routes. Firstly, direct pathway: surfactant and inorganic species of which charges are opposite interact together directly (S^+I^- and S^-I^+). Another is the indirect pathway, occurring when the charges of surfactant and inorganic species are the same, so the counter ions in solution get involved as charge compensating species for example the S^+XI^+ path takes place under acidic conditions, in the presence of halogenide anions ($X^- = Cl^-$ or Br^-) and the $S^-M^+I^-$ route is characteristic of basic media, in the existence of alkaline cation ($M^+ = Na^+$ or K^+). Figure 2.8 shows the possible hybrid inorganic-organic interfaces.

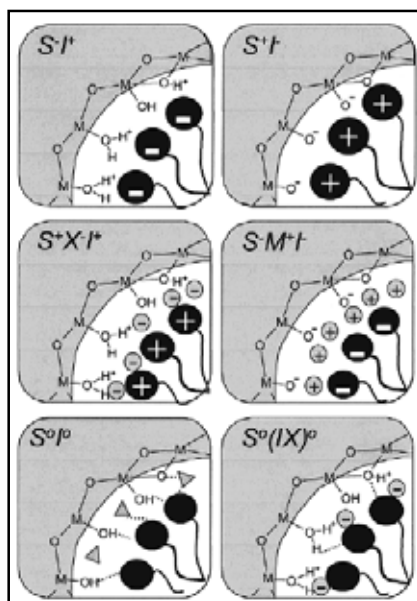


Figure 2.8 Schematic representation of the different types of silica-surfactant interfaces. Dashed line corresponded to H-bonding interactions [40].

In case of non-ionic surfactant (S^0 or N^0), the main interaction between template and inorganic species is hydrogen bonding or dipolar, which is called neutral path i.e. S^0I^0 and S^0FI^+ . Nowadays, non-ionic surfactants give important commercial advantages in comparison to ionic surfactants because they are easily removable, nontoxic, biodegradable and relatively cheap.

2.8.2.3 Formation mechanism of mesoporous materials

Mechanism of mesoporous formation can be classified on the basis of synthetic route into three types exhibited in Figure 2.9:

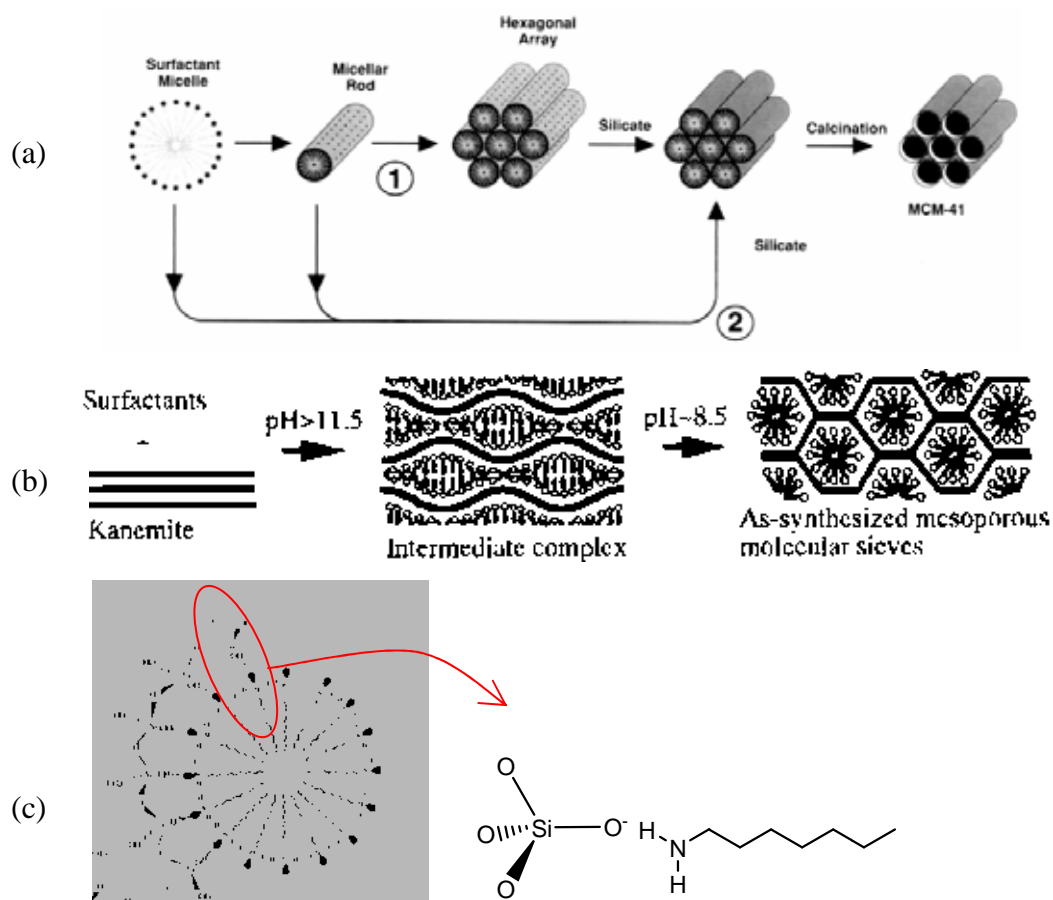


Figure 2.9 Mechanism of mesoporous formation (a) LCT of MCM-41 formation, (b) Folding sheet formation of FSM-16 and (c) H-bonding interaction in HMS formation [41-42].

(a) *Liquid crystal Templating mechanism: i.e.* MCM-41. From Figure 2.12(a) there are two main pathways; firstly, liquid crystal phase is intact before silicate species are added or another pathway is the addition of the silicate results in the ordering of the subsequent silicate-encased surfactant micelles.

(b) *Folding sheet formation: i.e.* FSM-16. The intercalation of ammonium surfactant into hydrate sodium silicate, which composes of single layered silica sheets called “kanemite” (ideal composition $\text{NaHSi}_2\text{O}_5 \cdot 3\text{H}_2\text{O}$), produces the lamellar-to-hexagonal phase in FSM-16. After the surfactants are ion exchanged into layered structure, the silicate sheets are thought to fold around the surfactants and condense into a hexagonal structure.

(c) *Hydrogen-bonding interaction*: The neutral templating produces mesoporous materials with thicker walls and higher thermal stability as compared to the LCT-derived silicates.

2.8.3 Synthesis strategy of mesoporous material using block-copolymer as structure directing agent

In the synthesis of mesoporous materials such as MCM-41, FSM-16 ionic surfactant *i.e.* the cationic, alkyltrimethyl ammonium (C_nTA^+ , $8 < n < 18$), and anionic surfactant, tertiary amine ($C_nH_{2n+1}N^+(CH_3)_3$) are used as template, respectively. These syntheses are done in extreme (alkaline) pH condition and the obtained materials have pore size in the range of 15 to 100 Å only. However, by this mean, two limitations occur:

- (1) The lower stability of the obtained materials: due to the thinner pore wall of materials (8-13 Å).
- (2) Difficult to expanding the pore size: the ionic surfactants give a limited pore size. The only way to expand the pore size is in employing swelling agents such as 1,3,5-trimethyl benzene, involving complicate synthesis.

Thus, the block copolymer has been used to solve these problems. Generally, amphiphilic block copolymer has been used in the field of surfactants, detergent manufacturing, emulsifying, coating, *etc.* The properties of block copolymer can be continuously tuned by adjusting solvent composition, molecular weight, or type of polymers. Figure 2.10 shows typical block copolymer used as templates.

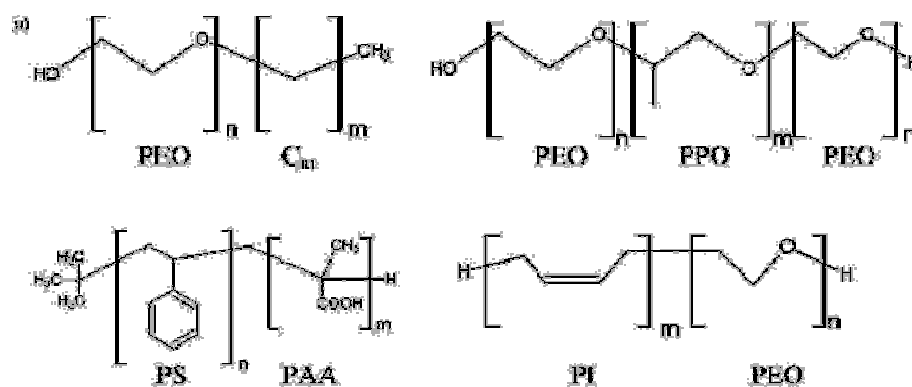


Figure 2.10 Block copolymer used in mesostructured generation [43].

Some advantages of using these block copolymer are:

- (1) *The thicker wall thickness* (about 15-40 Å), enhancing hydrothermal and thermal stability of materials.
- (2) *Pore diameter can be tuned easier* by varying type or concentration of polymer.
- (3) *Easier to remove from mineral framework* by thermal treatment or solvent extraction. Due to the hydrogen bonding interaction between template and inorganic framework, therefore, it should be easier to dissociate as compared to ionic templates (electrostatic interaction).

Interaction between block copolymer template and inorganic species, calls hybrid interphase (HI), is particularly important, especially in PEO-PPO based one. Different possible interactions take place at the HI are schematized in Figure 2.11. Most of the fine HI characterization has been performed on PEO-based (di or triblock) templates. Melosh *et al.* [44] determined that in F127-templated silica monoliths, organization arose for polymer weight fractions higher than 40%. For lower polymericsilica ratios, non-ordered gels were formed. This lack of order was due to a relatively strong interaction (probably of H-bonding type) of the (Si—O—Si) polymers forming the inorganic skeleton with both PEO and PPO blocks.

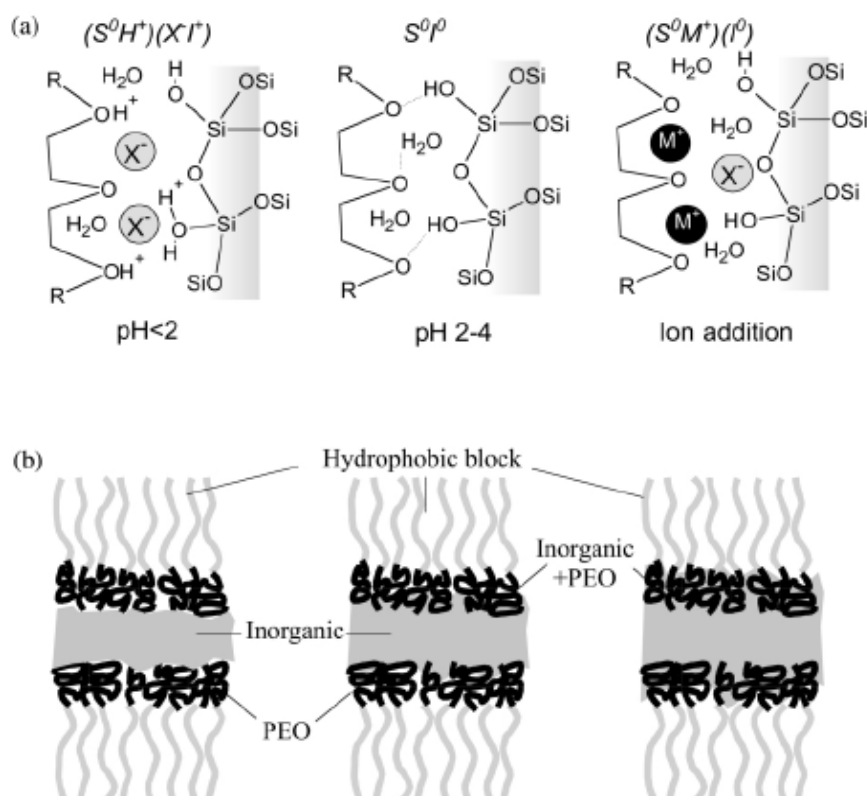


Figure 2.11 (a) Schematic view of the $(S^0H^+)(X^-)$, S^0I^0 , and $(S^0M^+)(I^0)$ hybrid interphases (HIs) (b) Three possible structures of a HI composed by a nonionic polymer and an inorganic framework [44].

2.9 SBA-15

2.9.1 Structure and properties of SBA-15

SBA-15 mesoporous material has been synthesized under acidic condition using triblock copolymer as a structure directing agent. This mesoporous material has shown higher hydrothermal stability as compared to MCM-41 due to its thicker pore walls (3.1-6.4 nm). They also possess uniform and hexagonal-structured channels similar to MCM-41 with larger pore size which makes them more desirable to deal with bulky molecules. Some properties of MCM-41 and SBA-15 are compared as described in Table 2.10. According to the properties listed in Table 2.10, SBA-15 shows a better performance than MCM-41 in almost all properties.

Table 2.10 Comparison of two well-known mesoporous materials, MCM-41 and SBA-15 in their characteristic properties [11,41].

Properties	MCM-41	SBA-15
Pore size (Å)	20-100	46-300
Pore volume (mL/g)	>0.7	0.8-1.23
Surface area (m ² /g)	>1000	690-1040
Wall thickness (Å)	10-15	31-64

2.9.2 Synthesis of SBA-15 and formation mechanism

For SBA-15 materials, aging time and temperature are particularly important. Some research found that mesoporous SBA-15 prepared from calcination of an ‘as-prepared’ hybrid precursor contained a significant fraction of microporosity; further aging of the precursor in the mother liquors leads to an improvement on the pore size distribution (Figure 2.12), in agreement with the first work by Stucky *et al.* [11].

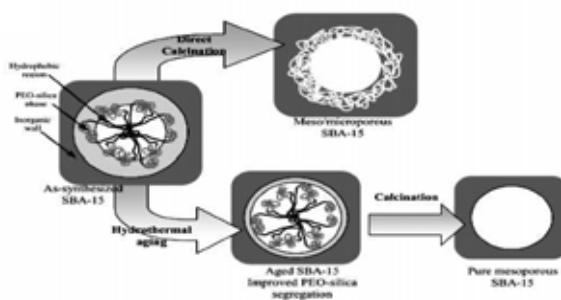
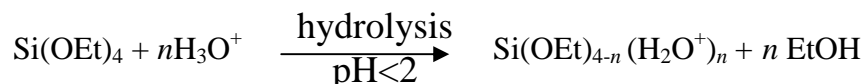


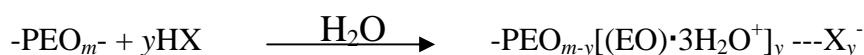
Figure 2.12 Pore evolution upon thermal treatment, depending on pre-treatment and aging [43].

Aging of an as-prepared precipitate at 80–100°C seems to help segregation of the PEO blocks and the inorganic framework, by promoting condensation of the latter. High temperatures also change the polymer behavior. It is known that for $T > 60^\circ\text{C}$, PEO blocks become less hydrophilic and expel water similar to PPO blocks when the

temperature is higher than 40°C [30]. For a mechanism, firstly alkoxysilane species (TMOS or TEOS) are hydrolyzed as:



This is followed by partial oligomerization at the silica. Furthermore, at this condition, the PEO parts of surfactant associate with hydronium ions as followed:



Next, coordination sphere expansion around the silicon atom by anion coordination of the form X^-SiO_2^+ may play an important role. The hydrophilic PEO blocks are expected to interact with the protonated silica and thus be closely associated with the inorganic wall. During the hydrolysis and condensation of the silica species, intermediate mesophase is sometimes observed and further condensation of silica species and organization of the surfactant and inorganic species result in the formation of the lowest energy silica-surfactant mesophase structure allowed by solidifying network.

2.10 FSM-16

2.10.1 Structure and properties of FSM-16

FSM-16 mesoporous material has been synthesized using surfactant from kanemite as a silicon source. This mesoporous material has an ordered one-dimensional large pore system similar to the mesoporous silicate MCM-41 [45]. They have shown slight higher hydrothermal stability as compared to MCM-41 due to its thicker pore walls about 20 nm. Some properties of MCM-41 and FSM-16 are compared as described in Table 2.11.

Table 2.11 Comparison of two well-known mesoporous materials, MCM-41 and FSM-16 in their characteristic properties [41,46].

Properties	MCM-41	FSM-16
Pore size (Å)	20-100	15-32
Pore volume (mL/g)	>0.7	~0.78
Surface area (m ² /g)	>1000	770-1050
Wall thickness (Å)	10-15	> 20

2.10.2 Synthesis of FSM-16 and formation mechanism

The formation mechanism of the mesoporous material FSM-16 derived from SiO₄ tetrahedral in the single silicate layers of kanemite. When kanemite is allowed to react with alkyl-trimethylammonium ions, the surfactant molecules are intercalated between the kanemite sheet, after which the adjacent silicate layers meet together in a periodic way and condense to form a three-dimensional highly ordered mesoporous material. The structure of FSM-16 with surfactant is shown along the pore direction in Figure 2.13.

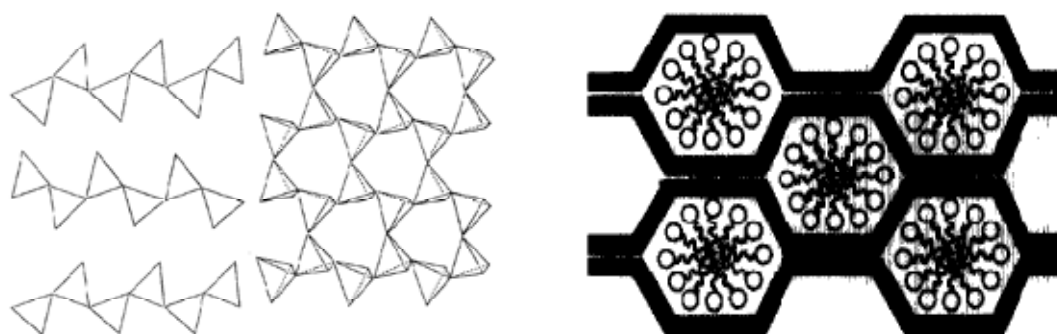


Figure 2.13 formation mechanism of (a) silicate structure of disilicate (H₂Si₂O₅) and (b) structure of FSM-16 with surfactant [45,46].

2.11 Step in a heterogeneous catalytic reaction [47]

In heterogeneous catalysis, the catalytic action involves the adsorption of reactant molecules on active sites on the surface of the solid catalysts; therefore, the transport of those molecules from the fluid phase to the surface, where the catalytic reaction effectively occurs, must be considered in the general mechanism. Similarly, the molecules of the reaction products are eventually desorbed and transferred in the opposite direction from inside the solid pores to the fluid phase.

Hougen and Watson and others have broken down the steps that occur on a molecular scale in the following manner.

1. Mass transfer of reactants from the main body of the fluid to the gross exterior surface of the catalyst particle.
2. Molecular diffusion and/or Knudsen flow of reactants from the exterior surface of the catalyst particle into the interior pore structure.
3. Chemisorptions of at least one of the reactants on the catalyst surface.
4. Reaction on the surface.
5. Desorption of (chemically) adsorbed species from the surface of the catalyst.
6. Transfer of products from the interior catalyst pores to the gross external surface of the catalyst by ordinary molecular diffusion and/or Knudsen diffusion.
7. Mass transfer of products from the exterior surface of the particle into the bulk of the fluid.

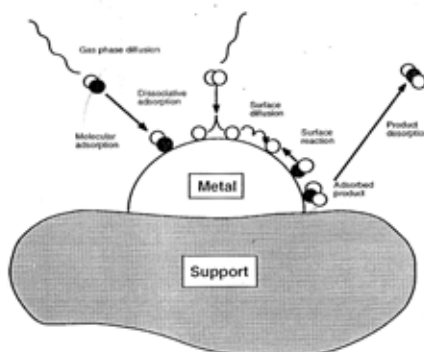


Figure 2.14 Steps in heterogenous catalysis [48].

Several of these steps are shown in Figure 2.13. Of course, if the catalyst is nonporous, steps 2 and 6 are absent. Steps 1, 2, 6, and 7 are obviously physical processes, while steps 3 to 5 are basically chemical in character. The rates of the various steps depend on a number of factors in addition to the concentration profiles of the reactant and product species.

Steps 1 and 7 are highly dependent on the fluid flow characteristics of the system. The mass velocity of the fluid stream, the particle size, and the diffusional characteristics of the various molecular species are the pertinent parameters on which the rates of these steps depend. These steps limit the observed rate only when the catalytic reaction is very rapid and the mass transfer is slow. Anything that tends to increase mass transfer coefficients will enhance the rates of these processes. Since the rate of these steps is only slightly influenced by temperature, the influence of these processes on the overall conversion rate will vary as the temperature changes. Their influence is often negligible at low temperatures, but may be quite significant at higher temperatures.

2.12 Modification of catalysts

Nowadays, the attachment of organic functionalities such as sulfonic acid groups to the surface of siliceous SBA-15 mesoporous material is an interesting research area in heterogeneous catalysis and green chemistry. Basically, two strategies have been generally used to anchor organic groups onto a mesostructured silica surface.

2.12.1 Direct synthesis

Direct synthesis consists of the co-condensation of siloxane and organosiloxane precursors in the presence of the corresponding structure-directing agent.

The preparation of sulfonic-acid modified mesostructured materials is illustrated in Figure 2.15. This method is simplicity, because the incorporation of the organic precursor and the formation of the mesoporous material occur in a single synthetic step. To have a useful catalyst after synthesis, one must be able to extract the template from within the pores to create porosity. Calcination the synthetic

material will destroy the incorporated organic functional groups. Extraction technique can be most effectively accomplished by ethanol solution [49-51].

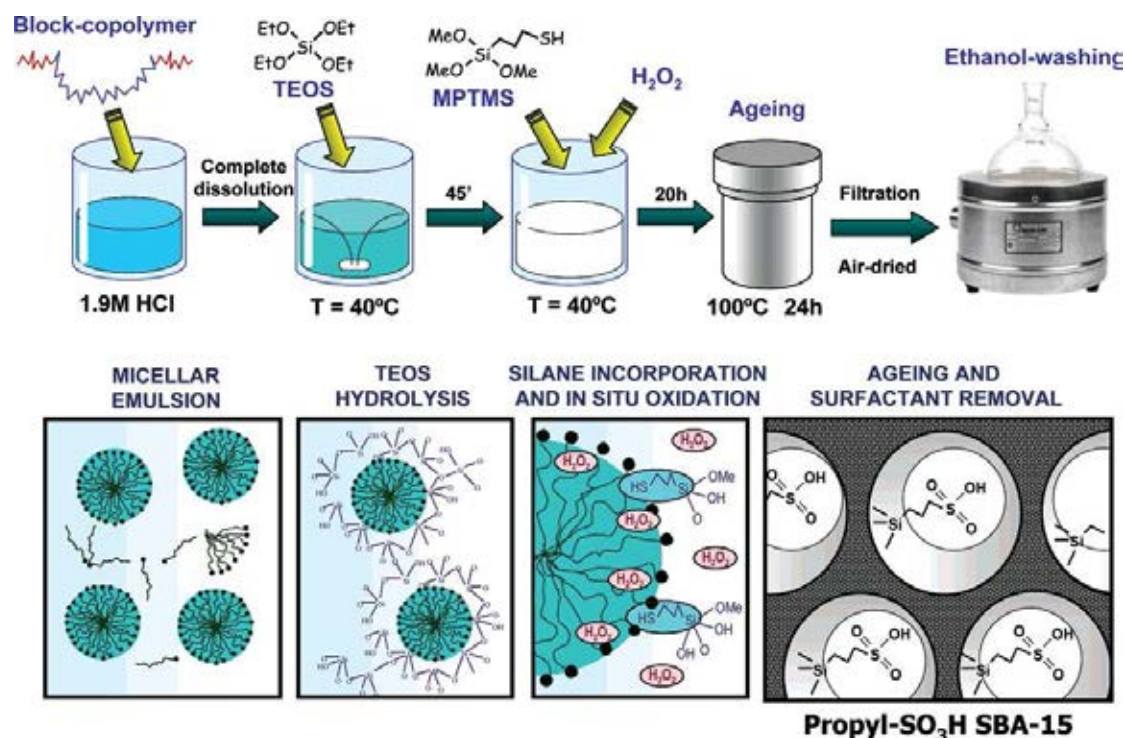


Figure 2.15 In-situ oxidation synthesis strategy for the preparation of sulfonic-acid-modified mesostructured materials [50].

2.12.2 Post synthesis (Grafting method)

Grafting procedure based on modification of the silica surface with organic groups through silylation reaction occurring on isolated ($\equiv\text{Si-OH}$) and germinal ($=\text{Si}(\text{OH})_2$) silanol groups using trichloro- or trialkoxyorganosilane and silylamines as organic precursors [50].

Synthesis of sulfonic functionalized SBA-15 by post synthesis is shown in Figure 2.16. In typical procedure, calcined SBA-15 is treated with a silating agent like 3-mercaptopropyltrimethoxysilane (MPTMS) in nonpolar solvent (commonly toluene) to immobilize thiol groups on the surface. These thiol functionalities are then oxidized, normally using hydrogen peroxide. The most apparent advantage of this procedure is good preservation of the mesostructure after post-modification.

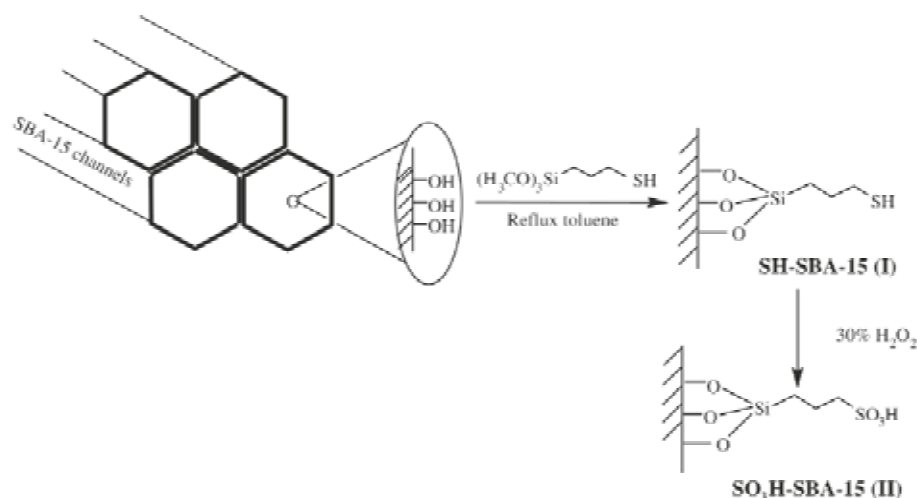


Figure 2.16 Post synthesis procedure for the preparation of sulfonic-acid-modified mesostructured materials [52].

2.13 Characterization of materials

2.13.1 X-ray powder diffraction (XRD)

X-ray powder diffraction (XRD) is an instrumental technique used for identification of minerals, as well as other crystalline materials. XRD is a technique in which a collimated beams of nearly monochromatic. X-rays is directed onto the flat surface of a relatively thin layer of finely ground material. XRD can provide additional information beyond basic identification. If the sample is a mixture, XRD data can be analyzed to determine the proportion of the different minerals present. Other obtained information can include the degree of crystallinity of the minerals present, possible deviations of the minerals from their ideal compositions, the structural state of the minerals and the degree of hydration for minerals that contain water in their structure.

XRD is a reliable technique that can be used to identify mesoporous structure. Typically, the XRD pattern of hexagonal symmetry shows five well-resolved peaks corresponding to lattice planes of Miller indices (100), (110), (200), (210), and (300) [40]. These XRD peaks appear at low angle (2θ angle between 0.5 and 3 degree) because the materials are not crystalline at atomic level, diffraction at higher angles are not observed.

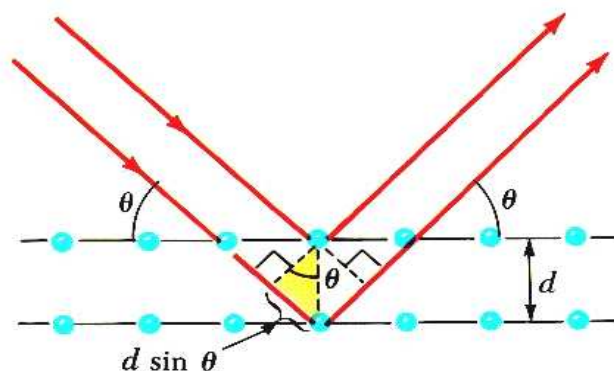


Figure 2.17 Diffraction of X-ray by regular planes of atoms [53].

Figure 2.17 shows a monochromatic beam of X-ray incident on the surface of crystal at an angle θ . The scattered intensity can be measured as a function of scattering angle 2θ . The resulting XRD pattern efficiently determines the different phases present in the sample. Using this method, Bragg's law is able to determine the interplanar spacing of the samples, from diffraction peak according to Bragg's angle.

$$n\lambda = 2d \sin\theta$$

Where the integer n is the order of the diffracted beam, λ is the wavelength; d is the distance between adjacent planes of the crystal (the d -spacings) and θ is the angle between the incident beam and these planes.

2.13.2 Nitrogen adsorption-desorption technique

The N_2 adsorption-desorption technique is used to classify the porous materials and its physical properties such as surface area, pore volume, pore diameter and pore-size distribution of solid catalysts. Adsorption of gas by a porous material is described by an adsorption isotherm, the amount of adsorbed gas by the material at a fixed temperature as a function of pressure. Porous materials are frequently characterized in terms of pore sizes derived from gas sorption data [54-55]. The IUPAC classification of adsorption isotherms is illustrated in Figure 2.18.

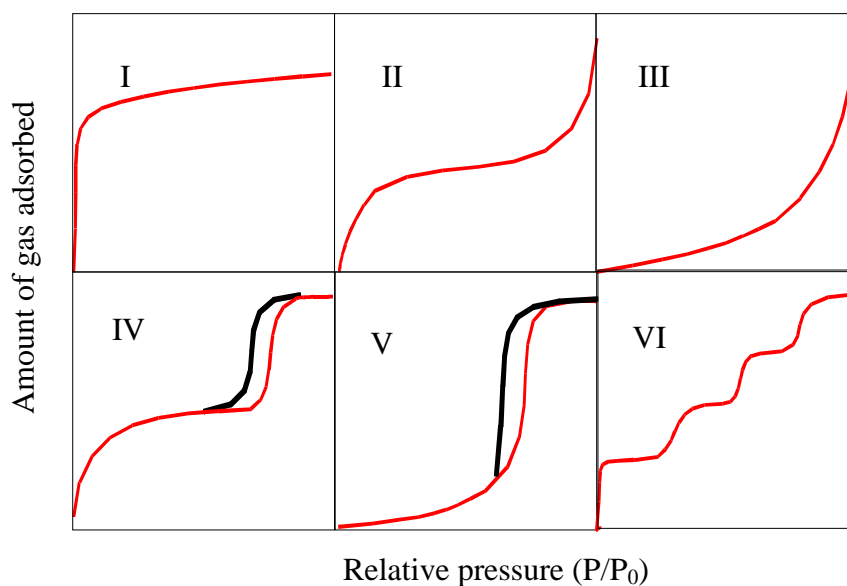


Figure 2.18 The IUPAC classification of adsorption isotherm [54].

As shown in Table 2.12, adsorption isotherms base on the strength of the interaction between the sample surface and adsorptive. Pore size distribution is measured by the use of nitrogen adsorption/desorption isotherm at liquid nitrogen temperature and relative pressures (P/P_0) ranging from 0.05-0.1. The large uptake of nitrogen at low P/P_0 indicates filling of the micropores ($<20 \text{ \AA}$) in the adsorbent. The linear portion of the curve represents multilayer adsorption of nitrogen on the surface of the sample, and the concave upward portion of the curve represents filling of mesoporous and macropores. The multipoint Brunauer, Emmett and Teller (BET) method is commonly used to measure total surface area.

$$\frac{1}{W[(P_0/P)-1]} = \frac{1}{W_m C} + \frac{C-1}{W_m C}(P/P_0)$$

Where W is the weight of nitrogen adsorbed at a given P/P_0 , W_m is the weight of gas to give monolayer coverage, and C is a constant that is related to the heat of adsorption. A slope and intercept are used to determine the quantity of nitrogen adsorbed in the monolayer and calculate the surface area. For a single point method, the intercept is taken as zero or a small positive value, and the slope from the BET

plot is used to calculate the surface area. The surface area depends upon the method used, as well as the partial pressures at which the data are collected.

Table 2.12 Features of adsorption isotherms.

Type	Interaction between sample surface and gas adsorbate	Porosity	Example of sample-adsorbate
I	relatively strong	Micropores	activated carbon-N ₂
II	relatively strong	Nonporous	oxide-N ₂
III	weak	Nonporous	carbon-water vapor
IV	relatively strong	Mesopore	silica-N ₂
V	weak	Micropores	
		Mesopore	activated carbon-water vapor
VI	relatively strong sample surface has an even distribution of energy	Nonporous	graphite-Kr

2.13.3 Scanning electron microscope (SEM)

The scanning electron microscope (SEM) has unique capabilities for analyzing surfaces and morphology of materials. It is analogous to the reflected light microscope, although different radiation sources serve to produce the required illumination. Whereas the reflected light microscope forms an image from light reflected from a sample surface, the SEM uses electrons for image formation. The different wavelength of these radiation sources result in different resolution levels: electron have much shorter wavelength than light photons, and shorter wavelength are capable of generating the higher resolution information. Enhanced resolution in turn permits higher magnification without loss of detail. The maximum magnification of the light microscope is about 2,000 times; beyond this level is “empty magnification”, or the point where increased magnification does not provide additional information. This upper magnification limit is a function of the wavelength of visible light, 2000

Å, which equal the theoretical maximum resolution of conventional light microscope. In comparison, the wavelength of electron is less than 0.5 Å, and theoretically the maximum magnification of electron beam instrument is beyond 800,000 times. Because of instrumental parameters, practical magnification and resolution limits are about 75,000 times and 40 Å in a conventional SEM [56]. The SEM consists basically of four systems:

1. The *illuminating/imaging system* produces the electron beam and directs it onto the sample.
2. The *information system* includes the data released by the sample during electron bombardment and detectors which discriminate among analyze these information signals.
3. The *display system* consists of one or two cathode-ray tubes for observing and photographing the surface of interest.
4. The *vacuum system* removes gases from the microscope column which increase the mean free path of electron, hence the better image quality.

2.13.4 Temperature-programmed desorption of ammonia (TPD) [57]

Temperature-Programmed Desorption (TPD) is a method to measure the acidic property of solid. On widely various solid acid catalysts, it was clarified that the desorption was controlled by the equilibrium between the gaseous and adsorbed ammonia under usually utilized experimental conditions. A theoretical analysis method - Curve-Fitting Method - was proposed based on the theory expressing the desorption process. On the other hand, the introduction of water vapor after the adsorption of ammonia selectively removed the unnecessary ammonia species hydrogen-bonded and that adsorbed on Lewis acid site which had been generated on basic oxide surface, and the ammonia or ammonium cation adsorbed on simply acidic site was preferentially detected -- Water Vapor Treatment Method --. By these new methods, one can precisely determine the number of acid sites, the acid strength and its distribution on almost all of the solid samples. The amount of ammonia desorbing above some characteristic temperature is taken as the acid-site concentration, and the peak desorption temperatures have been used to calculate heats of adsorption. The

activity depends on many factors, but the Brønsted-acid site density is usually one of the most crucial parameters.

CHAPTER III

EXPERIMENTALS

3.1 Instruments and apparatus

3.1.1 Oven and furnace

Crystallization of SBA-15 and FSM-16 during the synthesis was carried out at a temperature of 100°C in static condition using UM-500 oven as heater. The calcination was performed on a Carbolite RHF 1600 muffle furnace in air. Calcination of SBA-15 and FSM-16 were conducted in order to remove moisture and organic template from the catalyst. The temperature program used for the calcination of SBA-15 and FSM-16 were showed in Figure 3.1.

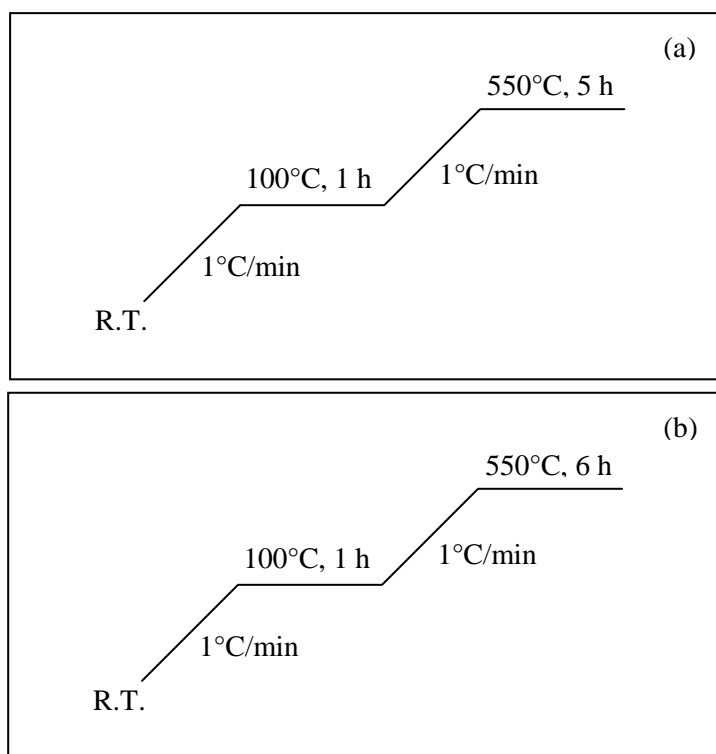


Figure 3.1 The temperature program for the calcination of (a) SBA-15 and (b) FSM-16.

3.1.2 X-ray powder diffractometer (XRD)

The XRD patterns of synthesized mesoporous materials were identified using a Rigaku D/MAX-2200 Ultima⁺ X-ray diffractometer equipped with Cu target X-ray tube (40 kV, 30mA) at 2-theta angle between 0.5 to 3.00 degree for SBA-15 and 2-theta angle between 0.5 to 8.00 degree for FSM-16 with a scan speed of 1.00 degree/min and sampling width of 0.02 degree. The scattering slit, divergent slit and receiving slit were fixed at 0.5 degree, 0.5 degree, and 0.15 mm, respectively. The measured diffractograms were analyzed using MDI software (Jade 6.5).

3.1.3 Nitrogen adsorption-desorption technique

N₂ adsorption-desorption isotherms, BET specific surface area, and pore size distribution of the catalysts were carried out using a BEL Japan, BELSORP-mini instrument. The materials were weighted nearly 40 mg and weighted exactly after pretreatment at 400°C for 3 hrs. The functionalized materials were pretreated at 150°C for 3 hrs before each measurement.

3.1.4 Scanning electron microscope (SEM)

The morphology and particle sizes of the catalysts were observed using a JEOL JSM-6480 LV scanning electron microscope. All samples were coated with spluttering gold under vacuum.

3.1.5 Ammonia temperature-program desorption (NH₃-TPD)

Acid strength of catalyst was determined using the BEL-CAT Japan instrument. The pure material was weighted nearly 80 mg and pretreatment at 400°C for 20 min. The functionalized materials were pretreatment at 150°C for 3 hrs before each measurement.

3.1.6 Sulfur analyzer

The sulfur content of the catalysts was measured with a sulfur analyzer, model SC-132 from LECO Corporation, by combustion in oxygen at 1350°C and determination of SO₂ by the intensity of infrared adsorption bands.

3.1.7 Gas chromatograph (GC)

Reaction mixtures from ester synthesis were analyzed using a Varian CP 3800 gas chromatograph equipped with a 30 m length \times 0.25 mm inner diameter of CP-Sil 8 capillary column (equivalent to DB-5 and HP-5 column). The detector was a flame ionization detector (FID). The sample volumes were 1 μ L. The column oven heating program was illustrated in Figure 3.2.

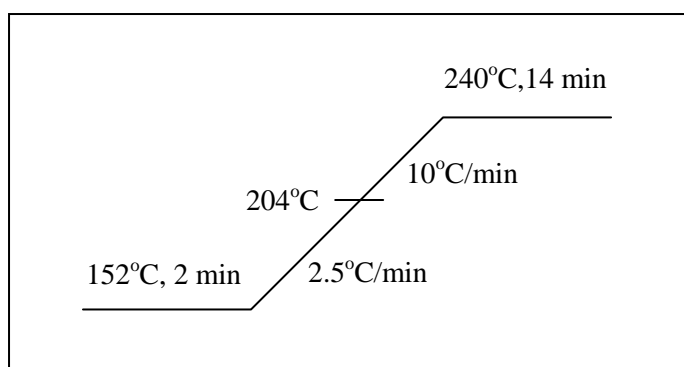


Figure 3.2 The GC heating condition for monoester and diester analysis.

3.1.8 Gas chromatograph-mass spectrometer (GC-MS)

Qualitative analysis of liquid sample was confirmed with GC-MS technique. GC system network of Varian CP-3800 gas chromatograph equipped with a 50 m length \times 0.25 mm inner diameter of VF-1ms capillary column, mass selective detector network of Varian Saturn 2200 GC/MS/MS was used.

3.1.9 Nuclear magnetic resonance spectrometer (NMR)

NMR spectra were recorded with a Varian Mercury⁺ 400 NMR spectrometer operated at 400 MHz for ^1H . The chemical shift in δ (ppm) was assigned with reference to the signal from the residual protons in deuterated solvents and using TMS as an internal standard in some cases.

3.1.10 Parr reactor

The esterification reaction of dicarboxylic acids (adipic acid, azelaic acid and sebacic acid) was performed in 100 ml PARR reactor. The temperature program for the reaction was shown in Figure 3.3.

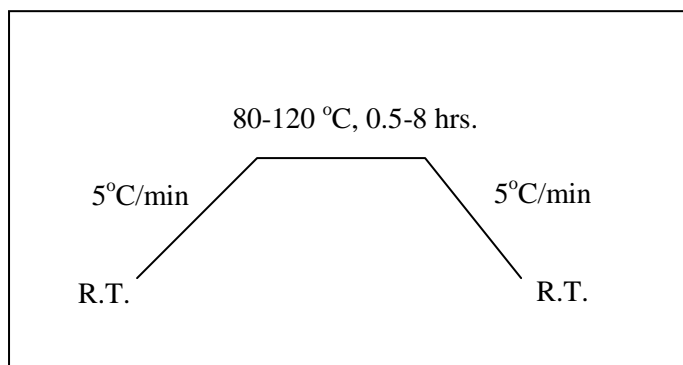


Figure 3.3 The temperature program for esterification reaction.

3.2 Chemicals

3.2.1 Chemicals for synthesis catalysts

1. Triblock copolymer pluronic P123 (PEO₂₀-PPO₇₀-PEO₂₀, average molecular weight = 5800) (Aldrich)
2. Tetraethyl orthosilicate, TEOS (Fluka, 98 %)
3. Hydrochloric acid, HCl (Fluka, 37 %)
4. (3-Mercaptopropyl)trimethoxysilane, MPTMS (Aldrich, 95 %)
5. 2-(4-Chlorosulfonylphenyl)ethyltrimethoxysilane, CSPETMS (Gelest, 50 % in methylene chloride)
6. Hydrogen peroxide (Merck, 30 %)
7. Toluene (CARLO ERBA, 99.5%)
8. Sulfuric acid, H₂SO₄ (Merck, 95-97%)
9. Sodium silicate, Water glass (C.Thai Chemical Company Limited)
10. Sodium hydroxide (Merck, 99%)
11. Cetyltrimethylammoniumbromide, CTMA (Fluka)
12. Deionized Water

3.2.2 Chemicals for esterification

1. Adipic acid (C₆H₁₀O₄) (Sigma Aldrich, 99%)
2. Azelaic acid (C₉H₁₆O₄) (Fluka, 99%)
3. Sebacic acid (C₁₀H₁₈O₄) (Sigma Aldrich, 99%)
4. 2-Ethyl-1-hexanol (C₈H₁₈O) (Sigma Aldrich, 99.6%)
5. *n*-Octanol (C₈H₁₈O) (Fluka, 99%)

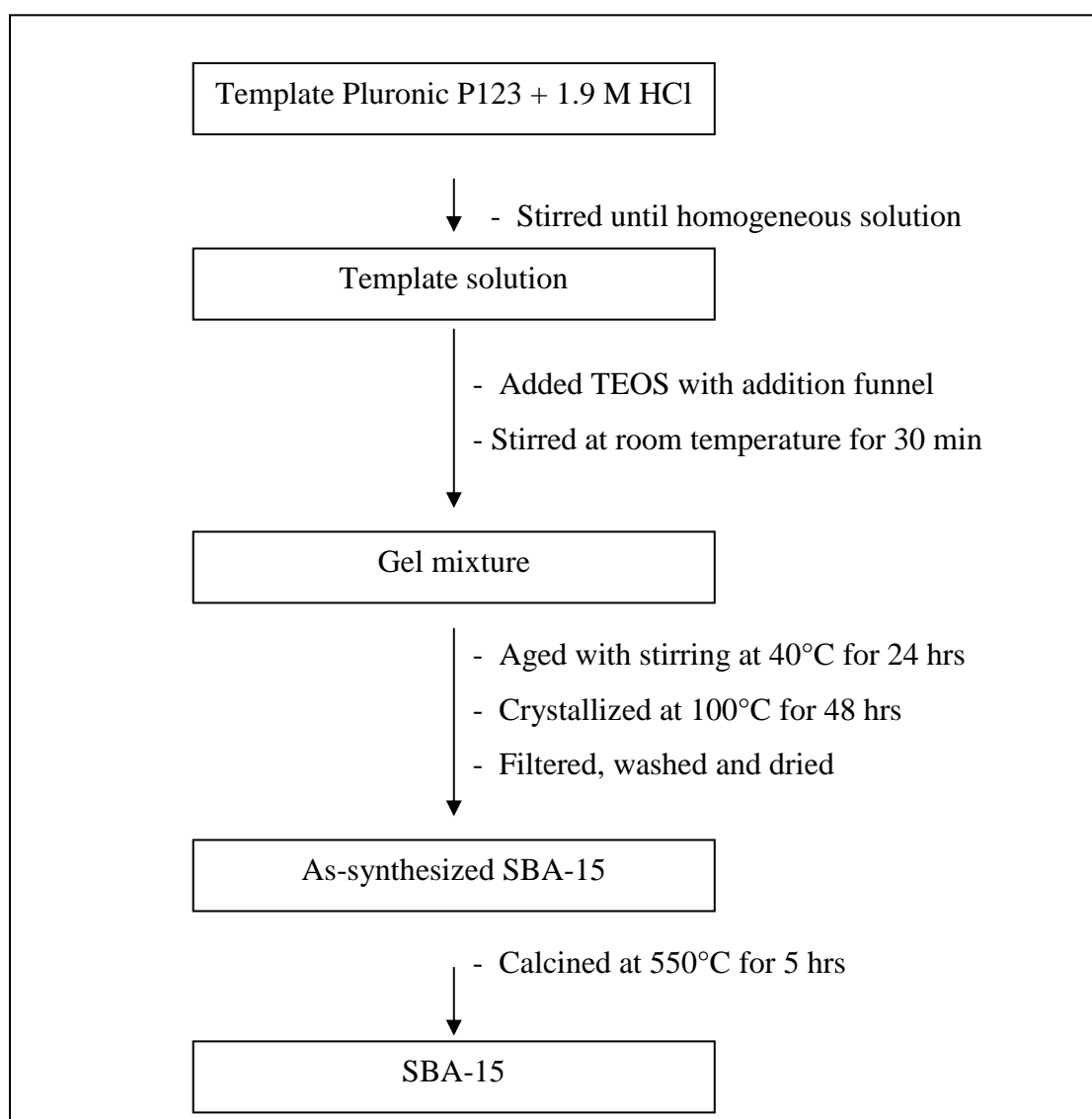
3.1.3 Chemicals for reaction product analysis

1. N-methyl-N-(trimethylsilyl)trifluoroacetamide, $C_6H_{12}F_3NOSi$
(Derivatization grade, Sigma Aldrich)
2. Eicosane ($C_{20}H_{42}$) (Sigma Aldrich, 99%)
3. Heptane (C_7H_{16}) (MERCK, 99%)

3.3 Synthesis of mesoporous materials (SBA-15 and FSM-16)

3.3.1 Synthesis SBA-15 by hydrothermal method

SBA-15 was synthesized using gel mole composition of 1.0TEOS: 0.0165 P123: 6.95 HCl: 140 H₂O reported by Stucky *et al.* [11]. In a typical procedure, triblock copolymer Pluronic P123 as template was dissolved in 1.9 M HCl solution at room temperature under stirring. Subsequently, TEOS was added dropwise and stirred for 30 min. Then, aged at 40°C for 24 hrs. with stirring. The resulting gel was transferred to a Teflon-lined autoclave for hydrothermal crystallization at 100°C for 48 hrs. As-synthesized SBA-15 was separated by filtration, washed with deionized water for several times, and dried overnight. The template was removed by calcined at 550°C for 5 hrs. The procedure for synthesizing the SBA-15 was illustrated in Scheme 3.1.

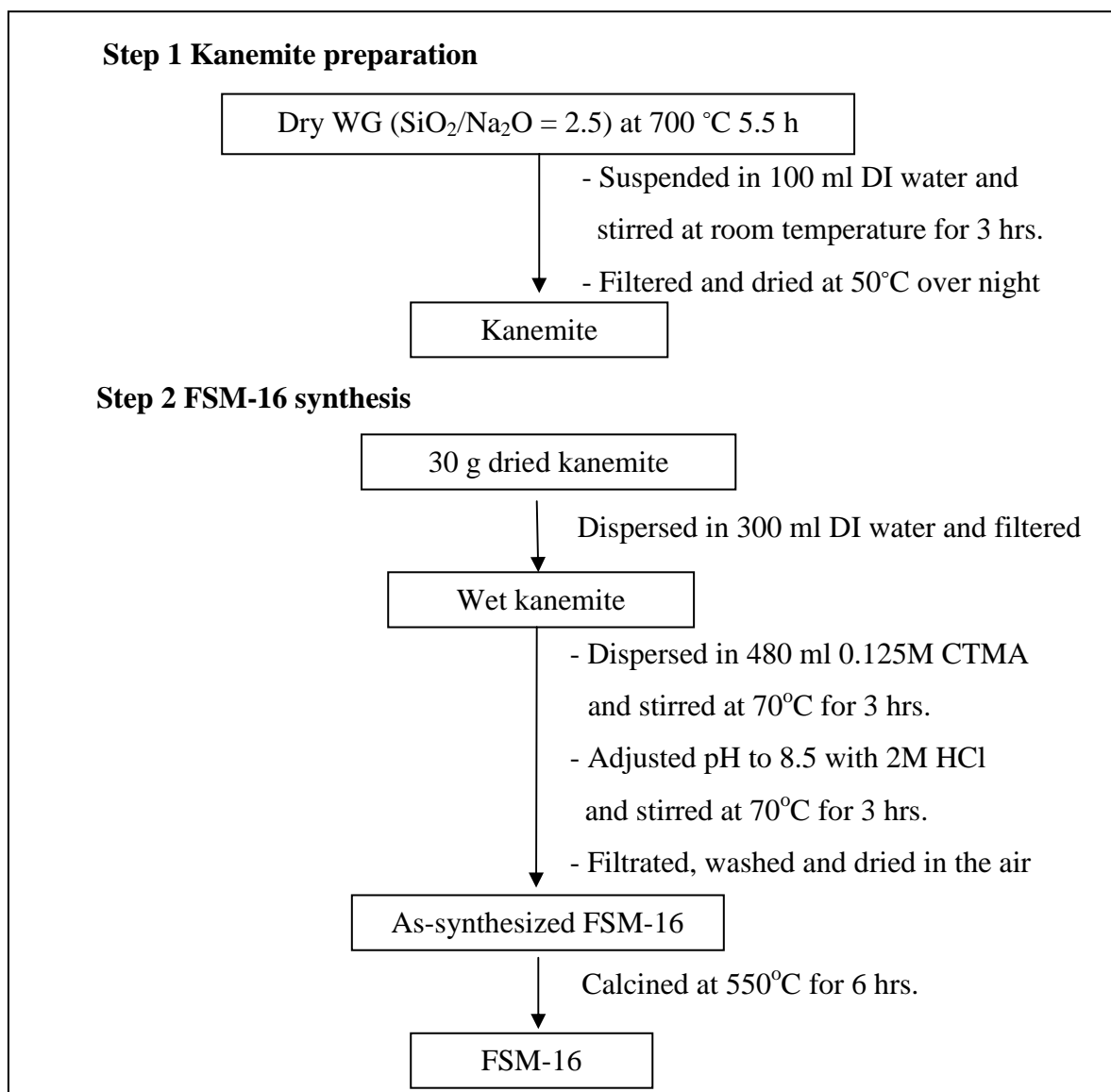


Scheme 3.1 Preparation diagram for SBA-15 by hydrothermal method.

3.3.2 Synthesis FSM-16 by hydrothermal method

FSM-16 was synthesized from the crystalline single-layered polysilicate kanemite ($\delta\text{-Na}_2\text{SiO}_5$) with aqueous solutions of organic surfactant molecules. Kanemite was synthesized using the gel mole composition of $\text{SiO}_2/\text{Na}_2\text{O} = 2.5$ developed from Wang *et al.* [14]. The FSM-16 material was prepared by a method similar to that used by Dhar *et al.* [15]. A typical synthesis procedure was as follows: 30 g of kanemite was dispersed in 300 ml of DI water and then stirred at room temperature for 3 hrs. Subsequently, the suspension was filtered out to obtain wet kanemite paste. All of the kanemite paste was dispersed in 480 ml of an aqueous

solution of 0.125 M 2-hexadecyltrimethylammonium chloride (CTMA) and then stirred at 70°C for 3 hrs. The suspension was kept stirring at 70°C for 3 hrs. while keeping the pH value at 8.5. After cooling, the solid product was filtered out, washed with water, dried in air and calcined at 550°C for 6 hrs.



Scheme 3.2 Preparation diagram for FSM-16 by hydrothermal method.

3.4 Sulfonic functionalized mesoporous materials

Three grams of mesoporous materials was suspended with (3-mercaptopropyl)tri-methoxysilane (for propyl sulfonic group), 2-(4-Chlorosulfonylphenyl)ethyl trimethoxysilane (for aryl sulfonic group) and toluene, refluxed at 60°C for 6 hrs. Then thiol groups were oxidized to sulfonic groups by 30% H₂O₂. The wet material was suspended in 0.2 M H₂SO₄ for 2 hrs [58]. Finally, the obtained product was filtered and dried in oven for overnight at 80°C.

3.5 Aluminium functionalized mesoporous materials

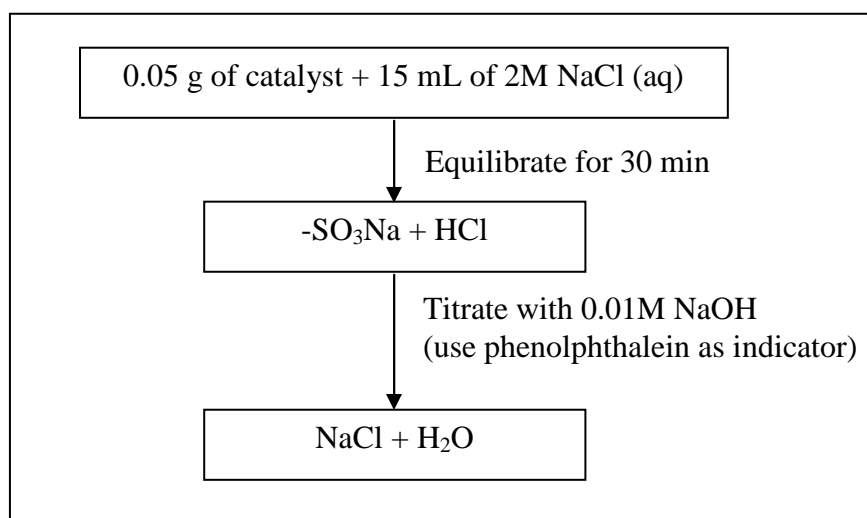
In this work, mesoporous materials were incorporated with aluminium *via* post synthesis. Alumination of calcined mesoporous were conducted by stirring 0.5 g of mesoporous material in 50 mL of water containing exact amounts of sodium aluminate at room temperature (RT) for 12 h which the stoichiometric amount of used sodium aluminate were shown in Table 3.1. The solid material was then filtered, washed with distilled water, and dried at room temperature. Then sodium ion in post-synthesized sample was removed by ion exchange with 0.01M NH₄Cl [59].

Table 3.1 Stoichiometric amounts of sodium aluminate in alumination of mesoporous materials with various Si/Al ratios

Si/Al molar ratio in gel	NaAlO ₂ dissolved in 50.0 mL H ₂ O (g)
10	0.0683
25	0.0275
50	0.0137
100	0.0068

3.6 Acid-base titration

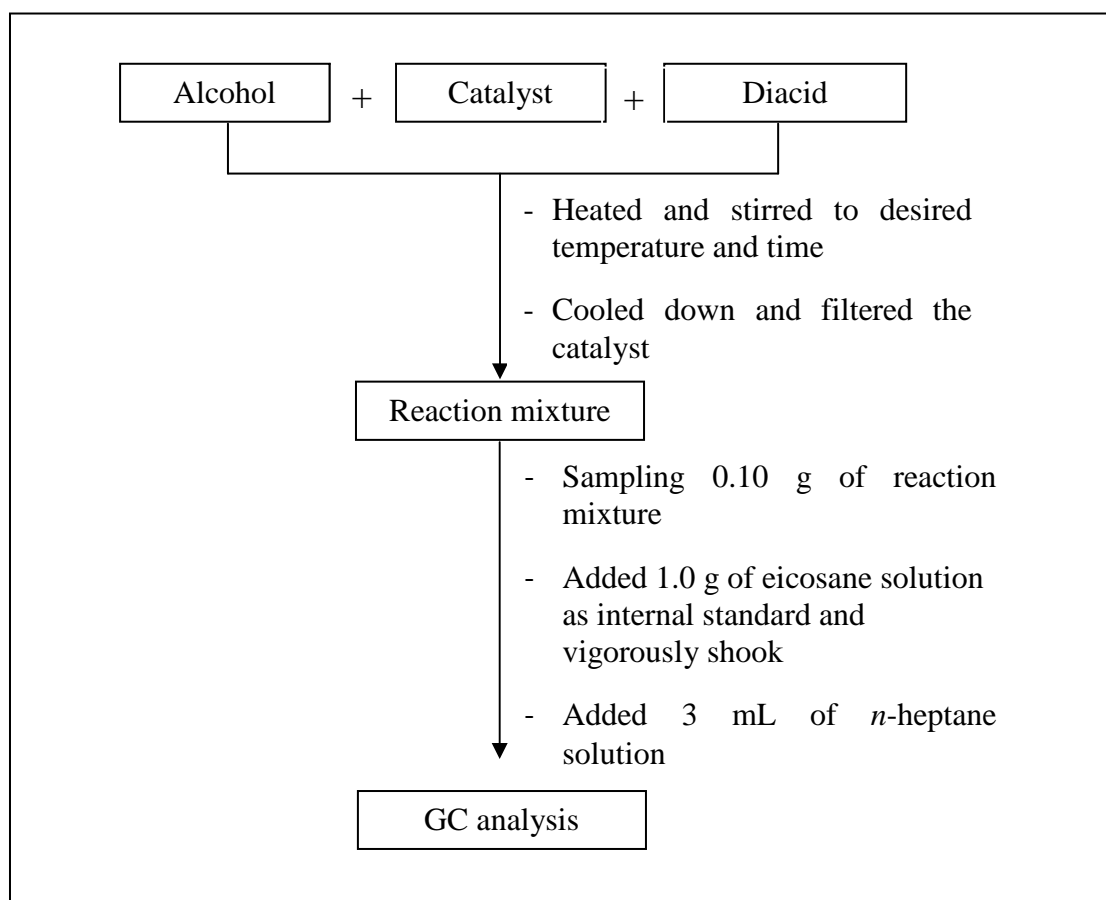
The acid capacities of sulfonic acid groups in the functionalized mesoporous materials were quantified using 2M NaCl solution as the ion-exchange agent (Scheme 3.3). Approximately 0.05xx g of the catalysts was exchanged with 15 ml of NaCl solution for 30 min under constant agitation at room temperature and titration with 0.01 M NaOH by using phenolphthalein as indicator [60].



Scheme 3.3 Diagram for acid-base titration.

3.7 Procedure in lubricant preparation

The synthesis of monoester and diester were carried out in stainless steel batch reactor. In each experiment, the total weight of diacid (adipic acid, azelaic acid or sebacic acid) and alcohol (2-ethyl hexanol or *n*-octanol) as five grams were added to PARR reactor (Scheme 3.4). After complete of the reaction, the reaction mixture was cooled down and then catalyst was separated from the reaction mixture by centrifuge. The obtained products were confirmed using GC-MS technique and compared to the authentic samples. Likewise, the reaction mixture was quantitatively analyzed by gas chromatography.



Scheme 3.4 Diagram for lubricating oil preparation and analysis.

3.8 Parameters affecting lubricant preparation

3.8.1 Effect of reaction time

The reaction was varied in the range 0.5-8 hours.

3.8.2 Effect of temperature

The reaction temperature was varied to 80, 90, 100, 110 and 120°C.

3.8.3 Effect of catalytic amount

In this work, the amount of catalyst was changed to 0 wt.%, 1 wt.%, 2 wt.%, 3 wt.%, 4 wt.%, 5 wt.% and 10 wt.% based on amount of substrate.

3.8.4 Effect of stirring speed

The stirring speed was varied to 50, 150 and 250 rpm.

3.8.5 Effect of 2-ethyl hexanol to adipic acid molar ratio

The mole ratio of 2-ethyl hexanol to adipic acid was studied at different reaction time of 1, 2, 3, 4 and 5

3.8.6 Effect of various catalysts

Catalytic activities of sulfonic functionalized SBA-15 and FSM-16 mesoporous materials were compared with Al-SBA-15, Al-FSM-16 and commercial catalysts such as H-ZSM-5, H-beta, Nafion SAC-13 and Amberlyst-15.

3.8.7 Effect of chain length of dicarboxylic acid

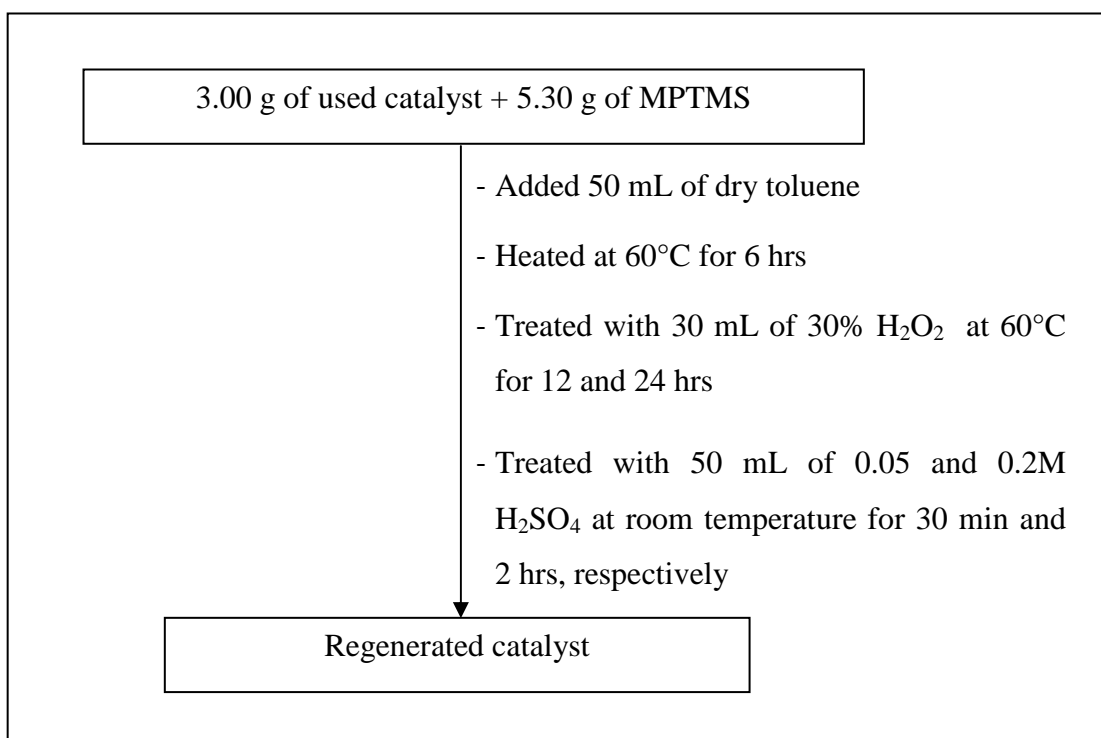
Esterification of various dicarboxylic acids with 2-ethyl-hexanol was carried out using adipic acid, azelaic acid and sebacic acid as reactants.

3.8.8 Effect of structure of alcohol

Esterification of adipic acid with various alcohols was carried out using *n*-octanol and 2-ethyl-1-hexanol as reactants.

3.9 Recycle of catalysts

After the first reaction, the used catalyst was filtered and washed several times with various solvents (hexane, acetone and methanol). The catalyst was dried at 80°C overnight, and then this catalyst was denoted as reused catalyst. The regenerated catalyst was grafting the used catalyst with MPMTS in toluene, H₂O₂ and H₂SO₄, respectively (Scheme 3.5). Then, catalyst was characterized by XRD, surface area analysis and SEM before testing in subsequent experiment. The reaction was performed in the similar way to described in Section 3.7.



Scheme 3.5 Regenerated catalyst preparation.

CHAPTER IV

RESULTS AND DISCUSSION

4.1 Synthesis of SBA-15 catalysts

4.1.1 The physico-chemical properties of sulfonic functionalized SBA-15

4.1.1.1 XRD results

Low angle X-ray powder diffraction patterns of SBA-15 mesoporous materials are shown in Figure 4.1. After removal of triblock copolymer template from the pores of materials, SBA-15-PrSO₃H and SBA-15-ArSO₃H showed one very intense peak and two weak peaks indexed to (100), (110) and (200) diffractions, respectively, indicating the prepared materials contained well-ordered hexagonal structure corresponding to pure SBA-15 [11]. In comparison with SBA-15, the diffraction peaks of sulfonic functionalized SBA-15 materials were slightly shifted to higher 2 theta values, indicating the presence of bulky functional groups on the surface of SBA-15 would decrease pore volume and wall thickness. Additionally, the sulfonic functionalized SBA-15 exhibited lower intensity compared with pure SBA-15 due to the organic group being incorporated into the mesoporous structure, leading to low crystallinity.

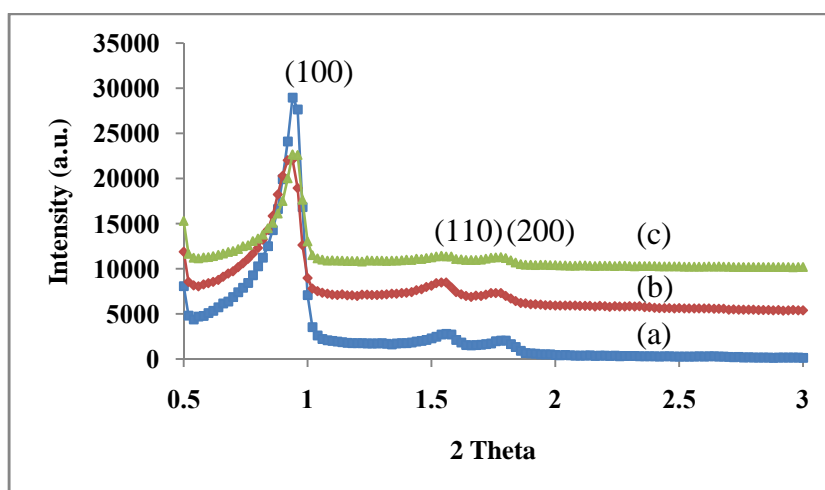


Figure 4.1 X-ray powder diffraction patterns of (a) SBA-15, (b) SBA-15-PrSO₃H and (c) SBA-15-ArSO₃H.

4.1.1.2 Sorption properties of sulfonic functionalized SBA-15

The N₂ adsorption-desorption isotherm and pore size distribution of functionalized SBA-15 catalysts are shown in Figure 4.2. It performed a type IV adsorption isotherm of IUPAC classification and exhibited a hysteresis loop H1-type which was a characteristic pattern of mesoporous materials [61]. Some physical properties derived from the adsorption isotherm of SBA-15 and sulfonic functionalized samples are compiled in Table 4.1. The total specific surface area of SBA-15-PrSO₃H and SBA-15-ArSO₃H were calculated using Brunauer, Emmett and Teller (BET) equation, which were found at 364 m²/g and 335 m²/g, respectively. These values exhibited lower surface area and mesopore volume when compared with the pure SBA-15 because the organo sulfonic functional transfer into pore structure that was corresponding with their intensity of XRD pattern results. Moreover, it also induced decreasing of surface area and pore volume. In part of pore size distribution, the synthetic materials were evaluated using Barrett-Joiner-Halenda (BJH) method. The narrow pore size distribution was found in SBA-15-PrSO₃H and SBA-15-ArSO₃H at the pore diameter of 9.23 nm which was the same as SBA-15.

Table 4.1 Textural properties of SBA-15 and sulfonic functionalized SBA-15.

Catalyst	Total specific surface area ^a (m ² ·g ⁻¹)	Pore size distribution ^b (nm)	Mesopore volume ^b (cm ³ ·g ⁻¹)	d ₍₁₀₀₎ ^c (nm)	Wall thickness ^d (nm)
SBA-15	735	9.23	1.05	9.45	1.68
SBA-15-PrSO ₃ H	365	9.23	0.67	9.40	1.62
SBA-15-ArSO ₃ H	335	9.23	0.57	9.38	1.60

^aCalculated using the BET plot method,

^bCalculated using the BJH method,

^cCalculated using XRD, Jade5.6,

^dCalculated as: a₀-pore size (a₀ = 2×d₍₁₀₀₎/√3)

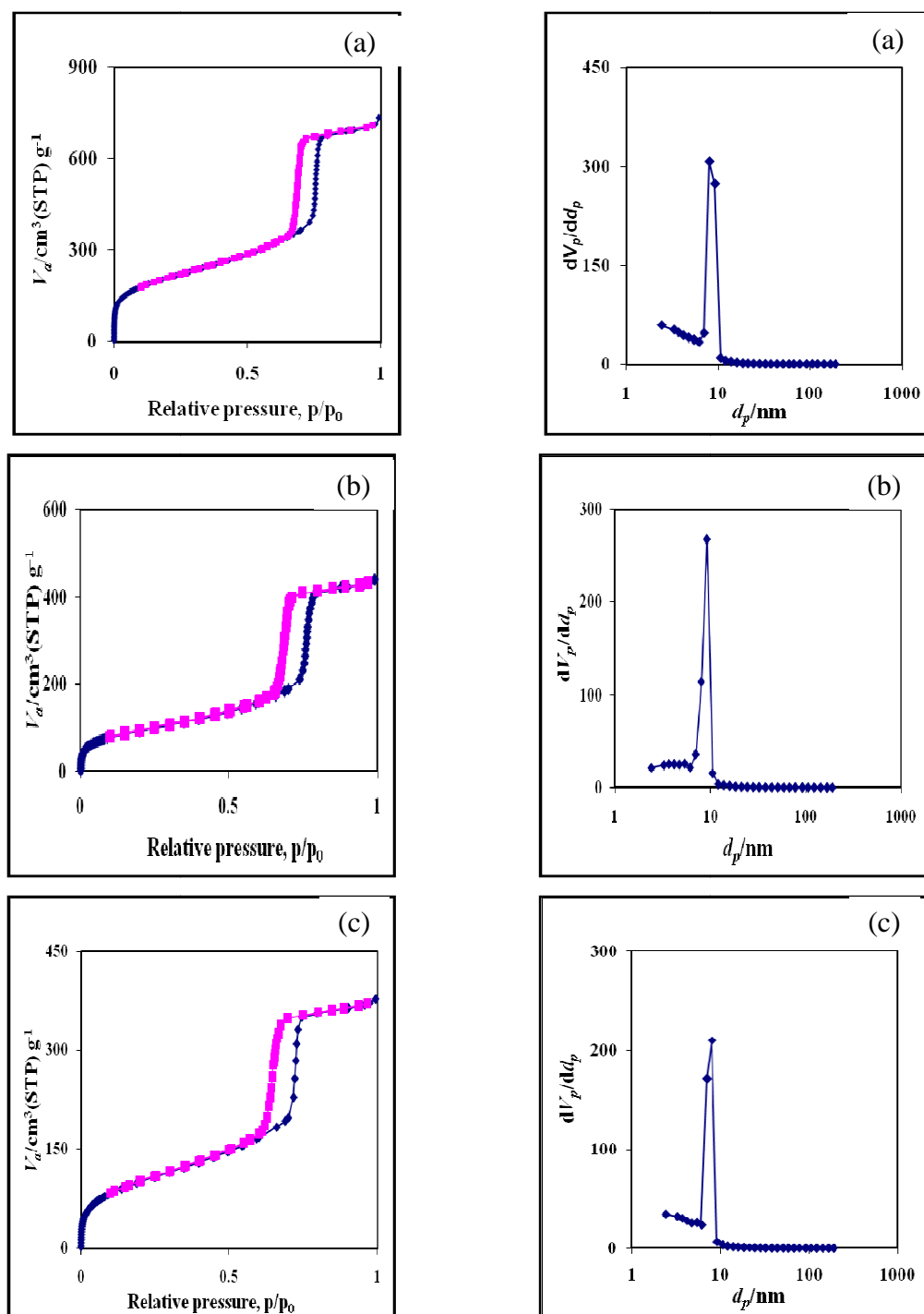


Figure 4.2 N_2 adsorption-desorption isotherm and BJH-pore size distribution of (a) SBA-15, (b) SBA-15-PrSO₃H and (c) SBA-15-ArSO₃H.

4.1.1.3 SEM images

The SEM images of pure SBA-15, SBA-15-PrSO₃H and SBA-15-ArSO₃H are illustrated in Figure 4.3. Morphology of SBA-15 was uniform rope-like particle shape aggregated particles. Furthermore, the average size of particle was $0.8 \times 1.0 \mu\text{m}$. For SEM images of SBA-15-PrSO₃H, the sample was aggregated particles with rope-like structure similar to pure SBA-15 with the average particle size was $0.7 \times 0.9 \mu\text{m}$. In the case of SBA-15-ArSO₃H, the sample showed uniform aggregated rope-like particles. In addition, the average particle size was $0.7 \times 0.8 \mu\text{m}$, which was slightly smaller than SBA-15-Pr-SO₃H. This observation was assumed that lower pore volume of SBA-15-ArSO₃H might affect on particle shapes.

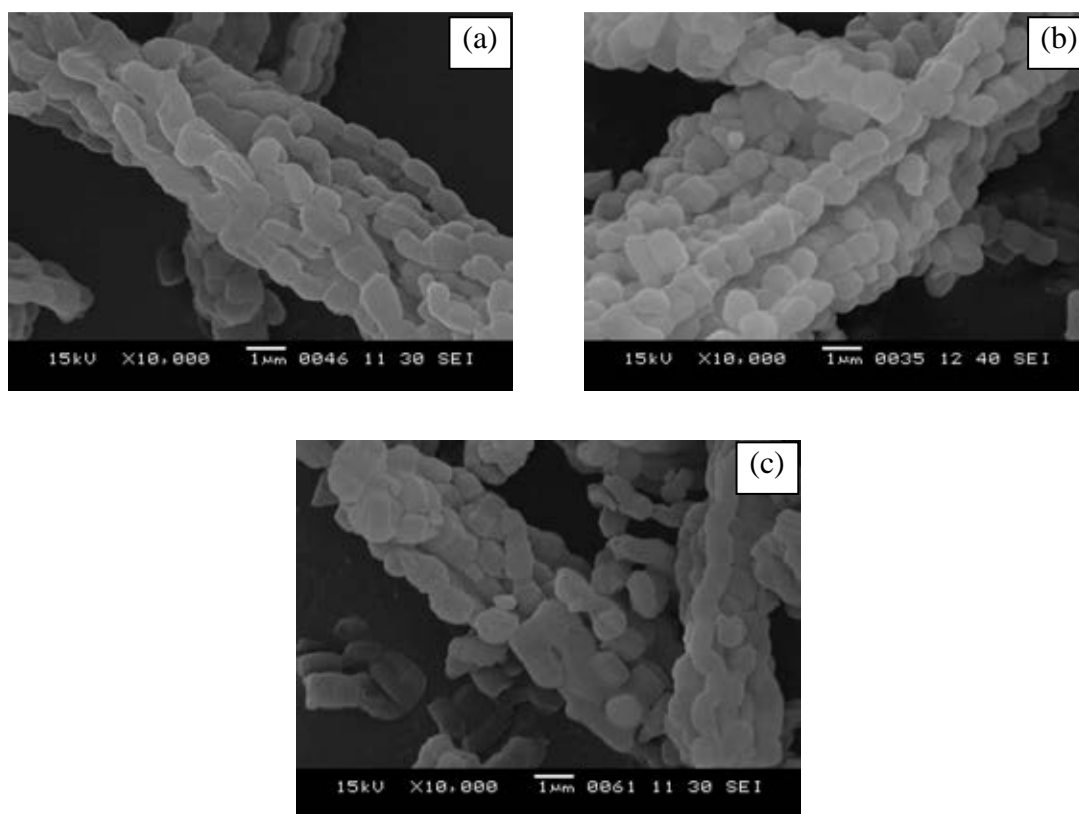


Figure 4.3 SEM images of (a) SBA-15, (b) SBA-15-PrSO₃H and (c) SBA-15-ArSO₃H.

4.1.1.4 Elemental analysis and acid-base titration

The number of sulfonic acid groups in the mesoporous silica was measured quantitatively by acid-base titration using sodium chloride as ion-exchange agent. The sulfur content of the modified mesoporous silica was determined by sulfur content analysis comply in Table 4.2. In this work, both SBA-15-Pr-SO₃H and SBA-15-ArSO₃H were synthesized using the same mole composition. As a result, the acid values and sulfur contents of two catalysts were no significant difference.

Table 4.2 Sulfur analysis and acid value of sulfonic functionalized SBA-15.

Catalyst	Sulfur analysis ^a (wt%)	H ⁺ content ^b (mmol/g)
SBA-15-PrSO ₃ H	2.82	1.38
SBA-15-ArSO ₃ H	3.04	1.40

^aSulfur analysis, measured from Sulfur analyzer,

^bAcid capacity defined as millimole of acid centers per gram of catalyst, obtained directly by titration (mmol H⁺/g)

4.1.2 The physic-chemical properties of aluminium functionalized SBA-15

4.1.2.1 XRD results

In this research, Al-SBA-15 was synthesized with Si/Al ratios in gel composition of 10, 25, 50 and 100 by alumination method following Kevan *et al.* [59]. The XRD patterns of Al-SBA-15 at various Si/Al ratios compared to calcined Si-SBA-15 are show in Figure 4.4. All XRD results indicated the catalysts retained the ordered structure of SBA-15 during the post synthesis process. The peaks of various Si/Al ratios in Al-SBA-15 exhibited increasing intensity of the (100) reflection plane along with decreasing aluminum contents. Additionally, XRD patterns of the modified materials were shifted slightly to higher angle comparing to Si-SBA-15 resulting from the shrinkage during the recalcination process [62].

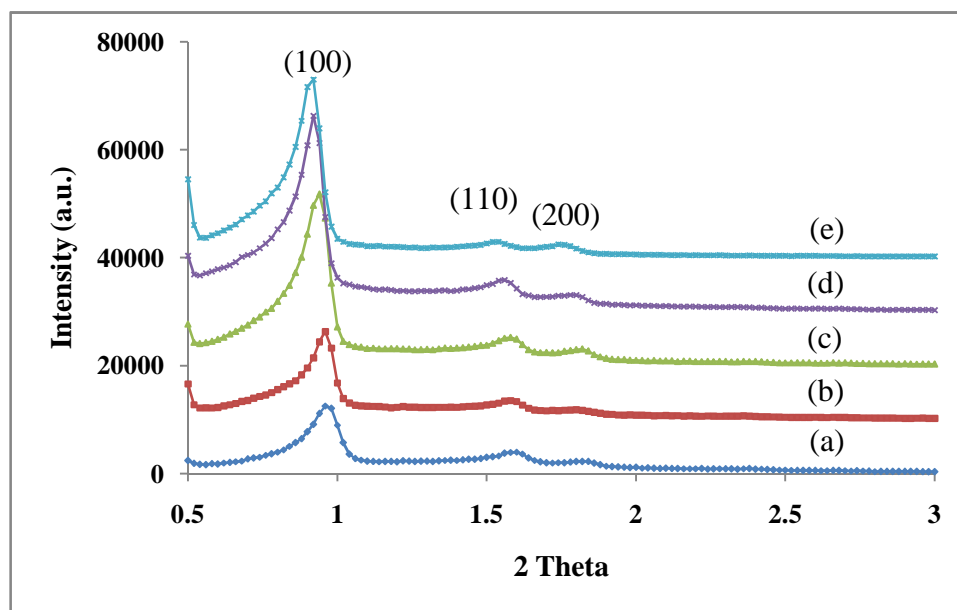


Figure 4.4 X-ray powder diffraction patterns of calcined Al-SBA-15 with various Si/Al mole ratios in reactant mixture (a) SBA-15(10), (b) Al-SBA-15(25), (c) Al-SBA-15(50), (d) Al-SBA-15(100) and (e) Al-SBA-15.

4.1.2.2 Sorption properties of Al-SBA-15

The N_2 adsorption-desorption isotherm of aluminated SBA-15 catalysts at various Si/Al mole ratios are shown in Figure 4.5. Although, modified materials were inserted Al ion in the framework, the isotherms were classified in type IV, similar to the pure SBA-15. Textural properties of calcined catalysts are shown in Table 4.3.

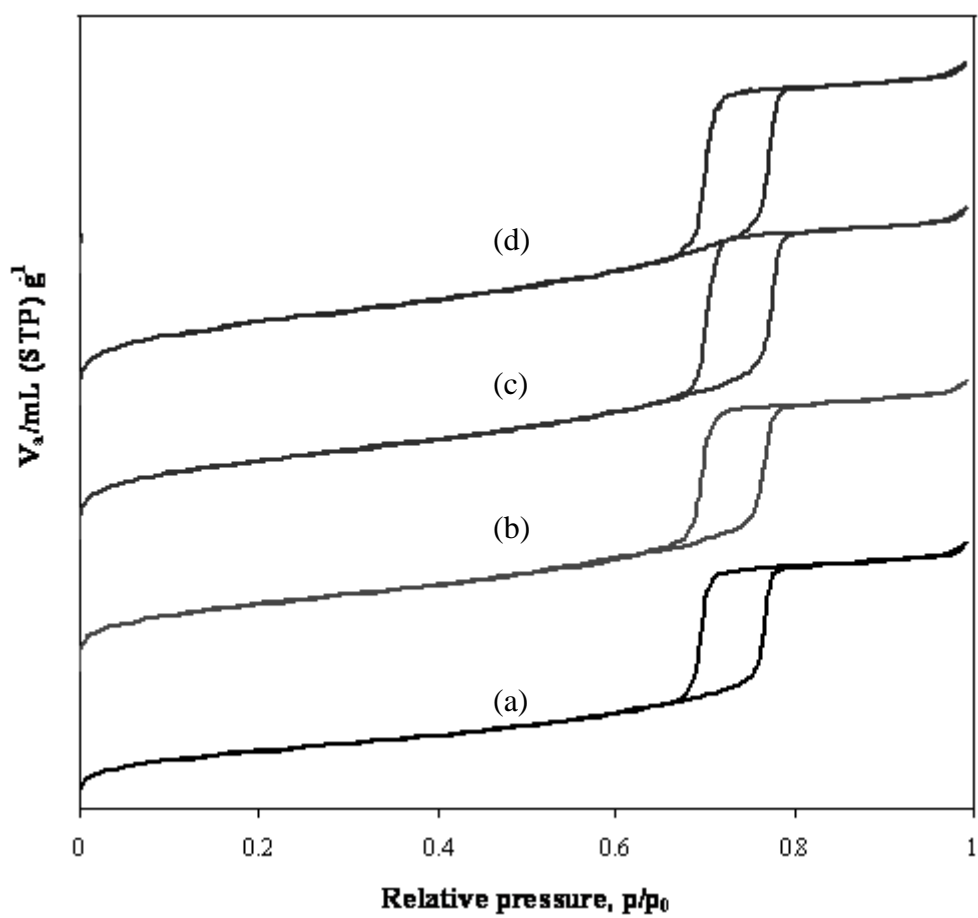


Figure 4.5 N_2 adsorption-desorption isotherms of (a) Al-SBA-15(10), (b) Al-SBA-15(25), (c) Al-SBA-15(50) and (d) Al-SBA-15(100).

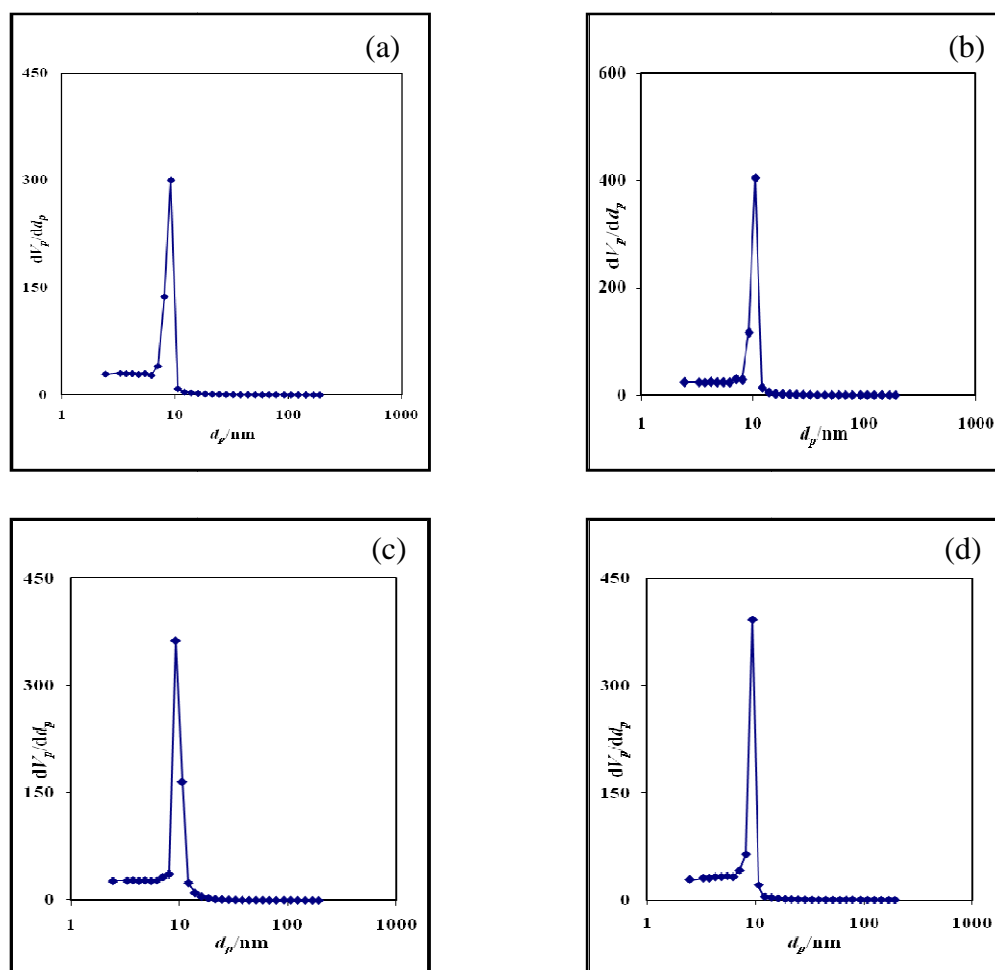


Figure 4.6 BJH-Pore size distributions of (a) Al-SBA-15(10), (b) Al-SBA-15(25), (c) Al-SBA-15(50) and (d) Al-SBA-15(100).

The pore size distribution obtained from BJH equation is shown in Figure 4.6. All samples exhibited a narrow distribution with a pore size of 9.23 nm. By comparing to the pore size of pure silica SBA-15 in Figure 4.2(a), the pore size of all Al-SBA-15 samples remains unchanged.

Table 4.3 Textural properties of SBA-15 and Al-SBA-15 with various Si/Al ratios.

Catalyst	Total specific surface area ^a (m ² ·g ⁻¹)	Pore size distribution ^b (nm)	Mesopore volume ^b (cm ³ ·g ⁻¹)	d ₍₁₀₀₎ ^c (nm)	Wall thickness ^d (nm)
SBA-15	735	9.23	1.05	9.45	1.68
Al-SBA-15(10)	409	9.23	0.78	9.19	1.38
Al-SBA-15(25)	447	9.23	0.86	9.23	1.43
Al-SBA-15(50)	467	9.23	1.00	9.43	1.66
Al-SBA-15(100)	494	9.23	1.04	9.62	1.88

^aCalculated using the BET plot method,

^bCalculated using the BJH method,

^cCalculated using XRD, Jade5.6,

^dCalculated as: a₀-pore size (a₀ = 2×d₍₁₀₀₎/√3)

Incorporated Al in the SBA-15 framework leads to a reduction in the amount of nitrogen up taken in SBA-15 depending on the amount of aluminum due to the decreasing of mesoporous volume. This result is in agreement with those in literatures [13, 63-64]. In addition, when Al content was increased, the d-spacing was decreased indicating that the distance from each plane was reduced. Considering the effect of aluminum content in catalysts, wall thickness was calculated in the same method as Stucky *et al.* [11]. The data showed that the wall thickness decreased when aluminum quantity increased, corresponding to the decrease of d-spacing as d₍₁₀₀₎ in the equation.

4.1.2.3 SEM images

The SEM images of modified acid SBA-15 samples are illustrated in Figure 4.7. All four Si/Al ratio samples showed small rod particles. From aluminum additions, the small rod particles were changed from the rope-like agglomeration. At Si/Al = 10, it performed many rod particles that broken out of the aggregation, whereas at higher Si/Al ratios (25-100) the eliminated particle found less and absent for pure SBA-15 as show in Figure 4.3. However, the rod shape of individual particle remained the same as precursor.

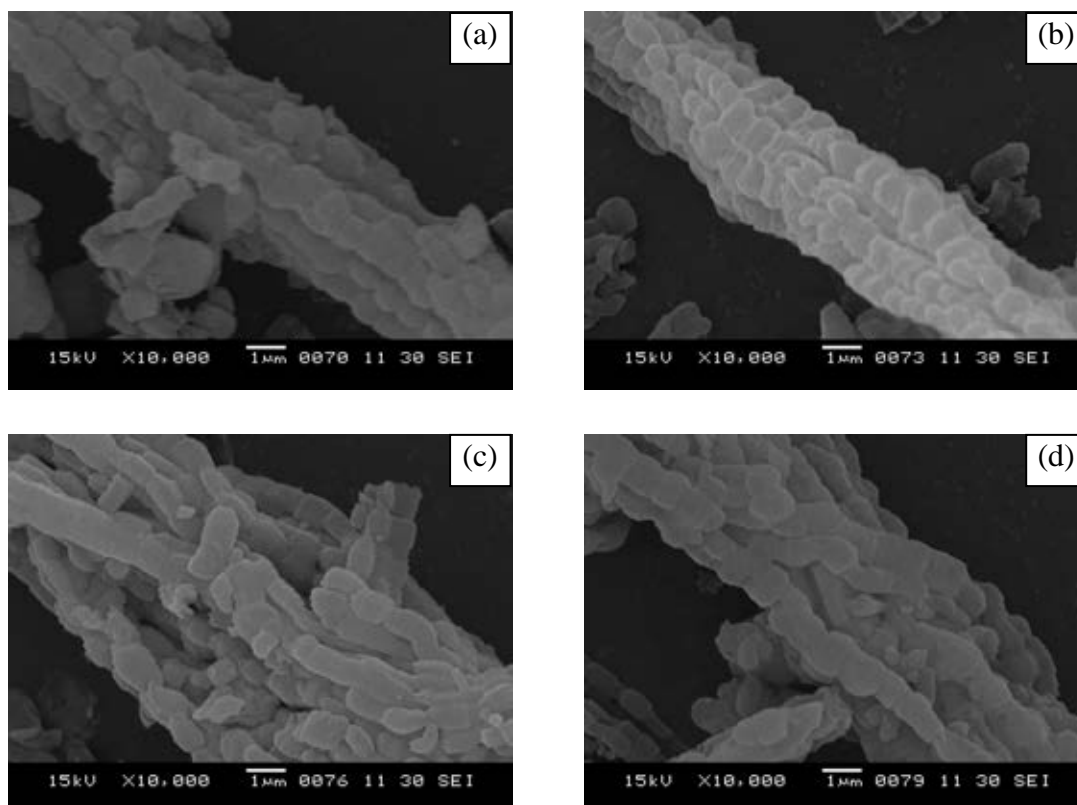


Figure 4.7 SEM images of (a) Al-SBA-15(10), (b) Al-SBA-15(25), (c) Al-SBA-15(50), and (d) Al-SBA-15(100).

4.1.2.4 Elemental analysis and acid-base titration

The number of aluminium in the mesoporous silica was measured quantitatively by acid-base titration using sodium chloride as ion-exchange agent. The acid sites quantities of Al-SBA-15 samples were increased following the aluminum contents. In addition, the elemental analysis result showed that the parts of aluminum were in the structure of catalyst. The Si/Al molar ratios in the catalysts for Al-SBA-15 materials were less than those in gel. In some cases, the structural framework of pure silica SBA-15 was collapsed, thus the silica in the framework was a smaller amount. The content of the alumina (Al_2O_3) in sodium aluminate as aluminum source was higher quantity than calculation.

Table 4.4 Elemental analysis and acid value of aluminium functionalized SBA-15.

Catalysts	Si/Al mole ratios		H ⁺ content ^c (mmol/g)
	in gel composition ^a	in catalysts ^b	
Al-SBA-15(10)	10	8.21	0.70
Al-SBA-15(25)	25	18.76	0.64
Al-SBA-15(50)	50	33.62	0.40
Al-SBA-15(100)	100	70.56	0.20

^aCalculated from reagent quantities,

^bAluminum (Al) was determined by ICP-AAS,

^cAcid capacity defined as millimole of acid centers per gram of catalyst, obtained directly by titration (mmol H⁺/g).

4.2 Synthesis of FSM-16 catalysts

The polysilicate kanemite ($\text{NaHSi}_2\text{O}_5 \cdot 3\text{H}_2\text{O}$) is a layered material which consists of single layer of SiO_4 . Kanemite could easily be prepared so it was used as a silicon source for synthesis of FSM-16. Comparison kanemite which was prepared by Wang *et al.* method [14], X-Ray powder diffraction pattern of kanemite in Figure 4.8 showed the same pattern which achieved the characteristic peaks at 2 theta as 8.7°, 22.3°, 24.5°, 26.0°, 28.9° and 36.3°, respectively.

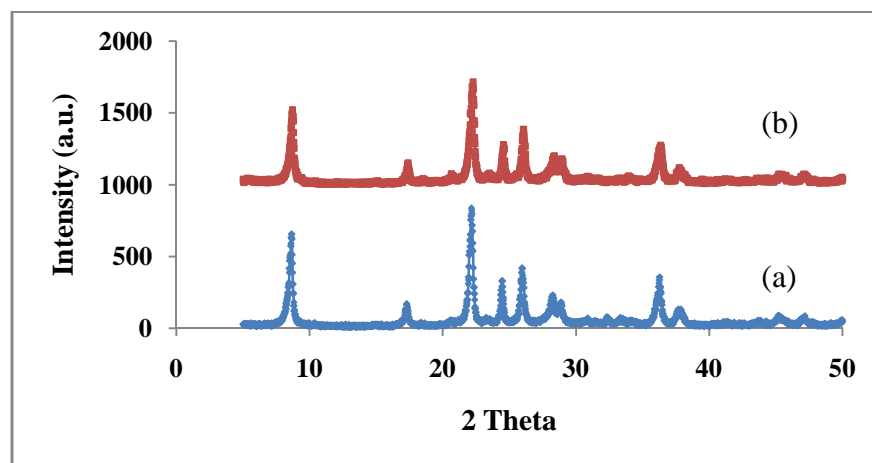


Figure 4.8 X-ray powder diffraction patterns of (a) reference kanemite by Wang *et al.* method and (b) synthetic kanemite.

The SEM images of kanemite at different magnifications were illustrated in Figure 4.9. Morphology of kanemite was irregular morphology with non-uniform sizes in the range 1-3 μm .

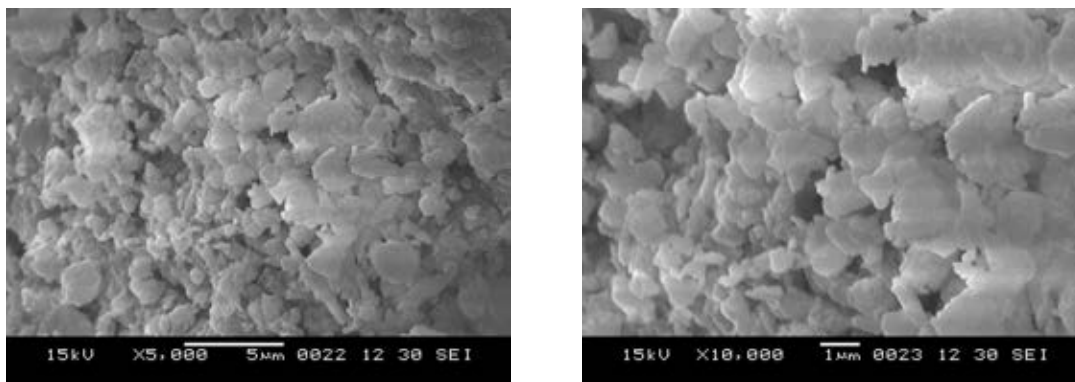


Figure 4.9 SEM images of kanemite at different magnifications
(a) $\times 5000$ and (b) $\times 10,000$.

4.2.1 The physico-chemical properties of sulfonic functionalized FSM-16

4.2.1.1 XRD results

X-ray powder diffraction patterns of all FSM-16 mesoporous materials are shown in Figure 4.10. FSM-16-PrSO₃H and FSM-16-ArSO₃H exhibited one very intense peak and two weak peaks at 2 theta of 2.3°, 4.1° and 4.7° for plane (100), (110) and (200), respectively. The sulfonic functionalized FSM-16 exhibited lower intensity compared to pure FSM-16, indicating the crystallinity of the prepared materials less than pure FSM-16 but contained hexagonal structure corresponding to pure FSM-16. In addition, the diffraction peaks of sulfonic functionalized FSM-16 materials were slightly shifted to higher 2 theta values, indicating the presence of bulky functional group on the surface of FSM-16 would decrease pore volume and wall thickness.

In comparison with SBA-15, the diffraction peaks of FSM-16 materials were shifted to higher 2 theta values. It performed FSM-16 contained lower d-spacing than SBA-15.

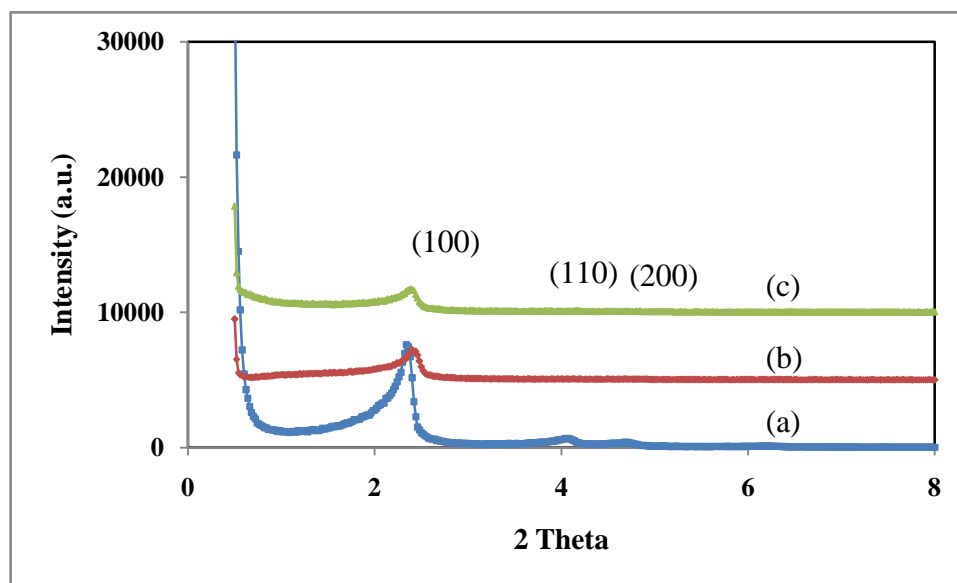


Figure 4.10 X-ray powder diffraction patterns of (a) FSM-16, (b) FSM-16-PrSO₃H and (c) FSM-16-ArSO₃H.

4.2.1.2 Sorption properties of sulfonic functionalized FSM-16

The N₂ adsorption-desorption isotherm and pore size distribution of functionalized FSM-16 catalysts are shown in Figure 4.11. It performed a type IV adsorption isotherm of IUPAC classification. Some physical properties derived from the adsorption isotherm of FSM-16 and sulfonic functionalized samples are compiled in Table 4.5. The total specific surface area and pore volume of pure FSM-16 performed total surface area and pore volume as 928 m²/g and 1.13 cm³·g⁻¹, as FSM-16-PrSO₃H and FSM-16-ArSO₃H were found at, 570 m²/g, 0.57 cm³·g⁻¹ and 451 m²/g, 0.37 cm³·g⁻¹, respectively, which exhibited lower surface area and mesopore volume than pure FSM-16 because the organo sulfonic functional transfer into pore structure that was corresponding with their intensity of XRD pattern results. In part of pore size distribution, both of the synthetic materials had the narrow pore size distribution as 2.43 nm same as FSM-16.

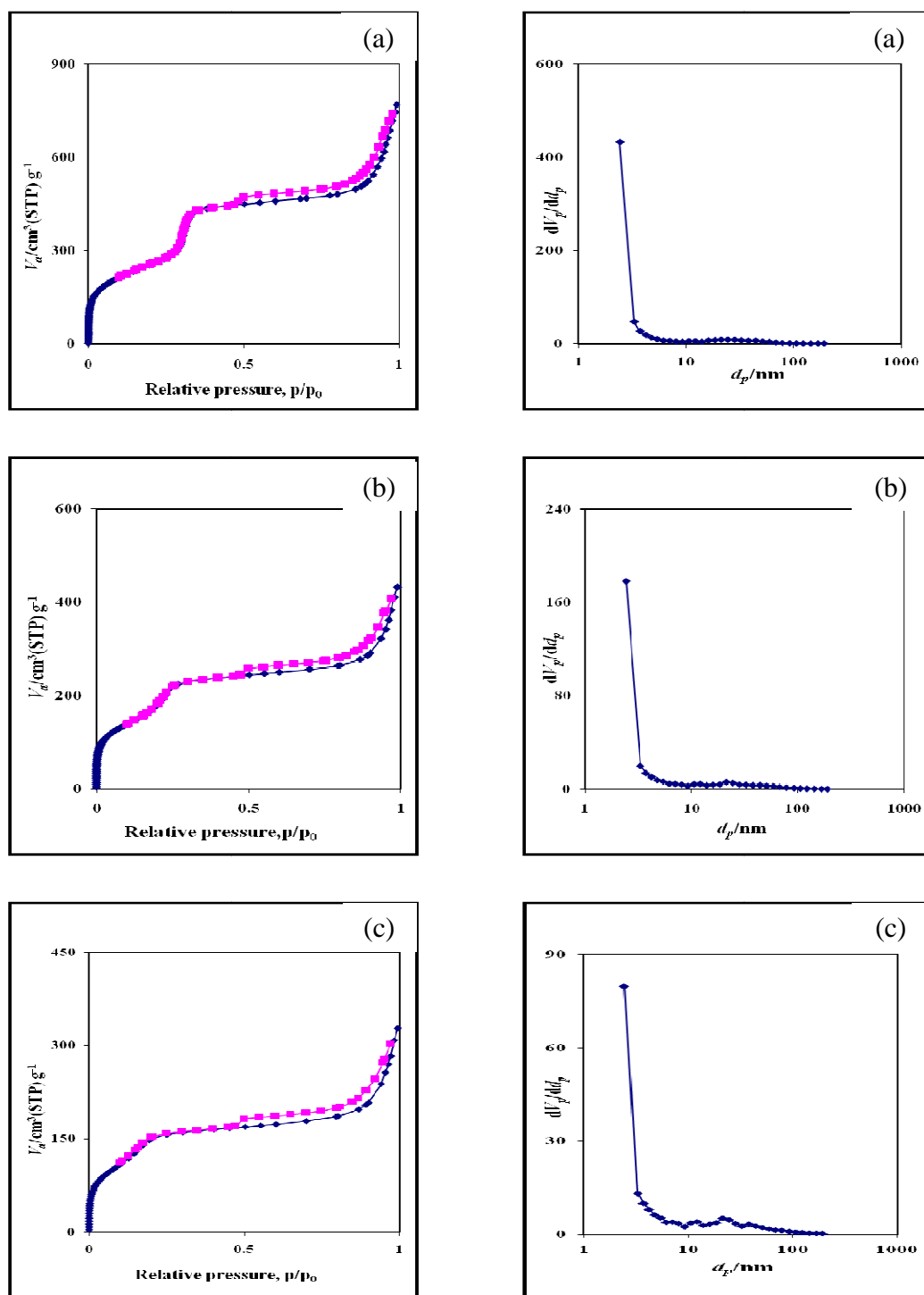


Figure 4.11 N_2 adsorption-desorption isotherm and BJH-pore size distribution of (a) FSM-16, (b) FSM-16-PrSO₃H and (c) FSM-16-ArSO₃H.

In comparison with SBA-15 (Table 4.1), the pure FSM-16 and sulfonic functionalized FSM-16 had more surface area and wall thickness than SBA-15 materials. It performed that all the sample of FSM-16 had higher hydrothermal stability as compared to SBA-15 materials.

Table 4.5 Textural properties of FSM-16 and sulfonic functionalized FSM-16.

Catalyst	Total specific surface area ^a (m ² ·g ⁻¹)	Pore size distribution ^b (nm)	Mesopore volume ^b (cm ³ ·g ⁻¹)	$d_{(100)}$ ^c (nm)	Wall thickness ^d (nm)
FSM-16	928	2.43	1.13	3.77	1.92
FSM-16-PrSO ₃ H	570	2.43	0.57	3.71	1.85
FSM-16-ArSO ₃ H	451	2.43	0.37	3.68	1.82

^aCalculated using the BET plot method,

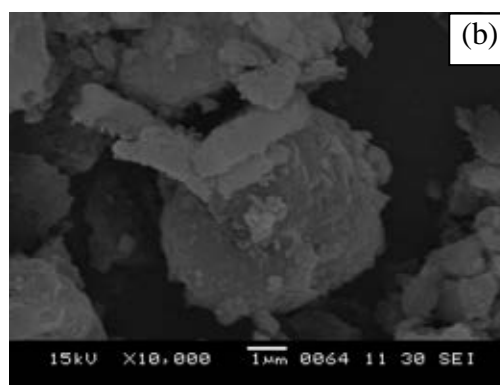
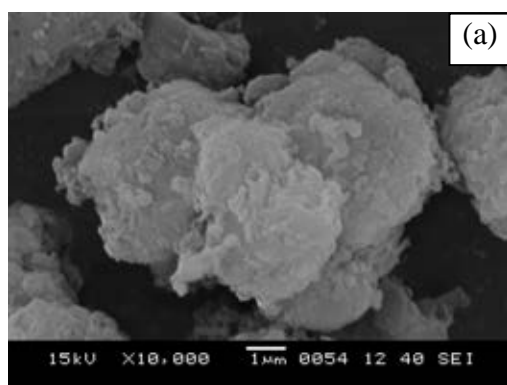
^bCalculated using the BJH method,

^cCalculated using XRD, Jade5.6,

^dCalculated as: a_0 -pore size ($a_0 = 2 \times d_{(100)} / \sqrt{3}$)

4.2.1.3 SEM images

The SEM images of pure FSM-16, FSM-16-PrSO₃H and FSM-16-ArSO₃H are illustrated in Figure 4.12. Morphology of sulfonic functionalized FSM-16 samples were similar to pure FSM-16 which were irregular particle shape. They indicated that morphology of the original kanemite aggregated to irregular shape. The average sizes of all catalysts in the range 5-8 μm.



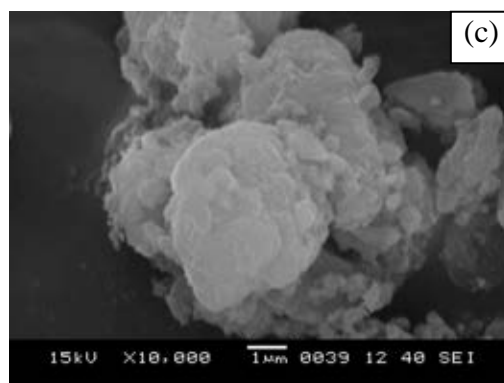


Figure 4.12 SEM images of (a) FSM-16, (b) FSM-16-PrSO₃H and (c) FSM-16-ArSO₃H.

4.2.1.4 Elemental analysis and acid-base titration

The number of sulfonic acid groups in the mesoporous silica was measured quantitatively by acid-base titration using sodium chloride as ion-exchange agent. The sulfur content of the modified mesoporous silica was determined by sulfur content comply in Table 4.6.

Table 4.6 Sulfur analysis and acid value of sulfonic functionalized FSM-16.

Catalyst	Sulfur analysis ^a (wt%)	H ⁺ content ^b (mmol/g)
FSM-16-PrSO ₃ H	2.36	1.08
FSM-16-ArSO ₃ H	2.62	1.14

^aSulfur analysis, measured from Sulfur analyzer,

^bAcid capacity defined as millimole of acid centers per gram of catalyst, obtained directly by titration (mmol H⁺/g)

In comparison with sulfonic acid group in SBA-15 (Table 4.2), the acid value and sulfur content of sulfonic functionalized SBA-15 were higher than sulfonic FSM-16 due to the large pore diameter of SBA-15 thus, the organosulfonic group could be easy incorporate into the pore.

4.2.2 The physico-chemical properties of aluminium functionalized FSM-16

4.2.2.1 XRD results

Al-FSM-16 were synthesized with Si/Al ratios in gel composition of 10, 25, 50 and 100 by alumination method following Kevan *et al.* [59]. After alumination, the XRD pattern showed hexagonal plane which implied to the thermal stability of

FSM-16 structure. The XRD pattern of Al-FSM-16 compared to calcined FSM-16 show in Figure 4.13. The peaks of four Si/Al ratios in Al-FSM-16 exhibited increasing intensity of the (100) reflection plane along with decreasing aluminum contents. Additionally, XRD patterns of the modified materials were shifted slightly to higher angle comparing to pure FSM-16 resulting from the shrinkage during the recalcination process or change in lattice parameters and d-spacing due to Al inclusion in crystal structure of FSM-16 [62].

In comparison with Al-SBA-15, the diffraction peaks of Al-FSM-16 materials were shifted to higher 2 theta values. It performed Al-FSM-16 contained shorter d-spacing than Al-SBA-15.

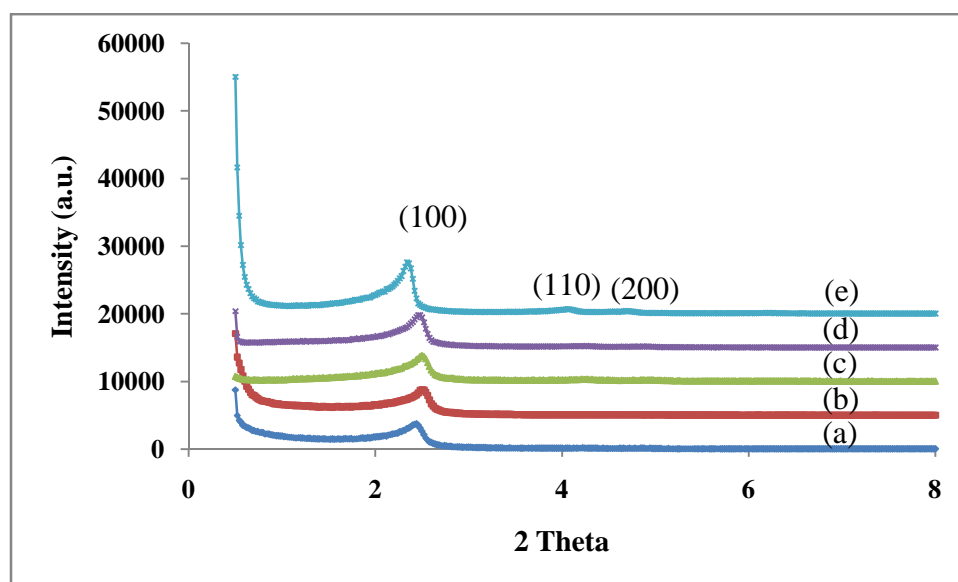


Figure 4.13 X-ray powder diffraction patterns of calcined Al-FSM-16 with various Si/Al mole ratios in reactant mixture (a) FSM-16(10), (b) Al-FSM-16(25), (c) Al-FSM-16(50), (d) Al-FSM-16(100) and (e) Al-FSM-16.

4.2.2.2 Sorption properties of Al-FSM-16

The N₂ adsorption-desorption isotherm of Al-FSM-16 catalysts in four Si/Al mole ratios are show in Figure 4.14. The samples performed type IV adsorption isotherm. The pore size distributions obtained from BJH equation are show in Figure 4.15. All sample exhibited a narrow distribution with the pore size of 2.43 nm. which small in comparison previous report by Wang *et al.* that was 0.6 nm. By

comparing to the pore size of pure silica FSM-16 in Figure 4.11(a), the pore size of all Al-FSM-16 samples still unchanged.

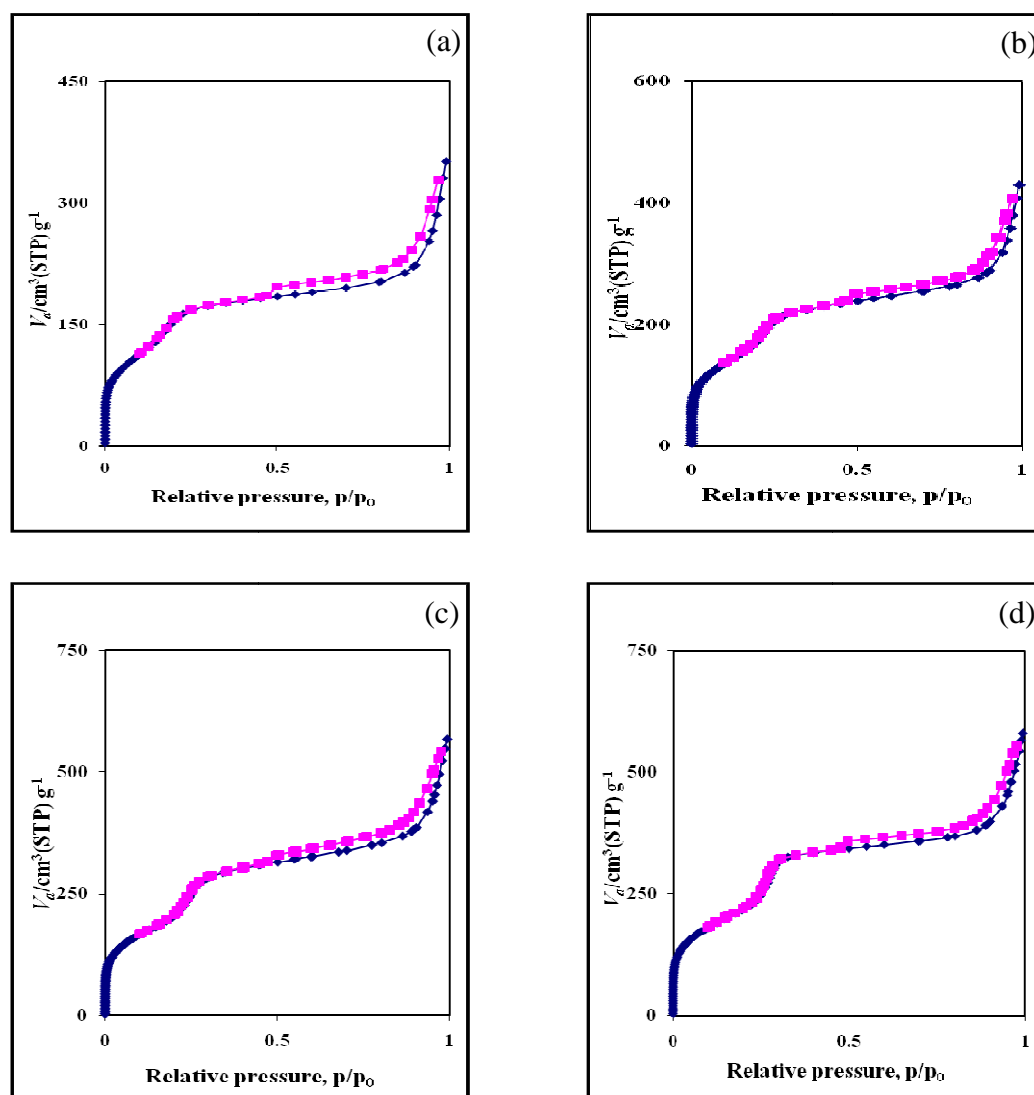


Figure 4.14 N_2 adsorption-desorption isotherms of (a) Al-FSM-16(10), (b) Al-FSM-16(25), (c) Al-FSM-16(50) and (d) Al-FSM-16(100).

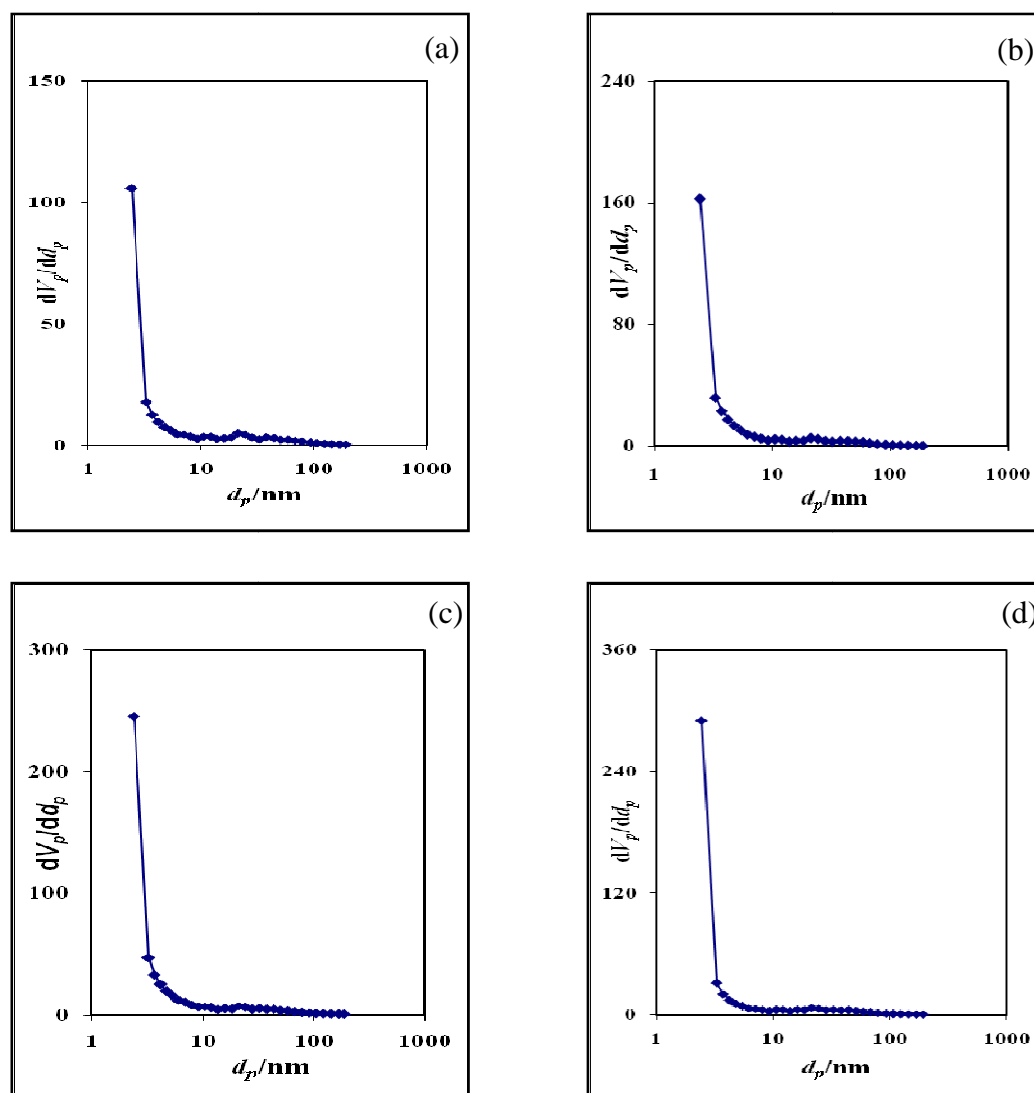


Figure 4.15 BJH-Pore size distributions of (a) Al-FSM-16(10), (b) Al-FSM-16(25), (c) Al-FSM-16(50) and (d) Al-FSM-16(100).

Incorporated Al in the FSM-16 framework led to a reduction in the amount of nitrogen up taken in FSM-16 depended on the quantities of aluminum. This result is in agreement with those in literatures [13, 63-64]. In addition, when Al content was increased, the d-spacing was decreased indicating that the distance from each plane was reduced. Considering the effect of aluminum content in catalysts (Table 4.7), the data showed the d-spacing and wall thickness decreased when aluminum quantity increased, corresponding to the decrease of d-spacing as $d_{(100)}$ in the Bragg's equation.

Table 4.7 Textural properties of FSM-16 and Al-FSM-16 with various Si/Al ratios.

Catalyst	Total specific surface area ^a (m ² ·g ⁻¹)	Pore size distribution ^b (nm)	Mesopore volume ^b (cm ³ ·g ⁻¹)	$d_{(100)}$ ^c (nm)	Wall thickness ^d (nm)
FSM-16	928	2.43	1.13	3.77	1.92
Al-FSM-16(10)	461	2.43	0.43	3.53	1.65
Al-FSM-16(25)	553	2.43	0.57	3.53	1.65
Al-FSM-16(50)	697	2.43	0.78	3.56	1.68
Al-FSM-16(100)	784	2.43	0.79	3.62	1.75

^aCalculated using the BET plot method,

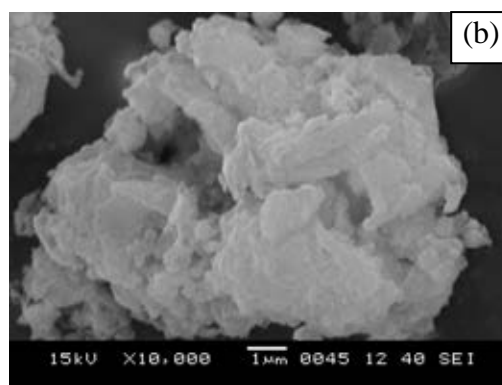
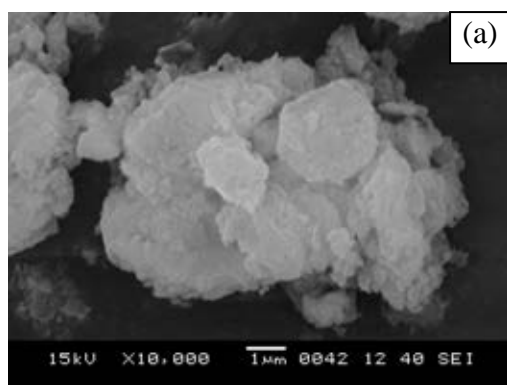
^bCalculated using the BJH method,

^cCalculated using XRD, Jade5.6,

^dCalculated as: a_0 -pore size ($a_0 = 2 \times d_{(100)} / \sqrt{3}$)

4.2.2.3 SEM images

The SEM images of acid modified FSM-16 samples are illustrated in Figure 4.16. All four Si/Al ratio samples showed irregular particle shape nearly same as sulfonic functionalized FSM-16. They indicated the morphology surface of the original kanemite was preserved. The average sizes of all Al-FSM-16 materials were in the range of 5-8 μm .



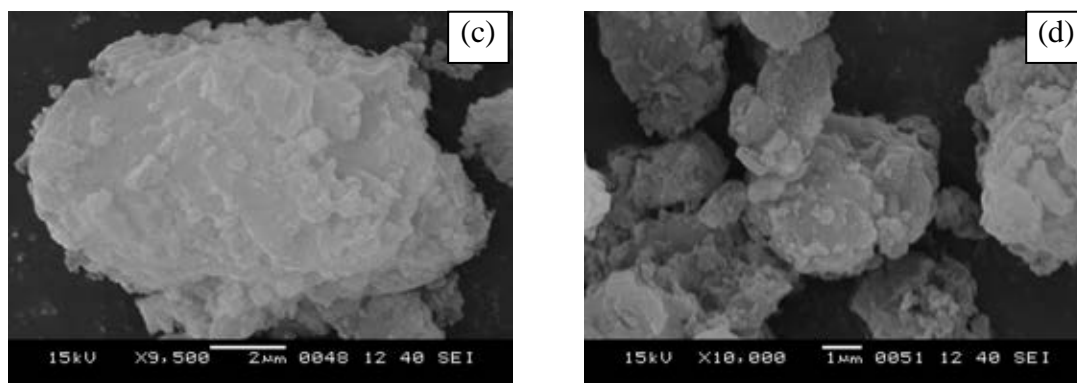


Figure 4.16 SEM images of (a) Al-FSM-16(10), (b) Al-FSM-16(25), (c) Al-FSM-16(50), and (d) Al-FSM-16(100).

4.2.2.4 Elemental analysis and acid-base titration

The number of aluminium in the mesoporous silica was measured quantitatively by acid-base titration using sodium chloride as ion-exchange agent. The acid site of Al-FSM-16 samples were increased following the aluminum contents. Moreover, the elemental analysis result showed that the parts of aluminum were in the structure of catalyst. The Si/Al molar ratios in catalysts of Al-FSM-16 were lower than those in gel. The results suggested that aluminium atoms had incorporated into the structure. The higher content of aluminium might be due to the loss of silica in framework. The agglomeration of silicon atoms was plausible for restriction silicon to access the framework.

In comparison with Al-SBA-15, the Al-FSM-16 materials showed higher Si/Al mole ratios in catalysts than Al-SBA-15. It performed Al-FSM-16 contained lower acid strength than Al-SBA-15 which corresponded to H^+ content.

Table 4.8 Elemental analysis and acid value of aluminium functionalized FSM-16.

Catalysts	Si/Al mole ratios		H^+ content ^c (mmol/g)
	in gel composition ^a	in catalysts ^b	
Al-FSM-16(10)	10	9.01	0.34
Al-FSM-16(25)	25	20.23	0.25
Al-FSM-16(50)	50	35.52	0.20
Al-FSM-16(100)	100	71.44	0.17

^aCalculated from reagent quantities,

^bAluminum (Al) was determined by ICP-AAS,

^cAcid capacity defined as millimole of acid centers per gram of catalyst, obtained directly by titration (mmol H^+ /g).

4.3 Comparison of synthetic catalysts

4.3.1 Acidity

The acid strength in the synthetic catalysts were measured quantitatively by acid-base titration using sodium chloride as ion-exchange agent. Table 4.9 show the propyl and aryl sulfonic mesoporous materials with contained high acid strength above 1.0 mmol/g. On the other hand, aluminium mesoporous silica matters contained less acidity around 0.70-0.17 mmol/g depend on Al content. Generally, esterification of dicarboxylic acid and alcohol could occur spontaneously but the acid catalyst was perferred to reduce reaction time and activation energy reaction owing to its higher acceleration ability. Thus, the suitable synthetic catalysts should be strong acid sulfonic functionalized mesoporous catalysts.

Although the aryl sulfonic mesoporous contained high acidity, but chemicals for grafting aryl sulfonic acid group was expensive. So, propyl sulfonic mesoporous matters were selected to be used in experiments.

Table 4.9 Acid value of synthetic catalysts.

Catalysts	Acid strength (mmol/g)
SBA-15-Pr-SO ₃ H	1.38
SBA-15-Ar-SO ₃ H	1.40
Al-SBA-15(Si/Al = 10)	0.70
Al-SBA-15(Si/Al = 25)	0.64
Al-SBA-15(Si/Al = 50)	0.40
Al-SBA-15(Si/Al = 100)	0.20
FSM-16-Pr-SO ₃ H	1.08
FSM-16-Ar-SO ₃ H	1.14
Al-FSM-16(Si/Al = 10)	0.34
Al-FSM-16(Si/Al = 25)	0.25
Al-FSM-16(Si/Al = 50)	0.20
Al-FSM-16(Si/Al = 100)	0.17

4.3.2 Hydrothermal stability test

4.3.2.1 XRD results

The hydrothermal stability test of SBA-15-PrSO₃H and FSM-16-PrSO₃H by hydrothermal method were examined by heating sample in boiling water for 24 hrs under reflux [65]. After hydrothermal stability test, both samples remained hexagonal structure. The crystallinity of SBA-15-PrSO₃H and FSM-16-PrSO₃H under hydrothermal stability test decreased less than catalysts before treatment (Figure 4.17). After hydrothermal stability test in case of FSM-16-PrSO₃H, peak at (100) were clearly shifted to higher 2-Theta value due to decreasing of wall thickness.

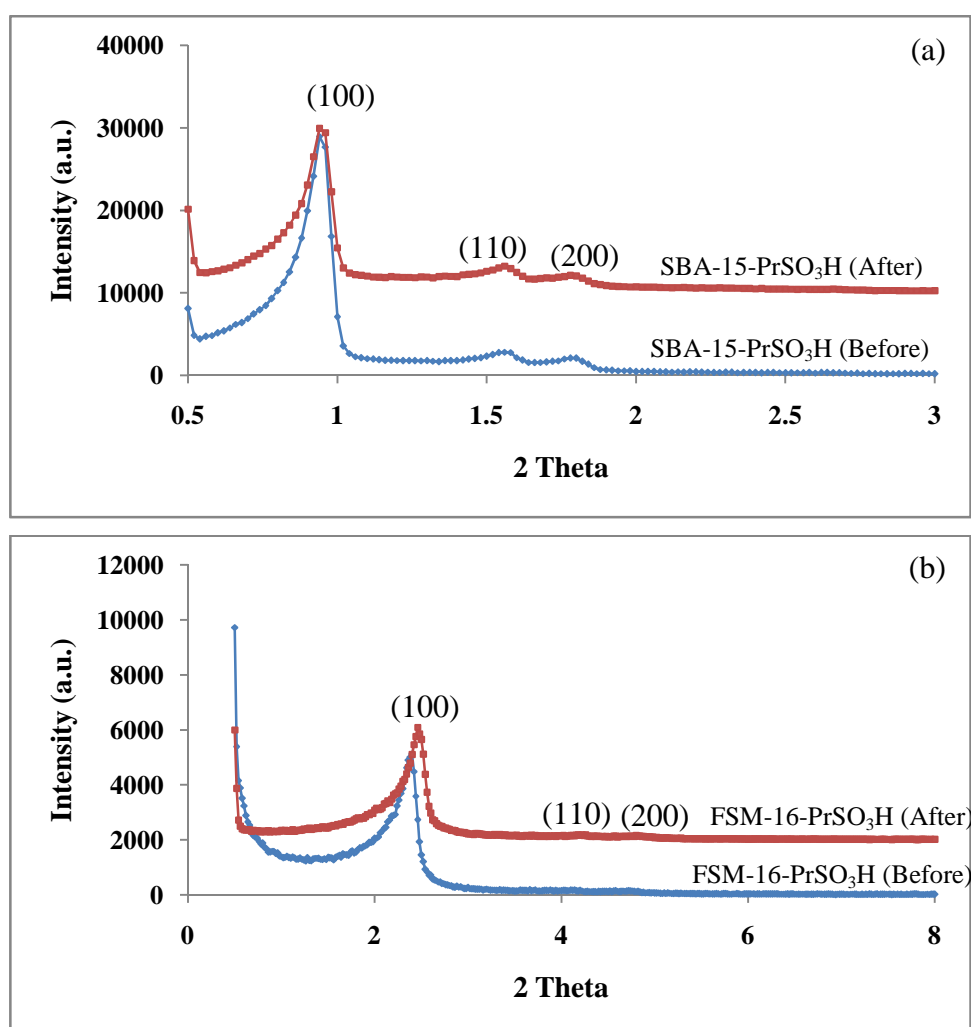


Figure 4.17 X-ray powder diffraction patterns of synthesized catalysts with hydrothermal method comparison with hydrothermal stability test (a) SBA-15-PrSO₃H and (b) FSM-16-PrSO₃H.

4.3.2.2 Sorption properties of synthetic catalysts

Both of the N₂ adsorption isotherms of before and after hydrothermal stability test of SBA-15-PrSO₃H and FSM-16-PrSO₃H samples remained type IV. The pore volume was increased while wall thickness was decreased after hydrothermal stability test (Table 4.10). A relative obviously decreasing on the wall thickness and surface area because the collapse of mesostructures and reconstruction of frameworks could be observed by the SEM [65-66].

Table 4.10 Textural properties of synthesized SBA-15-PrSO₃H and FSM-16-PrSO₃H with hydrothermal method before and after thermal stability test.

Catalyst	Total specific surface area ^a (m ² ·g ⁻¹)	Pore size distribution ^b (nm)	Mesopore volume ^b (cm ³ ·g ⁻¹)	Wall thickness ^d (nm)
SBA-15-PrSO ₃ H (before)	365	9.23	0.67	1.62
SBA-15-PrSO ₃ H (after)	254	9.23	0.82	1.61
FSM-16-PrSO ₃ H (before)	570	2.43	0.57	1.85
FSM-16-PrSO ₃ H (after)	466	2.43	0.67	1.82

^aCalculated using the BET plot method,

^bCalculated using the BJH method,

^cCalculated using XRD, Jade5.6,

^dCalculated as: a_0 -pore size ($a_0 = 2 \times d_{(100)} / \sqrt{3}$)

When comparison between SBA-15-PrSO₃H and FSM-16-PrSO₃H, the sulfonic functionalized FSM-16 contained high surface area and wall thickness than sulfonic functionalized SBA-15 materials. It performed that the FSM-16- PrSO₃H was higher hydrothermal stability than SBA-15- PrSO₃H material.

4.3.2.3 SEM images

The SEM images of hydrothermal stability samples are illustrate in Figure 4.18. Both before and after hydrothermal stability test samples exhibited the same morphology as precursor (the rope-like morphology for SBA-15-PrSO₃H and the irregular particle shape for FSM-16-PrSO₃H) but the particle size was reduced.

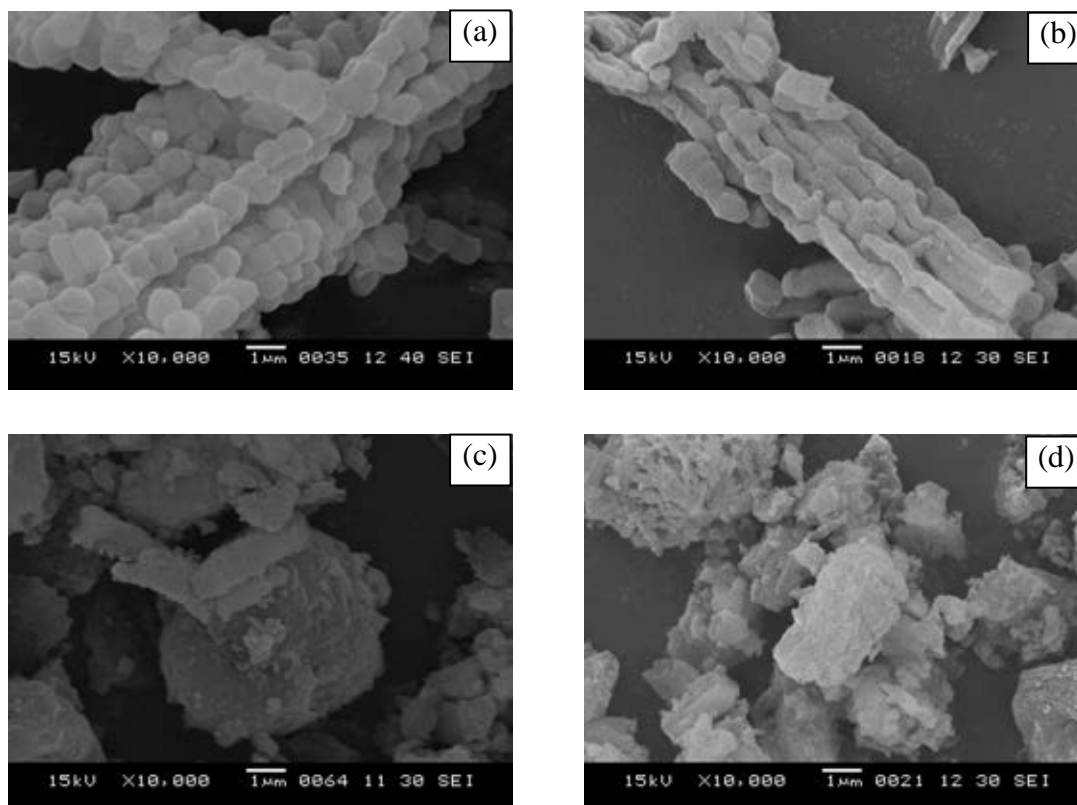


Figure 4.18 SEM images of catalytic synthesis (a) before, (b) after hydrothermal stability test of SBA-15-PrSO₃H and (c) before, (d) after hydrothermal stability test of FSM-16-PrSO₃H.

4.3.3 Acid leaching test

Leaching out of acid strength was determined by pH meter measuring the different between initial pH and final pH of solvent which stirred with catalysts at room temperature for 30 min. As showed in Table 4.11, FSM-16-PrSO₃H showed less leaching out of acid strength than SBA-15-PrSO₃H both in DI water and 2-ethyl hexanol solvent. Therefore, FSM-16-PrO₃H was able to be an efficient catalyst.

Table 4.11 Leaching out of synthetic catalysts.

Catalysts	Solvent					
	DI water			2-Ethyl hexanol		
	pH _{initial}	pH _{end}	ΔpH	pH _{initial}	pH _{end}	ΔpH
SBA-15-PrSO ₃ H	5.89	3.03	2.86	3.97	0.99	2.98
FSM-16-PrSO ₃ H	5.89	3.34	2.55	3.97	1.34	2.63

4.3.4 Initial rate, TON and TOF

Turnover number (abbreviated TON) was used to refer the maximum molecules of substrate could be converted into product per catalytic site. The term turnover frequency (abbreviated TOF) was used to refer to the turnover number per unit time. Initial rate, TON and TOF of synthetic catalysts in esterification of adipic acid and 2-ethyl hexanol at 30 min are show in Table 4.12

Table 4.12 Initial rate, TON and TOF of synthetic catalysts in esterification of adipic acid with 2-ethyl hexanol at 30 min.

Catalyst	initial rate (mmol min ⁻¹)			TON ^d	TOF ^e (min ⁻¹)
	r _m ^a	r _d ^b	r _p ^c		
SBA-15-PrSO ₃ H	0.152	0.249	0.402	68.6	2.29
FSM-16-PrSO ₃ H	0.161	0.262	0.423	78.4	2.61

^aCalculated as: [{(% monoester yield × total reactant) / 100 } / M.W. of monoester] / time × 1000,

^bCalculated as: [{(% diester yield × total reactant) / 100 } / M.W. of diester] / time × 1000,

^cCalculated as: r_m + r_d,

^dCalculated as: (r_p × time) / (acid amount × catalytic amount),

^eCalculated as: TON/time.

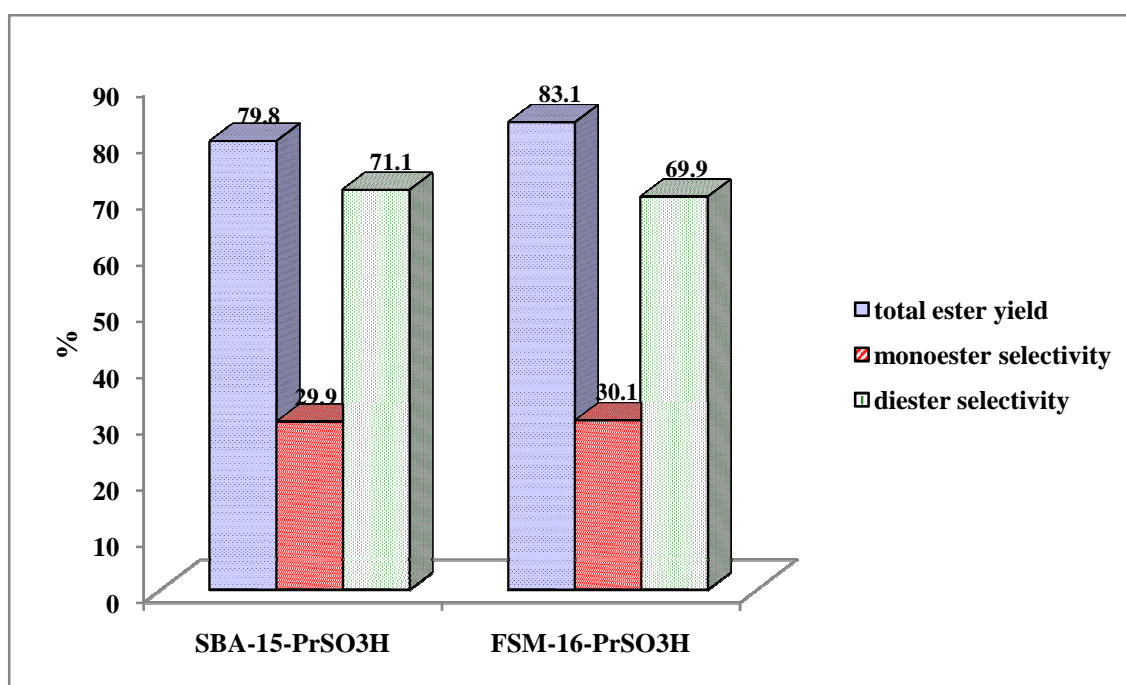


Figure 4.19 Ester yield and product selectivity over SBA-15-PrSO₃H and FSM-16-PrSO₃H.

As a result, FSM-16-PrSO₃H provided higher initial rate in both of monoester and diester than SBA-15-PrSO₃H. Moreover, TON and TOF of FSM-16-PrSO₃H, which indicated the maximum molecules of substrate could be converted into product per acid size of catalyst, were 78.4 and 2.61, respectively. According to these results, FSM-16-PrSO₃H was an appropriate catalyst for this experiment.

4.4 Catalytic activities of FSM-16-PrSO₃H in lubricant preparation

In this research, the catalytic performance of synthetic FSM-16-PrSO₃H was evaluated in monoester and diester preparation.

4.4.1 Effect of reaction time

The effect of reaction time was investigated. The catalytic activities of FSM-16-PrSO₃H are performed in Table 4.13. The reaction time of adipic acid esterification was varied in the range of 0.5-8 hrs.

Table 4.13 Effect of reaction time on ester yield and product distribution over FSM-16-PrSO₃H.

Time (h)	% ester yield			% ester selectivity	
	mono	di	total ester	mono	di
0.5	25.0	58.1	83.1	30.1	69.9
1	21.0	66.0	87.0	24.1	75.9
2	17.6	70.9	88.5	19.9	80.1
3	15.0	76.3	91.3	16.4	83.6
4	14.9	79.6	94.5	15.8	84.2
5	13.5	82.7	96.2	14.0	86.0
6	13.4	82.0	95.4	14.0	86.0
7	12.9	80.9	93.8	13.8	86.2
8	13.4	79.1	92.5	14.5	85.5

Esterification conditions: 2-ethyl hexanol/dicarboxylic acid mole ratio as 2; reaction temperature 100°C; catalytic amount 3wt.% base on reaction mixture; and stirring speed 150 rpm.

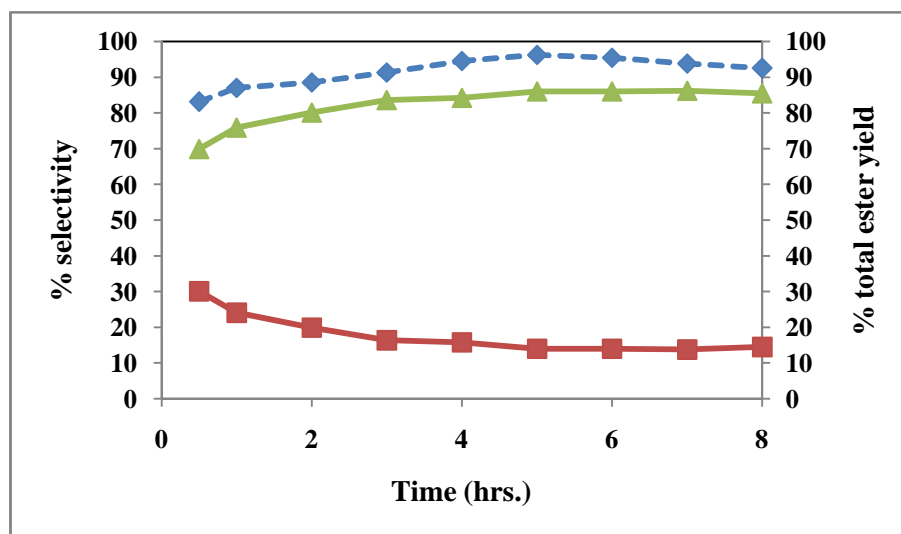


Figure 4.20 Influence of reaction time on the ester yield over FSM-16-PrSO₃H. Reaction conditions: 2-ethyl hexanol/adipic acid mole ratio as 2; reaction temperature 100°C; catalytic amount 3 wt.%; stirring speed 150 rpm. (Symbols: (■) monoester selectivity, (▲) diester selectivity and (◆) total ester yield).

As a result, the total ester yield was increased till five hours, which was obviously raising from 83.1% to 96.2%. The highest yield was obtained at the reaction time as 5 hrs. when the reaction time continued to increase over 5 hrs., the total ester yield was a bit decreased. The effect of reaction time on promoting esterification can be explained because the esters were transformed back to starting material. Therefore, subsequent experiments were accomplished at 5 hrs.

4.4.2 Effect of reaction temperature

To determine the effect of reaction temperature, the experiments were conducted at temperature ranging from 80 to 120°C. As show the results in Table 4.14.

Table 4.14 Effect of reaction temperature on ester yield and product distribution over FSM-16-PrSO₃H.

Temperature (°C)	% ester yield			% ester selectivity	
	mono	di	total ester	mono	di
80	21.3	74.7	96.0	22.2	77.8
90	16.6	80.9	97.5	17.0	83.0
100	13.5	82.7	96.2	14.0	86.0
110	14.6	81.6	96.2	15.2	84.8
120	16.8	79.6	96.4	17.4	82.6

Esterification conditions: 2-ethyl hexanol/dicarboxylic acid mole ratio as 2; reaction time 5 hrs.; catalytic amount 3wt.% base on reaction mixture; and stirring speed 150 rpm.

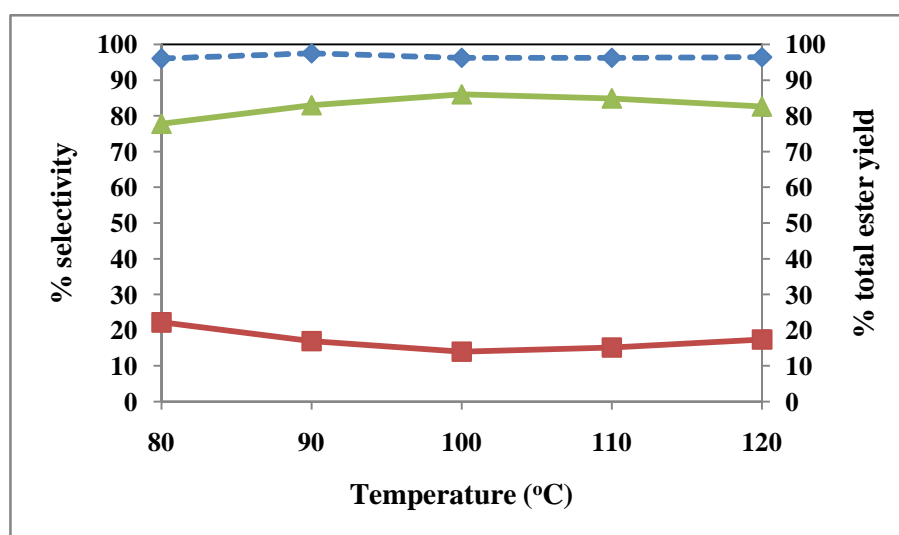


Figure 4.21 Influence of reaction temperature on the ester yield over FSM-16-PrSO₃H. Reaction conditions: 2-ethyl hexanol/adipic acid mole ratio as 2; reaction time 5 hrs.; catalytic amount 3 wt.%; stirring speed 150 rpm. (Symbols: (■) monoester selectivity, (▲) diester selectivity and (◆) total ester yield).

Table 4.14 show the influence of reaction temperature on the ester yield and selectivity. The formation of ester products was promoted concomitantly with an increase in the selectivity to diester when the temperature was raised from 80 to 100°C. As the reaction temperature was increased, all reactant molecules will gain more kinetic energy that will eventually accelerate the mass transfer rate between the

reactants-catalyst phases that resulted in the formation of diesters in a shorter time [67]. However, the total ester yield was decreased inversely at temperature over 110°C. It should be due to a hydrolysis of the ester products with water, generated as the esterification by-product. According to these results, a reaction temperature of 100°C was selected.

4.4.3 Effect of catalytic amount

The effect of catalytic amount effect on ester yield and product distribution was studied using different amount of FSM-16-PrSO₃H. The catalyst amount was varied in the range of 0 to 10 wt.% based on reaction mixture. As see the result in Table 4.15.

Table 4.15 Effect of catalytic amount on ester yield and product distribution over FSM-16-PrSO₃H.

Catalytic amount (wt.%)	% ester yield			% ester selectivity	
	mono	di	total ester	mono	di
0	21.9	19.6	41.5	52.8	47.2
1	17.7	72.0	89.7	19.7	80.3
2	14.4	79.3	93.7	15.4	84.6
3	13.5	82.7	96.2	14.0	86.0
4	15.5	80.7	96.2	16.1	83.9
5	13.9	80.0	93.9	14.8	85.2
10	12.7	71.1	83.8	15.2	84.8

Esterification conditions: 2-ethyl hexanol/dicarboxylic acid mole ratio as 2; reaction time 5 hrs.; reaction temperature 100°C; and stirring speed 150 rpm.

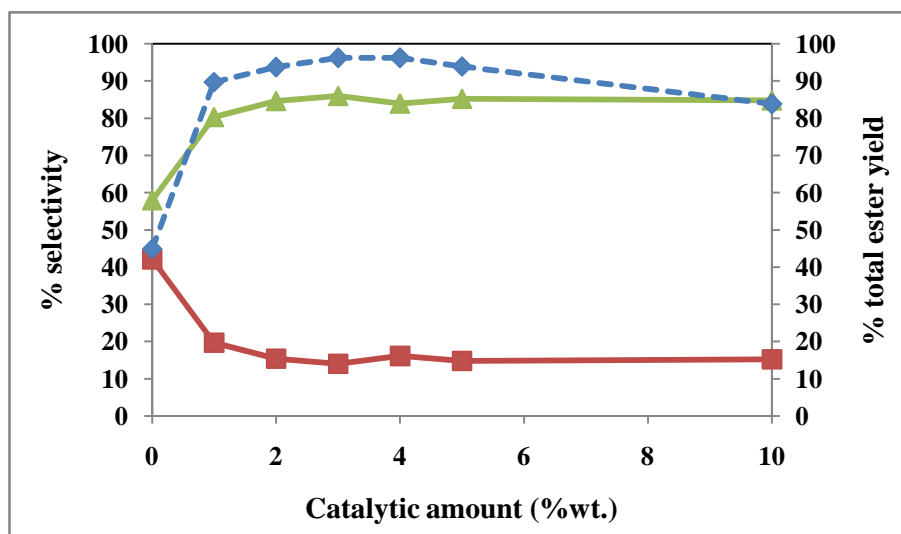


Figure 4.22 Influence of catalytic amount on the ester yield over FSM-16-PrSO₃H.

Reaction conditions: 2-ethyl hexanol/adipic acid mole ratio as 2; reaction time 5 hrs.; reaction temperature 100°C; stirring speed 150 rpm. (Symbols: (■) monoester selectivity, (▲) diester selectivity and (◆) total ester yield).

Without the addition of any catalyst, this result found that the esterification spontaneously occurred at 100°C which provided 41.5% of the total ester. Total ester yields and diester selectivity were increased when the amount of catalyst was raised in the reaction mixture. It was obvious that, with increased catalytic amount, the acid sites of catalyst for reaction were also increased. The highest yield (96.2%) was obtained at the catalytic amount of 3 wt.% by weight of reaction mixture. However, the yield slightly decreased at the catalytic amount over 3wt.%. This may be caused by the excess catalyst disturbed the mixing of dicarboxylic acid, alcohol and catalyst by phase reaction. Based upon these results, the catalytic amount used in the next experiments was 3 wt.% of the reaction mixture.

4.4.4 Effect of stirring speed

The effect of stirring speed on ester yield and product distribution over FSM-16-PrSO₃H is show in Table 4.16. The highest yield was obtained at the stirring speed 150 rpm. However, this effect on promoting esterification was not significant different.

Table 4.16 Effect of stirring speed on ester yield and product distribution over FSM-16-PrSO₃H.

stirring speed (rpm.)	% ester yield			% ester selectivity	
	mono	di	total ester	mono	di
50	14.9	81.1	96.0	15.5	84.5
150	13.5	82.7	96.2	14.0	86.0
250	14.5	83.1	97.6	14.9	85.1

Esterification conditions: 2-ethyl hexanol/dicarboxylic acid mole ratio as 2; reaction time 5 hrs.; reaction temperature 100°C; and catalytic amount 3wt.% base on reaction mixture.

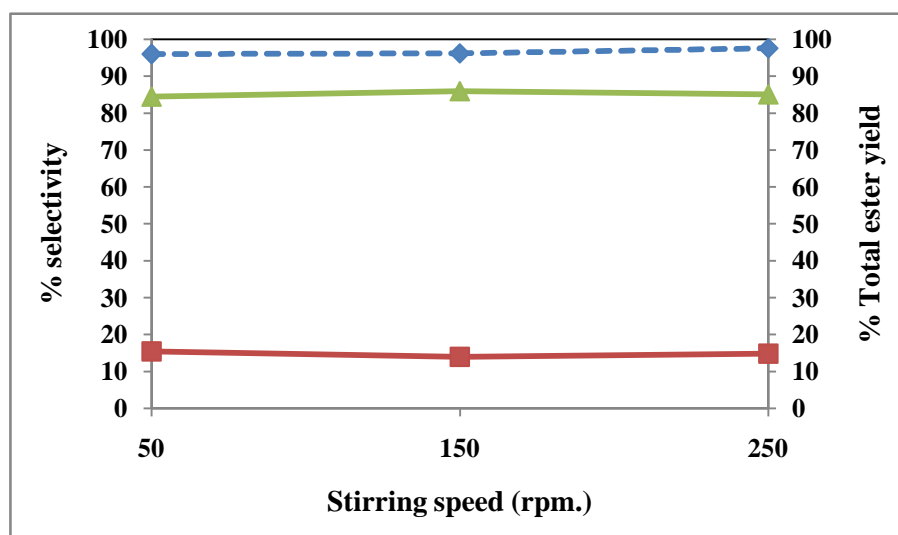


Figure 4.23 Influence of stirring speed on the ester yield over FSM-16-PrSO₃H. Reaction conditions: 2-ethyl hexanol/adipic acid mole ratio as 2; reaction time 5 hrs.; reaction temperature 100°C; catalytic amount 3 wt.%. (Symbols: (■) monoester selectivity, (▲) diester selectivity and (◆) total ester yield).

4.4.5 Effects of mole ratio of 2-ethyl hexanol to adipic acid

Effect of molar ratio of 2-ethyl hexanol to adipic acid on the esterification over FSM-16-PrSO₃H was also studied, as show in Table 4.17.

Table 4.17 Effect of 2-ethyl hexanol to adipic acid molar ratio on ester yield and product distribution over FSM-16-PrSO₃H.

2-ethyl hexanol : adipic acid molar ratio	% ester yield			% ester selectivity	
	mono	di	total ester	mono	di
1	24.3	12.3	36.6	66.4	33.6
2	13.5	82.7	96.2	14.0	86.0
3	7.8	89.3	97.1	8.0	92.0
4	7.1	90.3	97.4	7.3	92.7
5	6.9	91.9	98.8	7.0	93.0

Esterification conditions: reaction time 5 hrs.; reaction temperature 100°C; catalytic amount 3wt.% base on reaction mixture; and stirring speed 150 rpm.

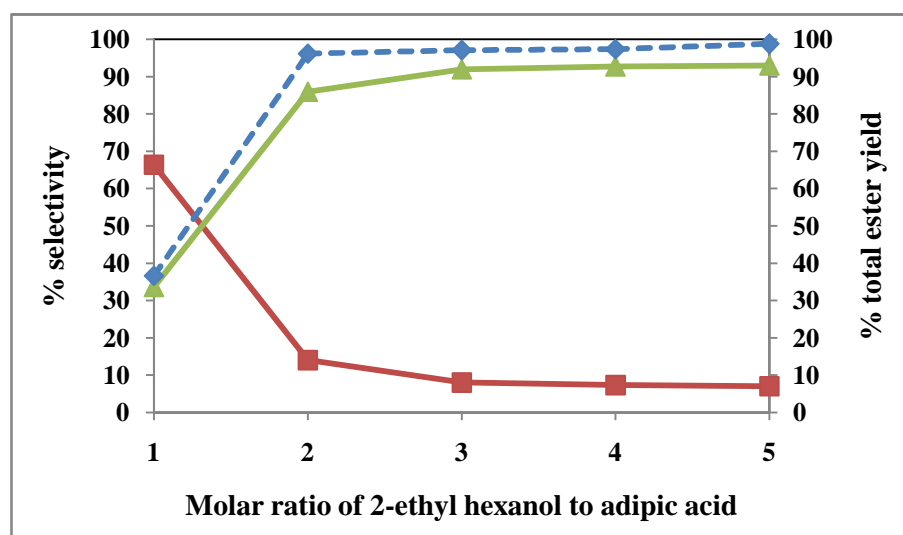


Figure 4.24 Influence of 2 ethyl hexanol to adipic acid mole ratio on the ester yield over FSM-16-PrSO₃H. Reaction conditions: reaction time 5 hrs.; reaction temperature 100°C; catalytic amount 3 wt.%; stirring speed 150 rpm. (Symbols: (■) monoester selectivity, (▲) diester selectivity and (◆) total ester yield).

The reaction results in Table 4.17 indicated an increasing of the total ester yield and diester selectivity depend on ratio between 2-ethyl hexanol and adipic acid. When the amount of 2-ethyl-1-hexanol was increased, the transformation of the monoester to diester was successfully facilitated by the excess of alcohol molecules.

Thus, the optimum condition was carried out over catalyst amount of 3% wt. of the reaction mixture at 100°C for 5 hrs. with stirring speed 150 rpm. and mole ratio of alcohol to carboxylic acid as 2 which exhibited highest 2-ethyl hexyl adipate esters yield as 96.2% with 86.0% of diester and 14.0% of monoester selectivities.

4.4.6 Effect of catalytic types

4.4.6.1 Homogeneous catalysts

The effect of homogeneous catalyst on esterification of adipic acid with 2-ethyl hexanol is show in Table 4.18.

Table 4.18 Effect of homogeneous catalysts on ester yield and product distribution.

Catalyst	% ester yield			% ester selectivity	
	mono	di	total ester	mono	di
H ₂ SO ₄	14.6	76.3	90.9	16.1	83.9
p-Toluene-SO ₃ H	18.8	73.5	92.3	20.4	79.6
FSM-16- PrSO ₃ H	13.5	82.7	96.2	14.0	86.0

Esterification conditions: 2-ethyl hexanol/dicarboxylic acid mole ratio as 2; reaction time 5 hrs.; reaction temperature 100°C; catalytic amount 3wt.% base on reaction mixture; and stirring speed 150 rpm.

In the case of sulfuric acid and organic sulfonic acid, the reaction was catalyzed by homogeneous catalyst provided lower total ester yield than FSM-16-PrSO₃H because the vigorous condition was not suitable for homogeneous catalysts.

4.4.6.2 Ion-exchange resins

Commercial sulfonic acid-based resins such as Amberlyst-15, Amberlyst-131 and Nafion SAC-13 were used in this study. Additionally, some characterization data corresponding to the commercial ion-exchange resins are depict in Table 4.19. In this case, the characterization was provided by the suppliers (Rohm & Hass for the Amberlyst resins and DuPont for Nafion SAC-13)

Table 4.19 Physicochemical and textural properties for ion-exchange resins^a

Catalyst	BET area (m ² ·g ⁻¹)	Pore size (Å)	Pore volume (cm ³ ·g ⁻¹)	Acid capacity ^b	Temp. limit (°C)
Amberlyst-15 (dry)	53	300	0.4	4.8	120
Amberlyst-131 (wet)	-	-	-	4.8	130
Nafion SAC-13	200	>100	0.6	0.12	200

^aProperties provided by the suppliers,^bMillimoles of acid centers per gram of catalyst

For commercial sulfonic acid-based resins such as Amberlyst-15, Amberlyst 131 and Nafion SAC-13, Amberlyst-15 performed the higher percentage of the total ester yield and the diester selectivity than Amberlyst-131 and Nafion SAC-13, respectively. Although Nafion SAC-13 had high surface area, but Amberlyst-15 contained 40 times higher in acid capacity. In the case of Amberlyst-131 wet, the presence of residual water, was likely to retard the reaction. Water molecule was a high affinity to the proton to the acid site, hampering the protonation of the diacid reaction. Thus, Amberlyst-15 performed the best catalytic performance in this reaction.

When comparison with FSM-16-PrSO₃H, although Amberlyst-15 contained high acid capacity, but FSM-16-PrSO₃H had higher surface area and pore volume which increased substrate contacting possibility on catalyst surface. In addition, it contained suitable pore size which increased diester selectivity.

Table 4.20 Effect of ion-exchange resins catalysts on ester yield and product distribution.

Catalyst	% ester yield			% ester selectivity	
	mono	di	total ester	mono	di
Amberlyst-15 (dry)	16.9	77.4	94.3	17.9	82.1
Amberlyst-131 (wet)	28.1	61.8	89.9	31.3	68.7
Nafion SAC13	38.2	46.8	85.0	44.9	55.1
FSM-16- PrSO ₃ H	13.5	82.7	96.2	14.0	86.0

Esterification conditions: 2-ethyl hexanol/dicarboxylic acid mole ratio as 2; reaction time 5 hrs.; reaction temperature 100°C; catalytic amount 3wt.% base on reaction mixture; and stirring speed 150 rpm.

4.4.6.3 Zeolites

A variety of zeolites, including H-MCM-22, commercial H-ZSM-5 and commercial H-Beta with $\text{SiO}_2/\text{Al}_2\text{O}_3$ ratios around 30, were used for catalysts. For H-MCM-22, this catalyst was prepared in laboratory. In order to investigate the effect of the structure on monoester and diester preparation, the physical properties of zeolites were characterized by N_2 adsorption, as show in Table 4.21. The total specific surface area and micropore volume decreased in the following order: H-beta > H-MCM-22 > H-ZSM-5. With respect to their microporous characteristics, ZSM-5 contained two types of pores which both formed by 10-membered oxygen rings. Beta zeolite had 12-ring pore opening in three directions. For MCM-22, the structure composed of two non-connected pore systems, one with 12-ring pores, and the other having 10-ring pores. Structures of ZSM-5, MCM-22 and Beta zeolite are show in Figure 4.25.

Table 4.21 Physicochemical and textural properties for zeolites.

Catalyst	Total specific surface area ^a ($\text{m}^2\cdot\text{g}^{-1}$)	Micropore distribution, d_p^b (nm)	External surface area, S_{ext}^c ($\text{m}^2\cdot\text{g}^{-1}$)	Micropore volume, V_p^c ($\text{cm}^3\cdot\text{g}^{-1}$)
H-ZSM-5 ($\text{SiO}_2/\text{Al}_2\text{O}_3 = 28.2$)	307.8	0.6	37.384	0.1208
H-MCM-22 ($\text{SiO}_2/\text{Al}_2\text{O}_3 = 30$)	417.86	0.6	64.463	0.1593
H-Beta ($\text{SiO}_2/\text{Al}_2\text{O}_3 = 30.3$)	501.6	0.6	40.271	0.2370

^aCalculated using the BET plot method,

^bCalculated using the MP plot method,

^cCalculated using the t-plot method.

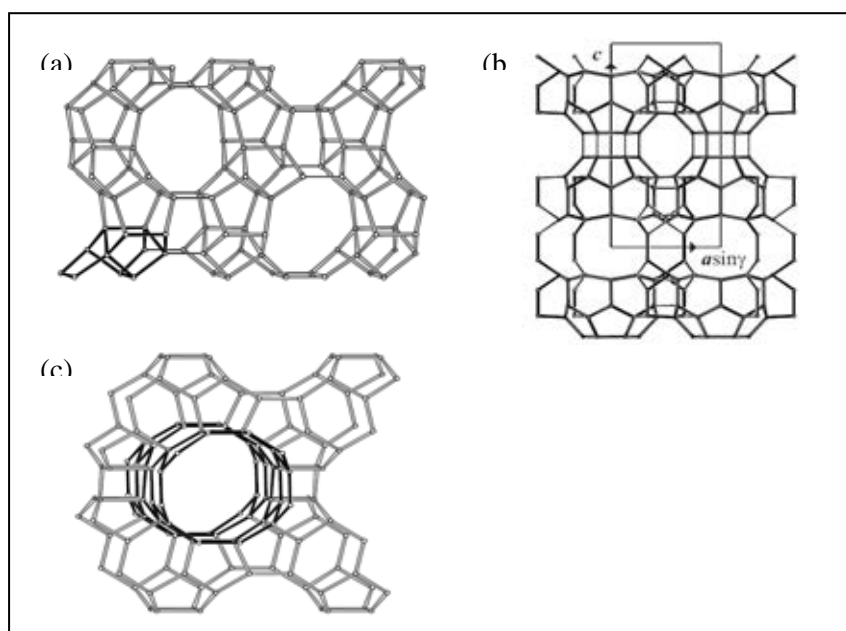


Figure 4.25 Structures of zeolites (a) ZSM-5, (b) MCM-22 and (c) Beta zeolite [68-70].

Among different zeolites, it was observed that H-beta with 12-membered ring channels performed high reactivity owing to an easier diffusion of the reactants and products in this large-pore zeolite. Contrastingly, H-ZSM-5 with 10-membered ring channels showed the lowest reactivity. This result indicated that pore-structure of zeolites affected on monoester and diester preparation.

In comparison with FSM-16-PrSO₃H, total ester yield and diester selectivity of FSM-16-PrSO₃H were higher than microporous materials. It was clear that the relatively large mesopores on derivitized FSM-16 facilitated the diffusion of the reactant and product molecules in lubricant synthesis.

Table 4.22 Effect of zeolite catalysts on ester yield and product distribution.

Catalyst	% ester yield			% ester selectivity	
	mono	di	total ester	mono	di
H-ZSM-5	21.6	24.7	46.3	46.7	53.3
H-MCM-22	25.8	26.9	52.7	49.0	51.0
H-beta	27.2	32.4	59.6	45.6	54.4
FSM-16- PrSO ₃ H	13.5	82.7	96.2	14.0	86.0

Esterification conditions: 2-ethyl hexanol/dicarboxylic acid mole ratio as 2; reaction time 5 hrs.; reaction temperature 100°C; catalytic amount 3wt.% base on reaction mixture; and stirring speed 150 rpm.

4.4.6.4 Mesoporous materials

At present, mesoporous material is an alternative in catalysis due to containing high surface area and large pore (2-50 nm). In this research, sulfonic mesoporous and aluminium mesoporous materials with Si/Al ratio from 10 to 100 mol mol⁻¹ had been investigated in monoester and diester synthesis. All catalysts were synthesized in this research. Additionally, the effect of mesoporous catalysts on ester yield and product distribution are summarize in Table 4.23.

Table 4.23 Effect of mesoporous catalysts on ester yield and product distribution.

Catalyst	% ester yield			% ester selectivity	
	mono	di	total ester	mono	di
SBA-15-PrSO ₃ H	13.6	81.0	94.6	14.4	85.6
SBA-15-ArSO ₃ H	15.0	82.2	97.2	15.4	84.6
FSM-16- PrSO ₃ H	13.5	82.7	96.2	14.0	86.0
FSM-16- ArSO ₃ H	15.5	83.4	98.9	15.7	84.3
Al-SBA-15 (Si/Al = 10)	26.9	18.4	45.3	59.4	40.6
Al-SBA-15 (Si/Al = 25)	24.6	18.2	42.8	57.5	42.5
Al-SBA-15 (Si/Al = 50)	23.3	16.9	40.2	58.0	42.0
Al-SBA-15 (Si/Al = 100)	17.8	14.7	32.5	54.8	45.2
Al-FSM-16 (Si/Al = 10)	26.7	18.6	45.3	58.9	41.1
Al-FSM-16 (Si/Al = 25)	23.4	17.9	41.3	56.7	43.3
Al-FSM-16 (Si/Al = 50)	23.2	16.8	40.0	58.0	42.0
Al-FSM-16 (Si/Al = 100)	16.4	16.4	32.8	50.0	50.0

Esterification conditions: 2-ethyl hexanol/dicarboxylic acid mole ratio as 2; reaction time 5 hrs.; reaction temperature 100°C; catalytic amount 3wt.% base on reaction mixtrue; and stirring speed 150 rpm.

The reaction results in Table 4.23 indicated sulfonic functionalized mesoporous catalysts provided higher total ester yield and diester selectivity than aluminium functionalized mesoporous due to the high acid strength.

When comparison between propyl sulfonic and aryl sulfonic mesoporous, they performed nearly activity but grafting chemicals for aryl sulfonic acid group was expensive. So, propyl sulfonic mesoporous was selected for using in this work.

4.4.7 Effects of chain length of dicarboxylic acid

The effects of carbon chain length of dicarboxylic acids, including adipic acid, azelaic acid and sebacic acid with the number of carbon atom of 6, 9 and 10, respectively, in the esterification with 2-ethyl hexanol over FSM-16-PrSO₃H are shown in Table 4.24.

Table 4.24 Effect of 2-ethyl hexanol to adipic acid molar ratio on ester yield and product distribution over FSM-16-PrSO₃H

Dicarboxylic acid	% ester yield			% ester selectivity	
	mono	di	total ester	mono	di
Adipic acid (C ₆ H ₁₀ O ₄)	13.5	82.7	96.2	14.0	86.0
Azelaic acid (C ₉ H ₁₆ O ₄)	9.6	75.7	85.3	11.3	88.7
Sebacic acid (C ₁₀ H ₁₈ O ₄)	9.5	71.9	81.4	11.7	88.3

Esterification conditions: 2-ethyl hexanol/dicarboxylic acid mole ratio as 2; reaction time 5 hrs.; reaction temperature 100°C; catalytic amount 3wt.% base on reaction mixture; and stirring speed 150 rpm.

The reaction results in Table 4.24 indicated the maximum yield of diester that obtained from adipic acid, giving the diester yield of 82.7 % and the diester selectivity of 86.0 %. The reactivity loss per additional –CH₂– moiety was greatest for the small diacids from adipic acid to sebacic acid. The size of diacid significantly affected the diester yield and the selectivity to diester as well. The two reasons contribute the decreasing of diacid reactivity with chain length: an inductive effect and a steric effect [71]. The inductive effect results from the increase in electron-releasing ability of the acid with lengthening alkyl chain. Although the inductive effect facilitates the protonation of the carbonyl oxygen, it also lowers the electrophilicity of the carbonyl carbon, resulting in a more energy-hindered rate-limiting nucleophilic attack by the alcohol. The steric component affecting dicarboxylic acid reactivity is also the decisive factor for acid-catalyzed esterification [72,73]. As a consequence of a steric effect, the ester yield of sebacic acid to the corresponding esters occurred at lesser extent. Since the diester possesses the largest molecular size in the reaction system, its formation is relatively limited within the confined space of the catalytic pores.

4.4.8 Effects of structure of alcohol

The reactivity differences with two kinds of alcohols of different structure (2-ethyl hexanol and *n*-octanol) for esterification with adipic acid at 100 °C catalyzed by FSM-16-PrSO₃H, as see in Table 4.25.

Table 4.25 Effect of structure of alcohol on ester yield and product distribution over FSM-16-PrSO₃H.

Alcohol	% ester yield			% ester selectivity	
	mono	di	total ester	mono	di
2-ethyl hexanol	13.5	82.7	96.2	14.0	86.0
<i>n</i> -octanol	14.8	59.4	74.2	19.9	80.1

Esterification conditions: 2-ethyl hexanol/dicarboxylic acid mol ratio as 2; reaction time 5 hrs.; reaction temperature 100°C; catalytic amount 3wt.% base on reaction mixtrue; and stirring speed 150 rpm.

It could be seen that both of the total ester yield and diester selectivity of branch alcohol was higher than linear alcohol. The effect of structure of alcohol on promoting esterification could be explained because the products from branch alcohol (2-ethyl hexyl mono adipate and 2-ethyl hexyl di adipate) had smaller size than the products from linear alcohol (Table 4.26). Therefore, they performed high reactivity ought to an easier diffusion of the reactants and products.

Table 4.26 Molecular width and length calculation by Hyper Chem program.

Molecules	Width (Å)	Length (Å)
Adipic acid	3.15141	10.0571
2-ethyl hexanol	5.90124	7.99991
<i>n</i> -octanol	2.52875	11.5495
2-ethyl hexyl mono adipate	9.15662	14.4568
2-ethyl hexyl di adipate	8.84553	12.8545
octyl mono adipate	10.1430	15.8834
octyl di adipate	9.02776	16.0203

4.5 Catalyst reusability

One of the main advantages of using heterogeneous catalysts is the ease of separation and can be reused in the successive catalytic cycles. In this research, FSM-16-PrSO₃H was used several times for esterification of adipic acid with 2-ethyl-1-hexanol using 3 wt.% of catalyst (based on reaction mixture). After complete reaction the catalyst was filtered, washed with several solvents (hexane, acetone and methanol) to remove substances, products and by-products adhering to the surface and active site of the catalysts, dried at 100 °C overnight and reused. The used and regenerated catalysts were characterized prior to testing in the next reactions.

4.5.1 Characterization of used catalysts

The XRD patterns of fresh and used FSM-16-PrSO₃H catalysts which washed with several solvents (hexane, acetone and methanol) are show in Figure 4.26. As a result, they still exhibited three characteristic peaks of hexagonal phase like the fresh catalyst. Additionally, the one very intense peak (100) and the two weak peaks indexed to (110) and (200) diffractions of reused catalysts exhibited lower intensity compare with fresh FSM-16-PrSO₃H.

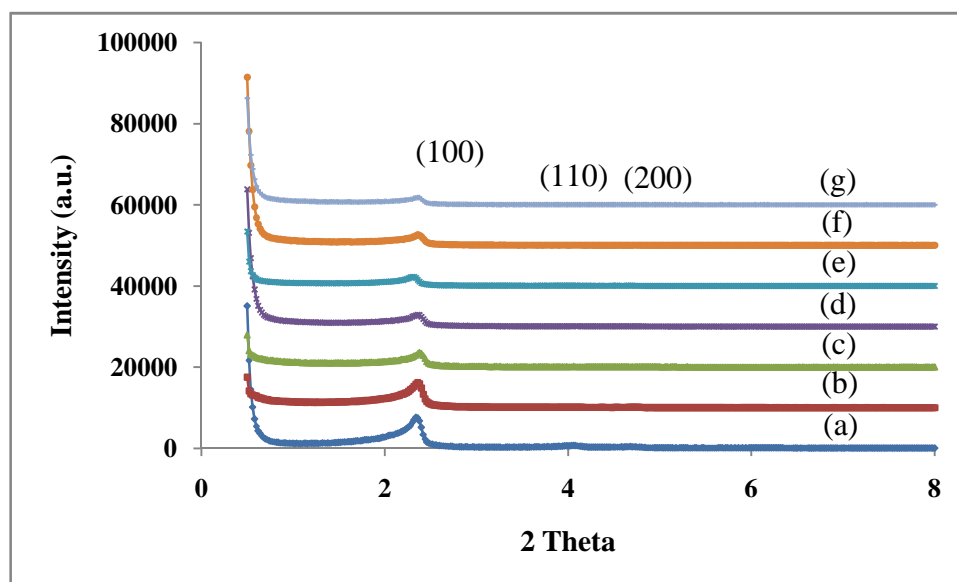


Figure 4.26 X-ray powder diffraction patterns of (a) fresh, (b) 1st used hexane, (c) 2nd used hexane, (d) 1st used acetone, (e) 2nd used acetone, (f) 1st used methanol and (g) 2nd used methanol FSM-16-PrSO₃H.

The adsorption-desorption isotherms of all catalysts showed the characteristic isotherm of mesoporous materials. The physical properties of reused catalysts are present in Table 4.27. Total specific surface area and pore volume decreased in the following solvent order: hexane > acetone > methanol. The used catalysts had the specific surface area was reduced as compared to the fresh one (570 m²/g) due to blockage of remaining organic molecules inside the mesoporous pore. However, all samples still remained a narrow pore size distribution of 9.23 nm, indicating the stability of synthetic catalyst.

Table 4.27 Textural properties of fresh and used FSM-16-PrSO₃H.

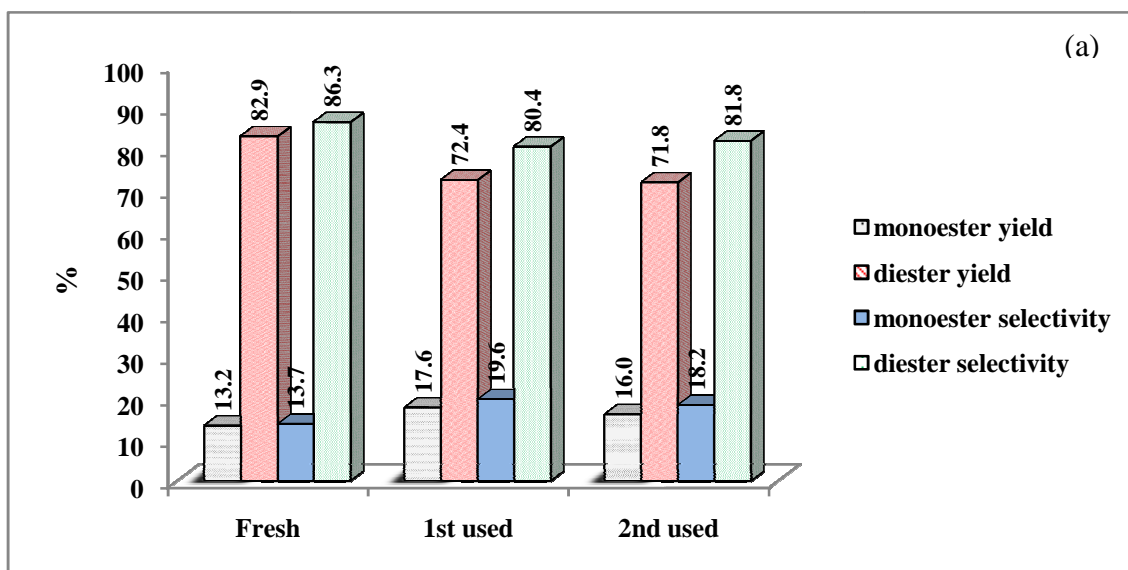
Catalyst	Total specific surface area ^a (m ² ·g ⁻¹)	Pore size distribution ^b (nm)	Mesopore volume ^b (cm ³ ·g ⁻¹)	Acid strength (mmol/g)
Fresh	569.55	2.43	0.5665	1.08
Hexane				
1 st used	520.36	2.43	0.5488	0.94
2 nd used	515.36	2.43	0.5151	0.74
Acetone				
1 st used	472.02	2.43	0.5461	0.86
2 nd used	433.57	2.43	0.4981	0.70
Methanol				
1 st used	219.67	2.43	0.3811	0.84
2 nd used	212.55	2.43	0.3530	0.56

^aCalculated using the BET plot method,

^bCalculated using the BJH method.

4.5.2 Activity of recycled FSM-16-PrSO₃H

According to the obtained results (Figures 4.27 (a)-(c)), it could be observed that the reused catalysts by hexane (non-polar solvent) provided the highest of diester yield and diester selectivity. The increasing monoester yield acquired from the reused catalyst by acetone and methanol which were moderate polar and polar solvents, respectively. These results might be because the reactants and the others by products were eroded from the acid sites of FSM-16-PrSO₃H by acetone resulted in the decrease acid site amount of the catalyst. For reused catalyst by methanol washing, the monoester was slightly increased and associated with the decrease in the diester yield. It could be postulated that the brunt hydrogen bonds occurred between the polar solvent and the acid site of the FSM-16-PrSO₃H, resulting in the depletion of acid site and the decrease in the diester yield. According to the results, hexane was an effective washing solvent to reused FSM-16-PrSO₃H.



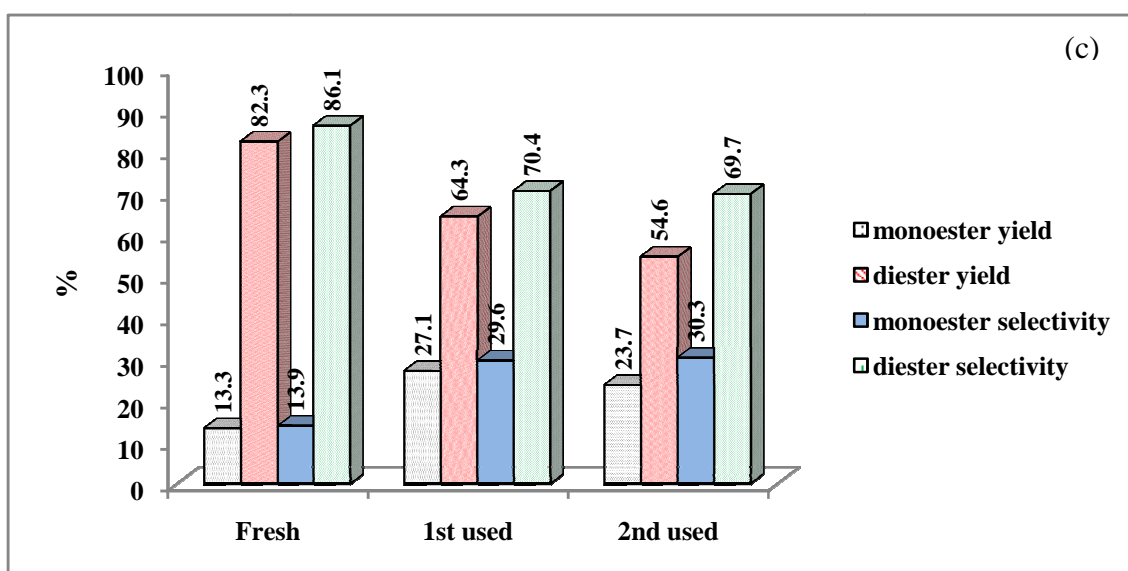
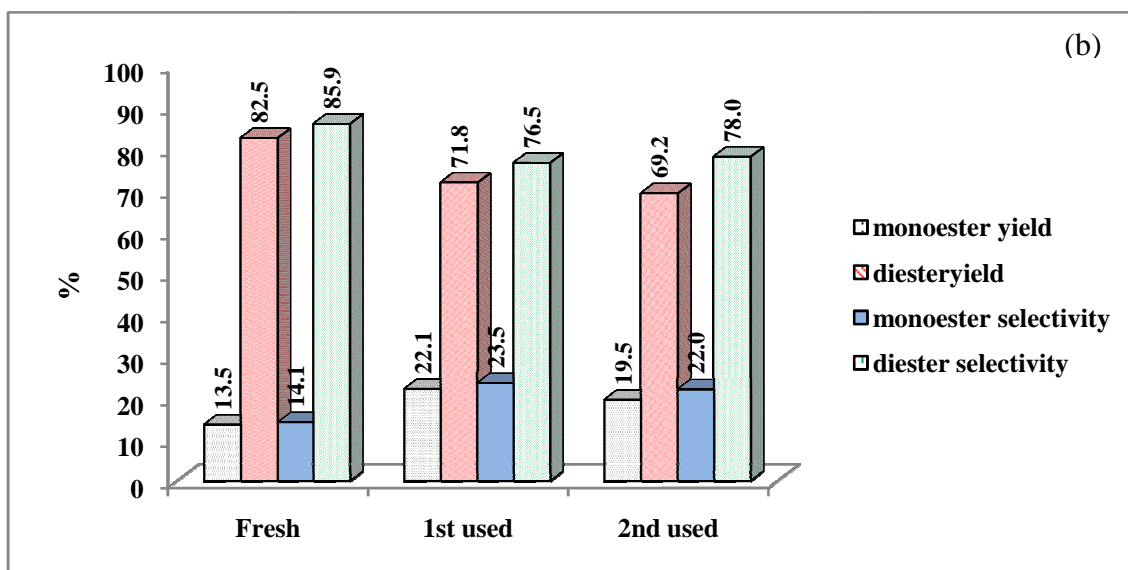


Figure 4.27 FSM-16-PrSO₃H deactivation following multiple reaction cycles of esterification of adipic acid with 2-ethyl hexanol at 100 °C with washing solvent (a) hexane, (b) acetone and (c) methanol and drying between cycles.

4.5.3 Characterization of regenerated catalysts

The XRD patterns of fresh, used and regenerated FSM-16-PrSO₃H catalysts which washed with hexane as are show in Figure 4.28. As a result, they still exhibited three characteristic peaks of hexagonal phase like the fresh catalyst. Additionally, the one very intense peak (100) and the two weak peaks indexed to (110) and (200) diffractions of reused and regenerated catalysts exhibited lower intensity compare with fresh FSM-16-PrSO₃H. However, the one very intense peak of regenerated had higher intensity than the used catalysts.

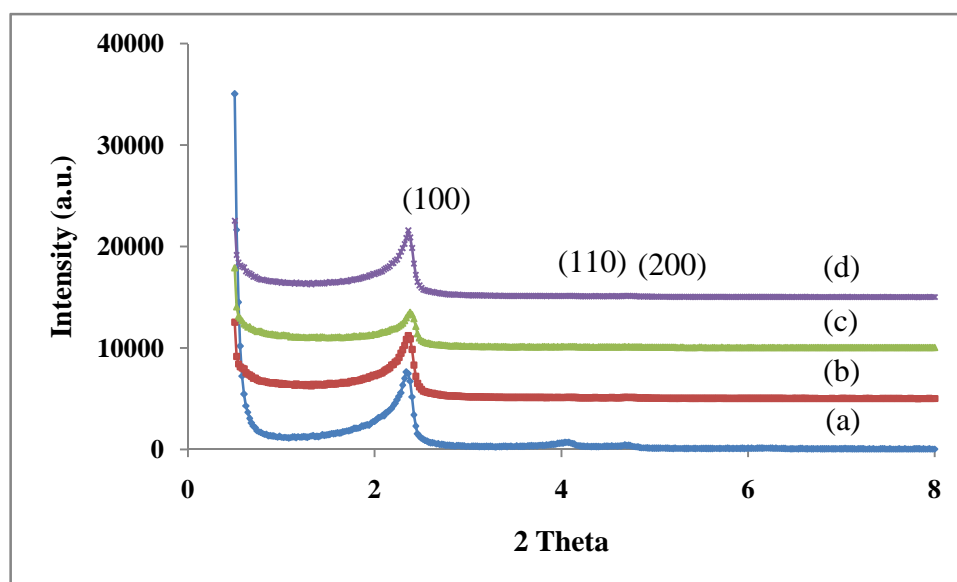


Figure 4.28 X-ray powder diffraction patterns of (a) fresh (b) 1st used hexane, (c) 2nd used hexane and (d) regenerated FSM-16-PrSO₃H.

The adsorption-desorption isotherms of all catalysts showed the characteristic isotherm of mesoporous materials. The specific surface area of regenerated catalysts was reduced as compared to the fresh one, while the acid strength was increased when compared with the used catalysts due to the regrafting of sulfonic group. However, all samples still remained a narrow distribution with the pore size of 2.43 nm, indicating the stability of synthetic catalyst.

Table 4.28 Textural properties of fresh and regenerated FSM-16-PrSO₃H.

Catalyst	Total specific surface area ^a (m ² ·g ⁻¹)	Pore size distribution ^b (nm)	Mesopore volume ^b (cm ³ ·g ⁻¹)	Acid strength (mmol/g)
Fresh	569.55	2.43	0.5665	1.08
1 st used	520.36	2.43	0.5488	0.94
2 nd used	515.36	2.43	0.5151	0.74
regenerated	389.77	2.43	0.4717	1.01

^aCalculated using the BET plot method,^bCalculated using the BJH method.

4.5.4 Activity of regenerated FSM-16-PrSO₃H

From physical property results, the regenerated catalyst was developed in order to improve its catalytic performance. As seen in Figure 4.29, after the used catalyst was regenerated, its catalytic activity was increased nearly to the fresh one. The diester yield was slightly decreased from 82.9 to 77.3% as compared to the fresh catalyst.

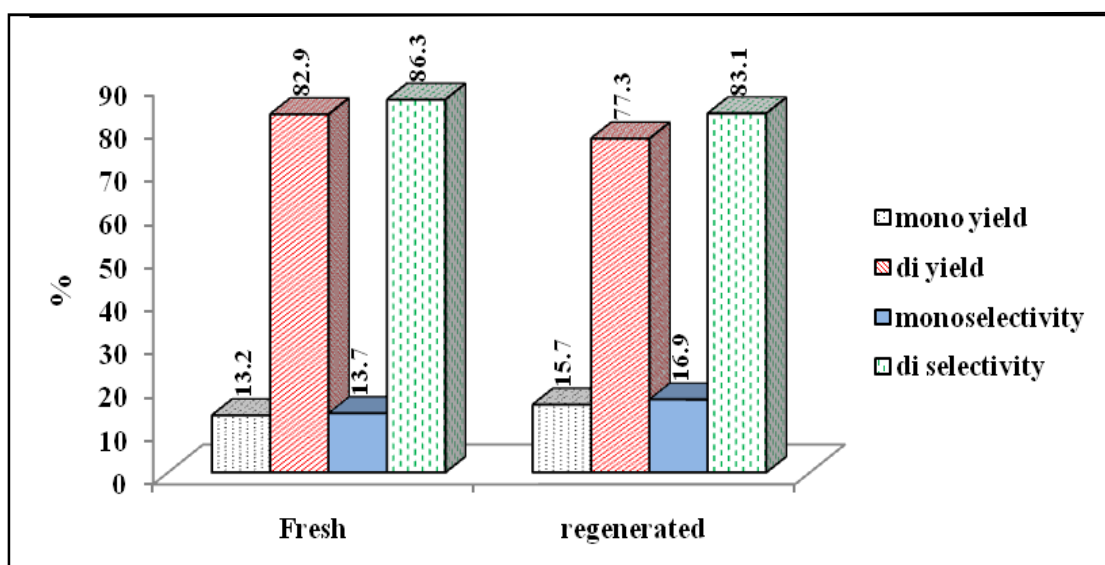


Figure 4.29 Activities of fresh and regenerated FSM-16-PrSO₃H using hexane as washing solvent.

CHAPTER V

CONCLUSIONS

SBA-15 and FSM-16 catalysts, which contained propyl sulfonic, aryl sulfonic or aluminium, were successfully synthesized via hydrothermal method. From characterization of all materials, XRD patterns of these catalysts exhibited the characteristic peaks of hexagonal structure. N₂ adsorption-desorption isotherms displayed type IV pattern which showed typical sorption isotherm of mesoporous structure. Morphology of samples were aggregated particles with rope-like structure and irregular shaped plates and particles to SEM for functionalized SBA-15 and FSM-16, respectively. Acid strength decreased in the following order: aryl sulfonic > propyl sulfonic > aluminium mesoporous. Although the aryl sulfonic mesoporous contained high acidity, but chemicals for grafting aryl sulfonic acid group was expensive. So, propyl sulfonic mesoporous was used in experiments. Moreover, FSM-16-PrSO₃H provided high initial rate, TON and TOF indicating it performed faster kinetic rate and can be more produce molecules of substrate converted into product than SBA-15-PrSO₃H. When comparison between synthetic catalysts, the FSM-16-PrSO₃H was the best efficient catalyst.

To study the catalytic activities of the synthetic materials, the FSM-16-PrSO₃H was selected in lubricating oil additive preparation. 2-ethyl hexyl adipate esters yield of FSM-16-PrSO₃H was 96.2% with 86.0% of diester and 14.0% of monoester selectivities. Furthermore, it could be concluded that the optimum condition on was carried out over catalyst amount of 3%wt. of the reaction mixture at 100°C for 5 hrs. with stirring speed 150 rpm. and molar ratio of alcohol to carboxylic acid as 2. The 2-ethyl hexanol to adipic acid molar ratio was found to be important factor controlling the diester yield and selectivity. At highest the alcohol to dicarboxylic acid ratio as 5, diester yield and diester selectivity were 98.8% and 93.0%, respectively. Additionally, the molecular size of dicarboxylic acid significantly affected the diester yield and the selectivity to diester as well. When the number of carbon in the linear alkyl chain was increased, the diacid yield and the diester yield were decreased due to the enhanced of steric effect.

In comparison with other solid catalysts, FSM-16-PrSO₃H showed higher reactivity than microporous materials. Thus, catalyst having medium pore size around 2 nm was more suitable for lubricating oil additive synthesis. Compared to ion-exchange resin, although SBA-15-Pr-SO₃H and Amberlyst-15 performed good catalytic performance due to giving high amount of diester yield, FSM-16-PrSO₃H exhibited higher surface area and pore volume which increased substrate contacting possibility on catalyst surface. In addition, it had suitable pore size which increased diester selectivity. Moreover, FSM-16-PrSO₃H could be reused and regenerated for two cycles. The catalytic activity of the reused catalyst exhibited no significant difference in the diester selectivity when using hexane as washing agent.

The suggestion for future work

1. Study in detail on physicochemical properties of synthetic diester.
2. Explore to the use of FSM-16-PrSO₃H to the other reaction.
3. Modify sulfonic functionalized porous material with other alkyl sulfonic acid groups to improve the activity of catalyst in lubricating oil preparation.

REFERENCES

- [1] Bartz, W.J. Ecotribology: Environmentally acceptable tribological practices. *Tribology International* 39(2006): 728–733.
- [2] Novotny-Farkas, F., Kotal, P., and Bohme, W. Condition monitoring of biodegradable lubricants. In: *2nd World Tribology Congress, Abstract of Papers* (2001): 313–316.
- [3] Rudnick, L.R. *Synthetic Mineral Oils and Bio-Based Lubricants: Chemistry and Technology*. Boca Raton: Taylor and Francis Group, 2006.
- [4] Smith, K., El-Hiti, G.A., Gamal, A., Jayne, A.J., and Butters, K. Acetylation of aromatic ethers using acetic anhydride over solid acid catalysts in a solvent-free system. Scope of the reaction for substituted ethers. *Organic and Biomolecular Chemistry* 1(2003): 1560.
- [5] Clark, J.H. Solid Acids for Green Chemistry. *Accounts of Chemical Research*. 35 (2002): 791–797.
- [6] Okamura, M., *et al.* Acid-Catalyzed Reactions on Flexible Polycyclic Aromatic Carbon in Amorphous Carbon. *Chemistry of Materials*. 18(2006): 3039–3045.
- [7] Reddy, C.R., Nagendrappa, G., and Prakash, B.S.J. Surface acidity study of Mn⁺-montmorillonite clay catalysts by FT-IR spectroscopy: Correlation with esterification activity. *Catalysis Communications*. 8(2007): 241-246.
- [8] Ma, Y., Wang, Q.L., Yan, H., Ji, X., and Qiu, Q. Zeolite-catalyzed esterification I. Synthesis of acetates, benzoates and phthalates *Applied Catalysis A: General*. 139(1996): 51-57.
- [9] Sharma, P., Vyas, S., and Patel, A. Heteropolyacid supported onto neutral alumina: characterization and esterification of 1° and 2° alcohol. *Applied Catalysis A: General*. 214(2004): 281-286.
- [10] Blagova, S., *et al.* Influence of ion-exchange resin catalysts on side reactions of the esterification of n-Butanol with acetic acid. *Chemical Engineering Science*. 61(2006): 753-765.
- [11] Stucky, G.D., *et al.* Triblock copolymer syntheses of mesoporous silica with periodic 50 to 300 angstrom pores. *Science*. 279(1998): 548-552.

- [12] Yang, L. M., Wang, Y. J., Luo, G. S., and Dal, Y. Y. Functionalization of SBA-15 mesoporous silica with thiol or sulfonic acid groups under the crystallization conditions. *Microporous and Mesoporous Materials*. 84(2005): 275-282.
- [13] Yue, Y., Bonaedet, A., Melosh, J. L., and Espinose, J. B. Direct synthesis of AISBA mesoporous molecular sieves: characterization and catalytic activities. *Chemical Communications*. (1999): 1967-1968.
- [14] Wang Z., et al. Preparation of stable mesoporous silica FSM-16 from water glass in the presence of cetylpyridium bromide. *Materials Chemistry and Physics*. 70(2001): 144-149.
- [15] Dhar M., et al. Novel highly active FSM-16 supported molybdenum catalyst for hydrotreatment. *Communication*. (2008): 5310-5311.
- [16] Gryglewicz, S., and Oko, F.A. Dicarboxylic acid esters as components of modern synthetic oils. *Industrial Lubrication and Tribology*. 57(2005): 128-132.
- [17] Mansoori, Y. Synthetic diester base oils from wastes of electrochemical production of sebacic acid. *Industrial Lubrication and Tribology*. 60(2008): 276–280.
- [18] Liu, Y., Lotero, E., and Goodwin, J.G. Effect of carbon chain length on esterification of carboxylic acids with methanol using acid catalysis. *Journal of Catalysis*. 243(2006): 221-228.
- [19] Özbay, N., Oktar, N., and Tapan, N.A. Esterification of free fatty acids in waste cooking oils (WCO): Role of ion-exchange resins. *Fuel*. 87(2008): 1789-1798.
- [20] Rahman, M.B.A., et al. Enzymatic synthesis of methyl adipate ester using lipase from *Candida rugosa* immobilised on Mg, Zn and Ni of layered double hydroxides (LDHs). *Journal of Molecular Catalysis B: Enzymatic*. 50 (2008): 33-39.
- [21] Reddy, C.R., Iyengar, P., Nagendrappa, G., and Prakash, B.S.J. Esterification of dicarboxylic acids to diesters over M^{n+} -montmorillonite clay catalysts. *Catalysis Letters*. 101(2005): 87-90.
- [22] Nagaraju, N., Chary, K.V., and Kirumakki, S.R. Esterification of alcohols with acetic acid over zeolites H β , HY and HZSM5. *Applied Catalysis A:*

General. 299(2006): 185-192.

- [23] Sastre, E., et al. Influence of the alkyl chain length of HSO₃-R-MCM-41 on the esterification of glycerol with fatty acids. *Microporous and Mesoporous Materials*. 80(2005): 33-42.
- [24] Sarin, R., Tuli, D.K., Sureshbabu, A.V., Misra, A.K., Rai, M.M., and Bhatnagar, A.K. Molybdenum dialkylphosphorodithioates: synthesis and performance evaluation as multifunctional additives for lubricants. *Tribology International*. 27(1994): 379-386.
- [25] Bannister, K.E. *Lubrication for industry. 1st edition*. New York: Industrail Press Inc., 1996.
- [26] Totten, G.E., Westbrook, S.R., and Shah, R.J. *Fuels and lubricants handbook: technology, properties, performance, and testing*. Glen Burnie: ASTM International, 2003.
- [27] Stachowiak, G.W., and Batchelor, A.W. *Engineering tribology. 3rd edition*. Oxford: Elsevier Inc., 2005.
- [28] Rudnick, L.R., and Shubkin, R.L. *Synthetic lubricants and high-performance functional fluids. 2nd edition*. New York: Marcel Dekker, Inc., 1999.
- [29] Mortier, R.M., Fox, M.F., and Orszulik, S.T. *Chemistry and Technology of Lubricants*. New York: Springer Science, 2010.
- [30] Activation energy [online]. Available from: http://en.wikipedia.org/wiki/Activation_energy [2011, February 14]
- [31] Hagen, J. *Industrial Catalysis*. New York: Weinheim Wiley, 1999.
- [32] Otera, J., and Nishikido, J. *Esterification: Methods, Reactions, and Applications. 2nd edition*. Germany: WILEY – VCH, 2010.
- [33] The McGraw-Hill Companies. *Reactions of Carboxylic Acids* [Online]. 2010. Available from: <http://www.mhhe.com/physsci/chemistry/carey/student/olc/graphics/carey04oc/ref/ch19reactioncarboxylicacids.html#esters> [2010, October 3]
- [34] Wakasugi, K., Misaki, T., Yamada, K., and Tanabe, Y. Diphenylammonium triflate (DPAT): efficient catalyst for esterification of carboxylic acids and for transesterification of carboxylic esters with nearly equimolar amounts of alcohols. *Tetrahedron Letters*. 41(2000): 5249 – 5252.

- [35] Ramalinga, K., Vijayalakshmi, P., and Kaimal, T.N.B. A mild and efficient method for esterification and transesterification catalyzed by iodine. *Tetrahedron Letters*. 43(2002): 879 – 882.
- [36] Takagaki, A., *et al.* Esterification of higher fatty acids by a novel strong solid acid. *Catalysis Today*. 116(2006): 157 – 161.
- [37] Kresge, C. T., Leonowicz, M. E., Roth, W. J., Vartuli, J. C., and Beck, J. S. Ordered mesoporous molecular sieves synthesized by a liquid-crystal template mechanism. *Nature*. 359(1992): 710-712.
- [38] Beck, J. S., and Vartuli, J. C. Recent advances in the synthesis, characterization and applications of mesoporous molecular sieves. *Current Opinion in Solid State and Materials Science*. 1(1996): 76-87.
- [39] Inagaki, S., and Fukushima, Y. Adsorption of water vapor hydrophobicity of ordered mesoporous silica, FSM-16. *Microporous and Mesoporous Materials*. 21(1998): 667-672.
- [40] Soler-Illia, G. J. A. A., Sanchez, C., Lebeau, B., and Patarin, J. Chemical strategies to design textured materials: from microporous and mesoporous oxides to nanonetworks and hierarchical structures. *Chemical Reviews*. 102(2002): 4093-4138.
- [41] Beck, J. S., Leonowicz, M. E., Roth, W. J., Vartuli, J. C., and Kresge, C. T. A new family of mesoporous molecular sieves prepared with liquid crystal templates. *Journal of the American Chemical Society*. 114(1992): 10834-10843.
- [42] Tanev, P. T., and Pinnavania, T. J. Mesoporous silica molecular sieves prepared by ionic and neutral surfactant templating: a comparison of physical properties. *Chemistry of Materials*. 8(1996): 2068-2079.
- [43] Soler-Illia, G. J. A. A., Crepaldi, E. L., Grosso, D., and Sanchez, C. Block copolymer-templated mesoporous oxides. *Current Opinion in Colloid and Interface Science*. 8(2003): 109-126.
- [44] Melosh, N.A., Lipic, P., Bates, F.A., and Stucky, G.D. Molecular and mesoscopic structure of transparent block copolymer silica monoliths. *Macromolecules*. 32(1999): 4332-4342.
- [45] Sakamoto, Y., *et al.* Structure analysis of mesoporous material 'FSM-16' studies

- by electron microscopy and X-ray diffraction. *Microporous and Mesoporous Materials*. 21(1998): 589-596.
- [46] Yamamoto, T., et al. Local structure of mesoporous silica FSM-16 studied by X-ray absorption spectroscopy. (2005): 1-9
- [47] Figueiredo, J.L., Pereira, M.M., and Faria, *Journal of Catalysis from theory to application: an integrated course*. Portugal: Imprensa Da Universidade De Coimbra, 2008.
- [48] University of South Carolina. *Building of a Heterogeneous Catalysis Reactor* [Online]. 2010. Available from:http://www.che.sc.edu/centers/RCS/smith/jake_smith_reactor_page.html [2010, October 15]
- [49] Athens, G. L., Shayib, R. M., and Chmelka, B. F. Functionalization of mesostructured inorganic-organic and porous inorganic materials. *Current Opinion in Colloid and Interface Science* 14(2009): 281-292.
- [50] Melero, J. A., Grieken, R. V., and Morales, G. Advances in the synthesis and catalytic applications of organosulfonic-functionalized mesostructured materials. *Chemical Reviews*. 106(2006): 3790-3812.
- [51] Wight, A. P., and Dais, M. E. Design and preparation of organic-inorganic hybrid catalysts. *Chemical Reviews*. 102(2002): 3589-3614.
- [52] Kureshy, R. I. et al. Sulfonic acid functionalized mesoporous SBA-15 as an efficient and recyclable catalysyt for the chromenes from chromanols. *Catalysis Communications*. 10(2009): 572-575.
- [53] Skoog, D. A. *Principles of Instrumental Analysis*. New York, Harcourt Brace College Publishers, 1997.
- [54] BET [online]. Available from: Basic operating principles of the sorptomatic, <http://saf.chem.ox.ac.uk/Instruments/BET/sorpoptprin> [2011, February 9]
- [55] Analysis software user's manual, Belsorp, Bel Japan, Inc.
- [56] Gabriel, B. L. *SEM: A User's Manual for Material Science*, Ohio: American Society for Metal, 1985.
- [57]. Hunger, M., Schenk, U., Breuninger, R., Glaser, R., and Weikamp, J. Characterization of the acid sites in MCM-41 type materials by spectroscopic and catalytic technique. *Microporous and Mesoporous*

- Materails*. 27 (1999): 261-271.
- [58] Reddy, S. S., Raju, B. D., Kumar, V. S., Padmasri, A. H., Narayanan, S., and Rama, R. K. S. *Catalysis Communications*. 8(2007): 261-266.
- [59] Zhaohua, L., Hartmann, M., Zhao, D.; Zhou, D., and Kevan, L. Alumination and ion exchange of mesoporous SBA-15 molecular sieve. *Chemistry of Materails*. 11(1999): 1621-1627.
- [60] Mbaraka, I. K., Radu, D. R., Lin, V. S. Y., and Shanks, B. H. Organosulfonic acid-functionalized mesoporous silicas for the esterification of fatty acid. *Journal of Catalysis*. 219(2003): 329-336.
- [61] Zhao, D. et al. Nonionic triblock and star diblock copolymer and oligomeric surfactant syntheses of highly ordered, hydrothermally stable, mesoporous silica structures. *Journal of the American Chemical Society*. 120(1998): 6024-6036.
- [62] Eswaramoorthi, I., and Dalai, A.K. Synthesis, characterization and catalytic performance of boron substituted SBA-15 molecular sieves, *Microporous and Mesoporous Materails*. 93(2006): 1.
- [63] Hu, W., et al. Acid sites in mesoporous Al-SBA-15 material as revealed by solid-state NMR spectroscopy. *Microporous and Mesoporous Materails*. 92(2006): 22-30.
- [64] Ooi, Y.; Zakaria, R., Mohamed, A. R., and Bhatia, S. Hydrothermal stability and catalytic activity of mesoporous aluminum-containing SBA-15. *Catalysis Communications*. 5(2004): 441-445.
- [65] Lou, G. S., Dai, Y. Y., Wang, Y. J., and Yang, L. M. Functionalization of SBA-15 mesoporous silica with thiol or sulfonic acid groups under the crystallization conditions. *Microporous and Mesoporous Materails*. 84(2005): 275-282.
- [66] Zhao, D., Ha, C. S., Park, S. S., Tu, B., Wu, Z., and Li, Q. Highly hydrothermal stability of ordered mesoporous aluminosilicates Al-SBA-15 with high Si/Al ratio. *Microporous and Mesoporous Materails*. 135(2010): 95-104.
- [67] Lam, M.K., Lee, K.T., and Mohamed, A.R. Sulfated tin oxide as solid superacid catalyst for transesterification of waste cooking oil: An optimization study. *Applied Catalysis B: Environmental*. 93(2009): 134-139.

- [68] MFI [online]. Available from: <http://www.iza-structure.org/databases/ModelBuilding/MFI.pdf> [2011, March 22].
- [69] MWW [online]. Available from: <http://www.iza-structure.org/databases/ModelBuilding/MWW.pdf> [2011, March 22
- [70]]. BEA [online]. Available from: <http://www.iza-structure.org/databases/ModelBuilding/BEA.pdf> [2011, March 22].
- [71] Taft, R.W. *Steric Effects in Organic Chemistry*. USA: Wiley, 1956.
- [72] Charton, M. Steric effects. IV. E1 and E2 eliminations. *Journal of the American Chemical Society*. 97(1975): 6159–6161.
- [73] Fujimoto, H., Mizutani, Y., Endo, J., and Jinbu, Y. Theoretical study of substituent effects. Analysis of steric repulsion by means of paired interact' orbitals. *The Journal of Organic Chemistry*. 54(1989): 2568–2573.

APPENDIX

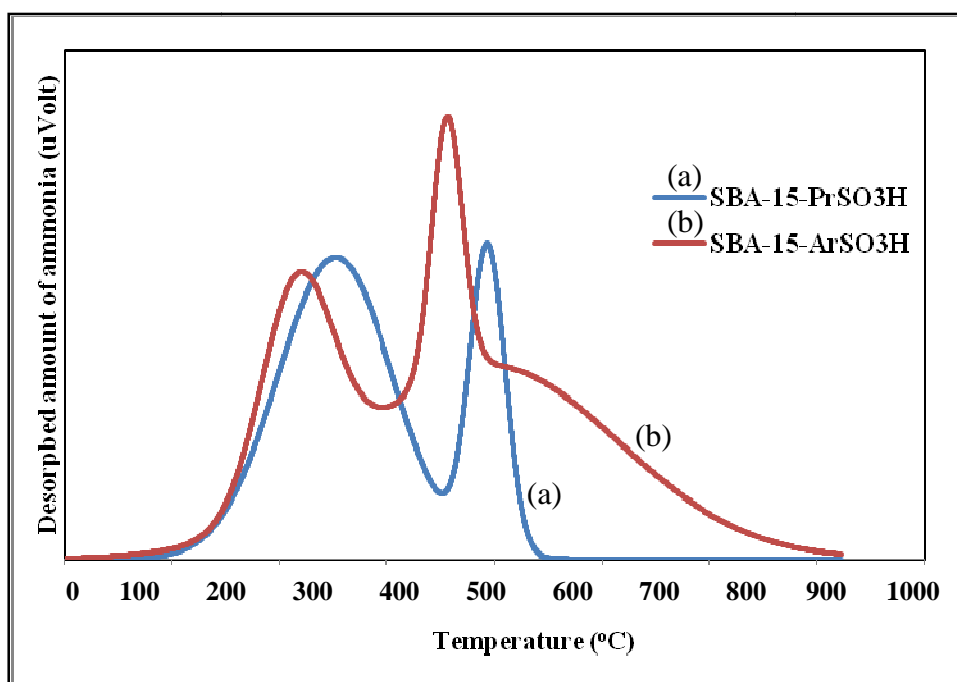


Figure A-1 NH_3 -TPD profile of (a) SBA-15-PrSO₃H and (b) SBA-15-ArSO₃H.

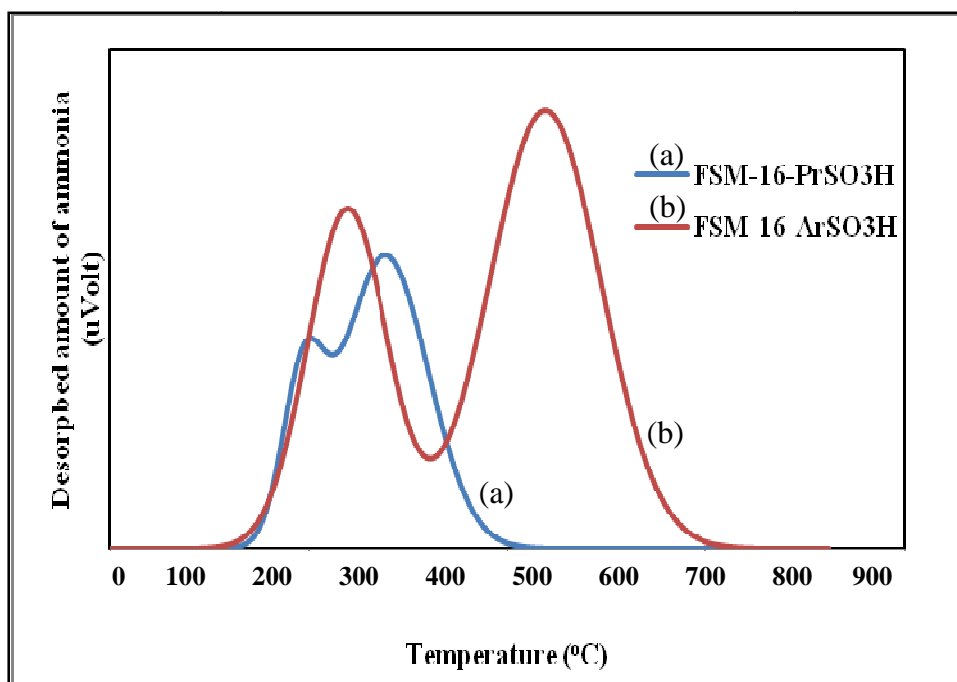


Figure A-2 NH_3 -TPD profile of (a) FSM-16-PrSO₃H and (b) FSM-16-ArSO₃H.

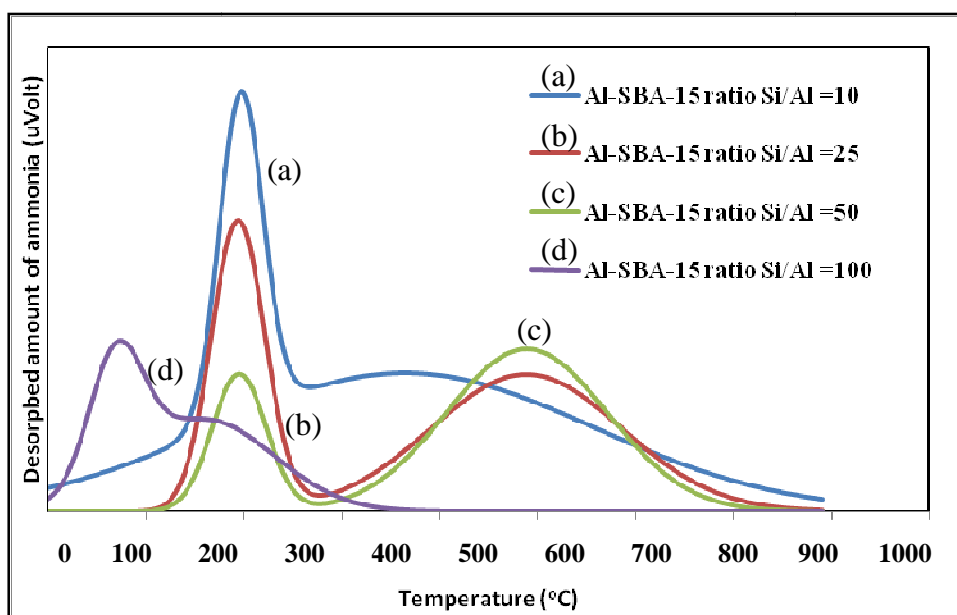


Figure A-3 NH_3 -TPD profile of (a) Al-SBA-15 ratio Si/Al=10, (b) Al-SBA-15 ratio Si/Al=25, (c) Al-SBA-15 ratio Si/Al=50 and (d) Al-SBA-15 ratio Si/Al=100.

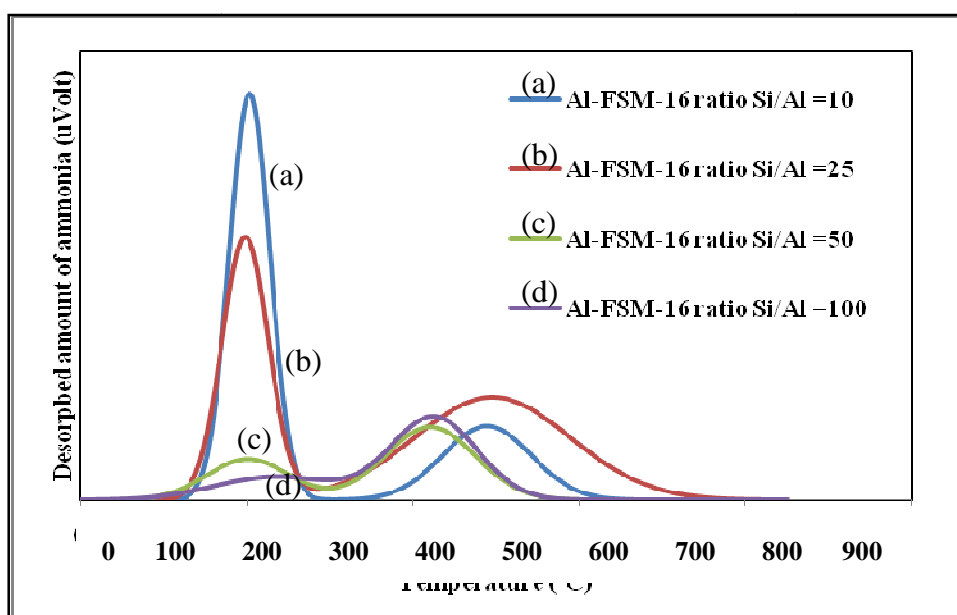


Figure A-4 NH_3 -TPD profile of (a) Al-FSM-16 ratio Si/Al=10, (b) Al-FSM-16 ratio Si/Al=25, (c) Al-FSM-16 ratio Si/Al=50 and (d) Al-FSM-16 ratio Si/Al=100.

1. Standard solution and calibration solution

1.1 2-ethyl hexyl monoadipate standard solution

1.1.1 Stock standard solution 1.0×10^{-1} M

A 0.1285 g of 2-ethyl hexyl monoadipate was accurately weighed in a 5 mL volumetric flask and made up to the mark with *n*-heptane.

1.1.2 Working standard solution (0.05, 0.01, 0.005 and 0.001 M)

The working standard solutions were prepared by dilution of the stock standard solution using a pipette and then made up to the mark with *n*-heptane.

1.2 2-ethyl hexyl diadipate standard solution

1.2.1 Stock standard solution 1.0×10^{-1} M

A 0.1855 g of 2-ethyl hexyl diadipate was accurately weighed in a 5 mL volumetric flask and made up to the mark with *n*-heptane.

1.2.2 Working standard solution (0.05, 0.01, 0.005 and 0.001 M)

The working standard solutions were prepared by dilution of the stock standard solution using a pipette and then made up to the mark with *n*-heptane.

1.3 Standard calibration solution

Five calibration solutions were prepared into a series of vials. The weight 2.5 g of stock and working 2-ethyl hexyl monoadipate and 2-ethyl hexyl diadipate solutions were transferred into the five vials and added 0.5 g of internal standard 1.2×10^{-1} M eicosane stock solution to the five standard solutions. Then, a 1 μ L of each reaction mixture was analyzed by GC technique under the condition described in Section 3.1.7. Preparation of calibration solution were listed in Table A-1 and A-2

Remark: The preparation of stock standard solution for other esters were performed in the similar calculation to described in Section 1.1,1.2 and 1.3.

Table A-1 Preparation of standard 2-ethyl hexyl monoadipate calibration solution.

2-ethyl hexyl monoadipate calibration solution	1	2	3	4	5
1.0 x 10 ⁻¹ M (g)	2.50				
5.0 x 10 ⁻² M (g)		2.50			
1.0 x 10 ⁻² M (g)			2.50		
1.0 x 10 ⁻³ M (g)				2.50	
5.0 x 10 ⁻³ M (g)					2.50
Internal standard solution 1.2 x 10 ⁻¹ M (g)	0.50	0.50	0.50	0.50	0.50

Table A-2 Preparation of standard 2-ethyl hexyl diadipate calibration solution.

2-ethyl hexyl diadipate calibration solution	1	2	3	4	5
1.0 x 10 ⁻¹ M (g)	2.50				
5.0 x 10 ⁻² M (g)		2.50			
1.0 x 10 ⁻² M (g)			2.50		
1.0 x 10 ⁻³ M (g)				2.50	
5.0 x 10 ⁻³ M (g)					2.50
Internal standard solution 1.2 x 10 ⁻¹ M (g)	0.50	0.50	0.50	0.50	0.50

2. Calibration function

The calibration function was given by the following expression, obtained from the experimental data using the linear regression method.

Linear regression equation: $Y = aX + b$

2.1 2-ethyl hexyl mono adipate calibration function

$$M_{\text{HMA}}/M_{\text{eicosane}} = a(A_{\text{HMA}}/A_{\text{eicosane}}) + b$$

M_{HMA} = the mass of 2-ethyl hexyl mono adipate (g)

M_{eicosane} = the mass of internal standard (eicosane, g)

A_{HMA} = the peak area of 2-ethyl hexyl mono adipate

A_{eicosane} = the peak area of eicosane

In regression function X was represented by the term of $A_{\text{HMA}}/A_{\text{eicosane}}$ while Y was $M_{\text{HMA}}/M_{\text{eicosane}}$.

2.2 2-ethyl hexyl di adipate calibration function

$$M_{\text{HDA}}/M_{\text{eicosane}} = a(A_{\text{HDA}}/A_{\text{eicosane}}) + b$$

M_{HDA} = the mass of 2-ethyl hexyl di adipate (g)

M_{eicosane} = the mass of internal standard (eicosane, g)

A_{HDA} = the peak area of 2-ethyl hexyl di adipate

A_{eicosane} = the peak area of eicosane

In regression function X was represented by the term of $A_{\text{HDA}}/A_{\text{eicosane}}$ while Y was $M_{\text{HDA}}/M_{\text{eicosane}}$.

Remark: Calibration function for other esters was performed in the similar calculation to describe in Section 2.1 and 2.2.

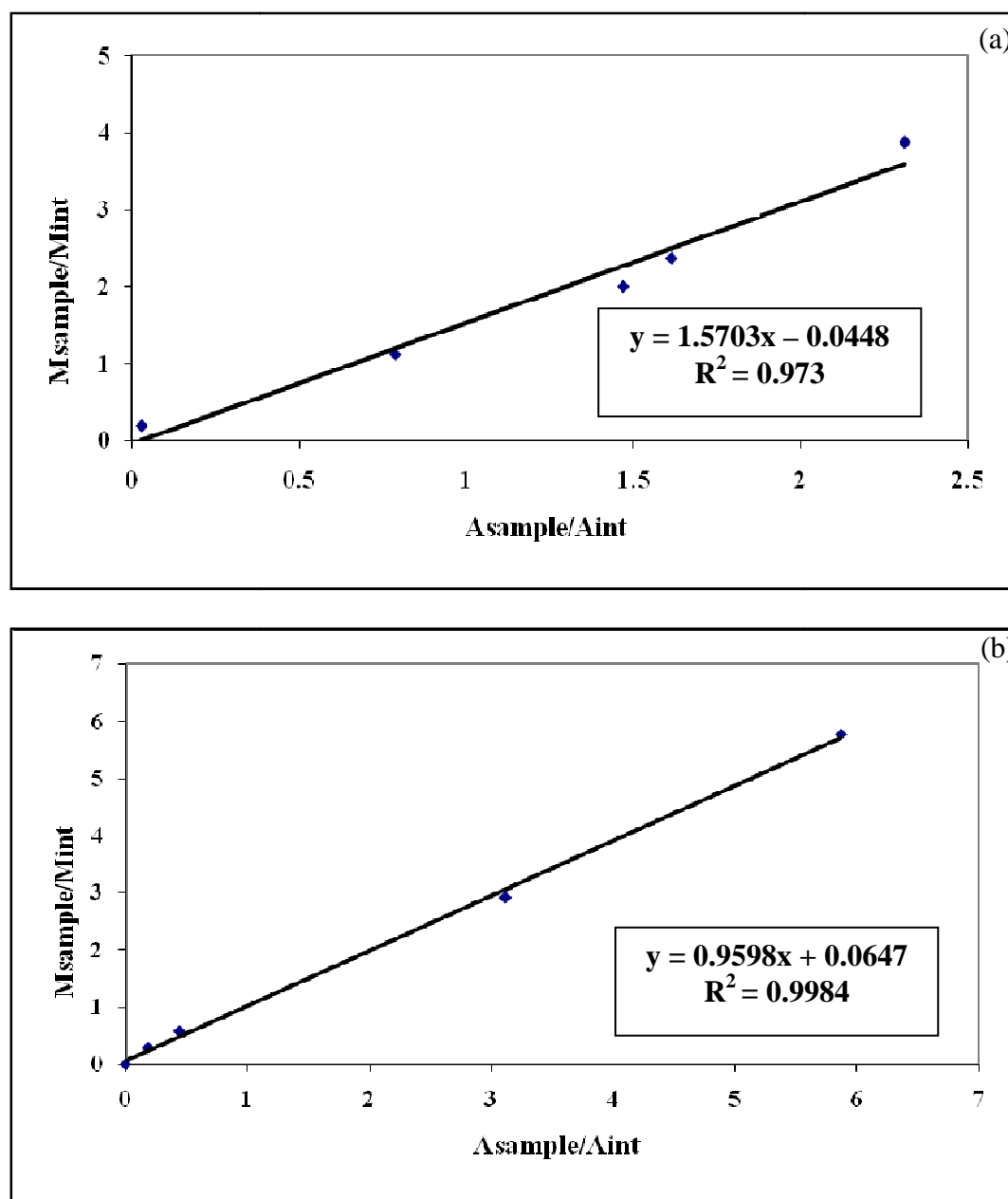


Figure A-5 Calibration curve of (a) 2-ethyl hexyl mono adipate and (b) 2-ethyl hexyl di adipate.

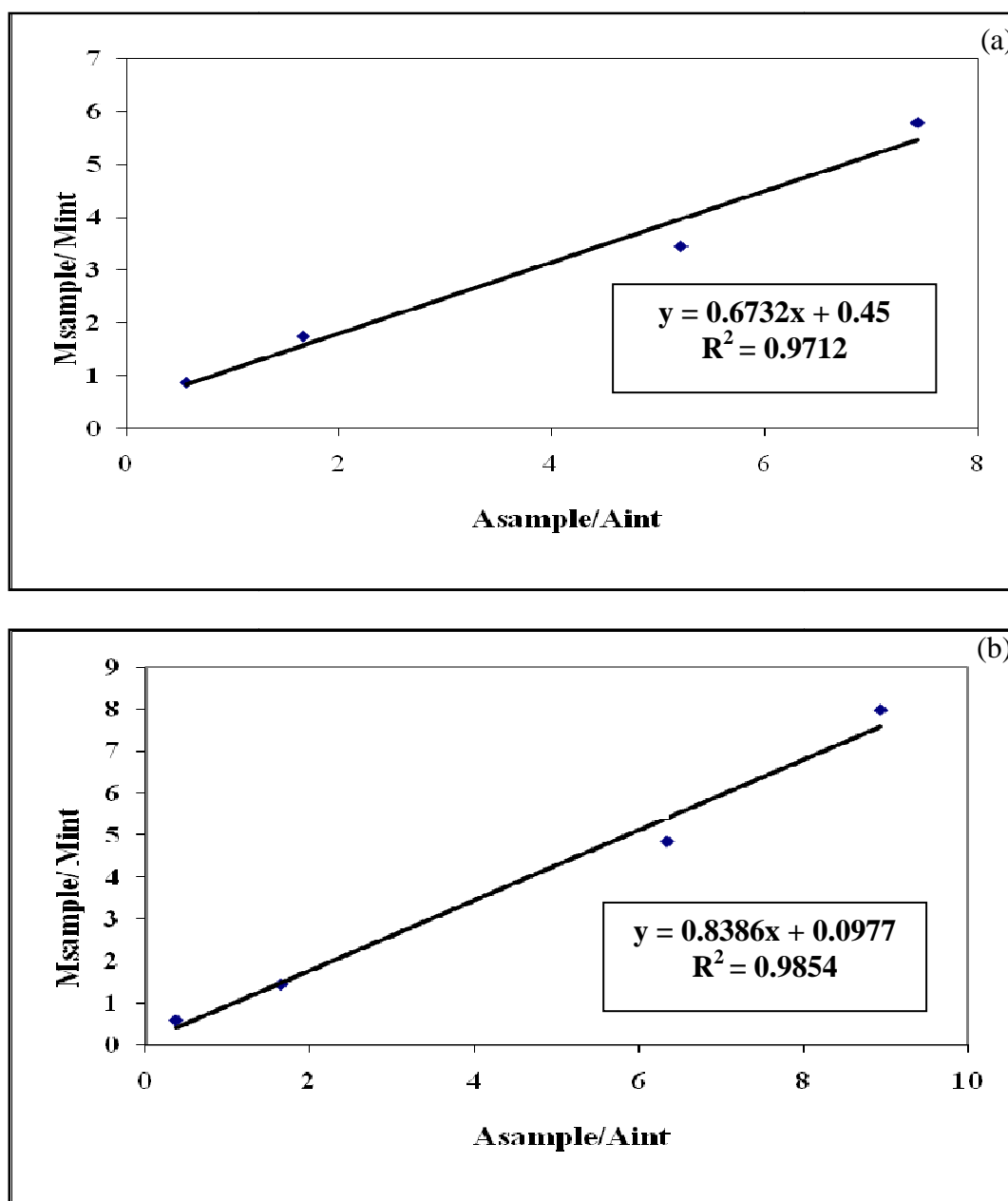


Figure A-6 Calibration curve of (a) 2-ethyl hexyl monoazelate and (b) 2-ethyl hexyl diazelate.

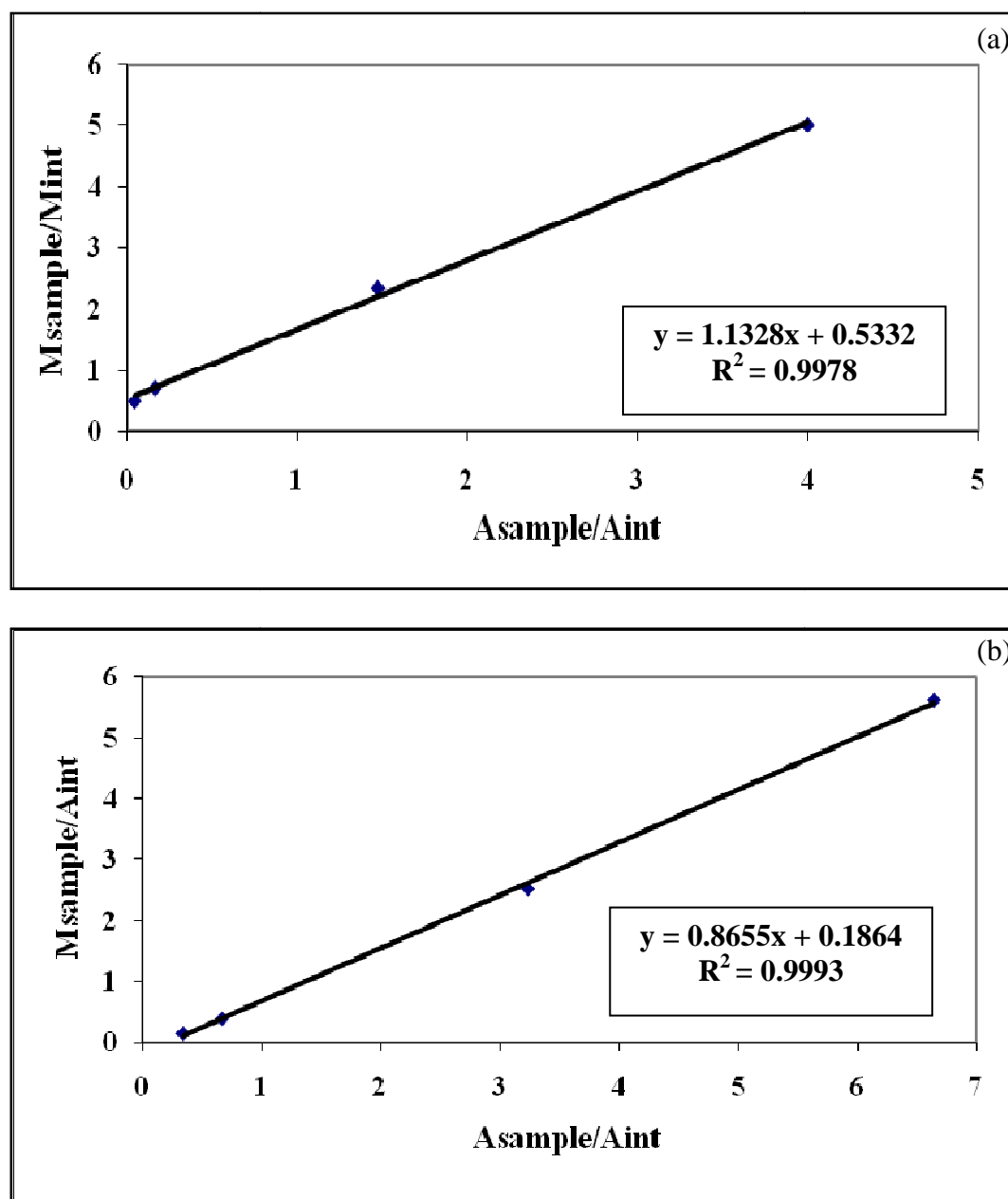


Figure A-7 Calibration curve of (a) 2-ethyl hexyl monosebacate and (b) 2-ethyl hexyl disebacate.

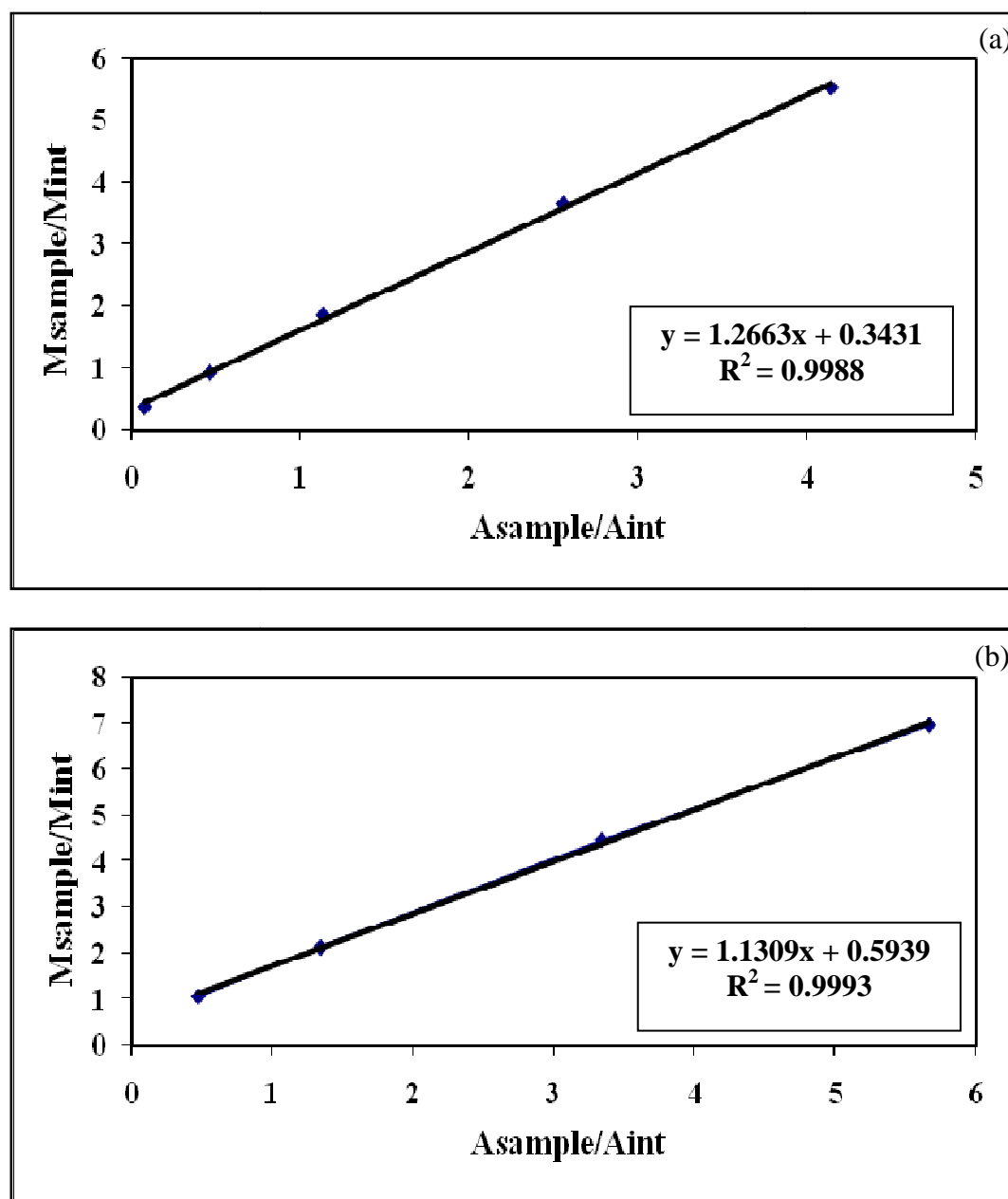


Figure A-8 Calibration curve of (a) octyl monodipate and (b) octyl diadipate.

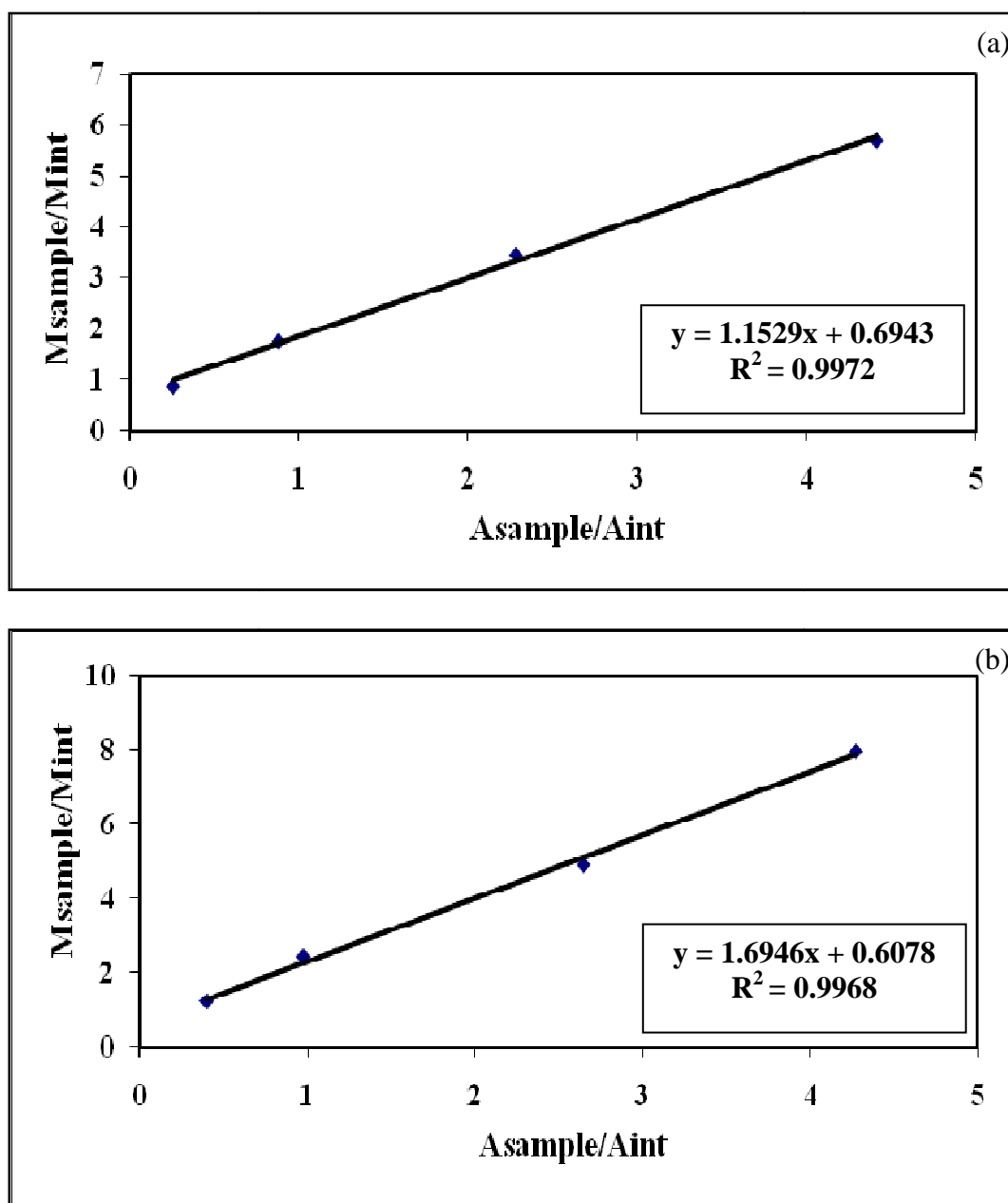


Figure A-9 Calibration curve of (a) octyl monoazolate and (b) octyl diazolate.

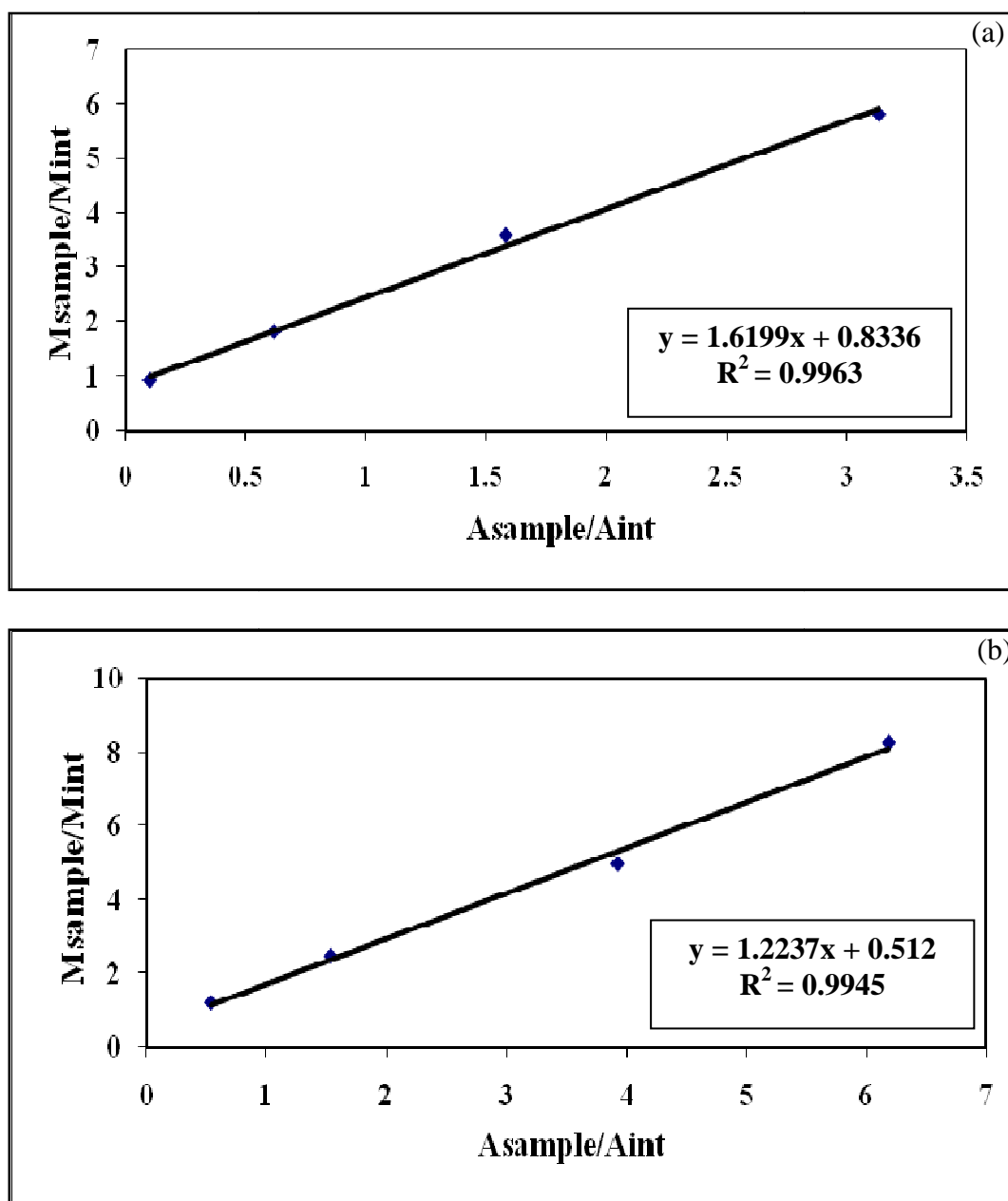


Figure A-10 Calibration curve of (a) octyl monosebacate and (b) octyl disebacate.

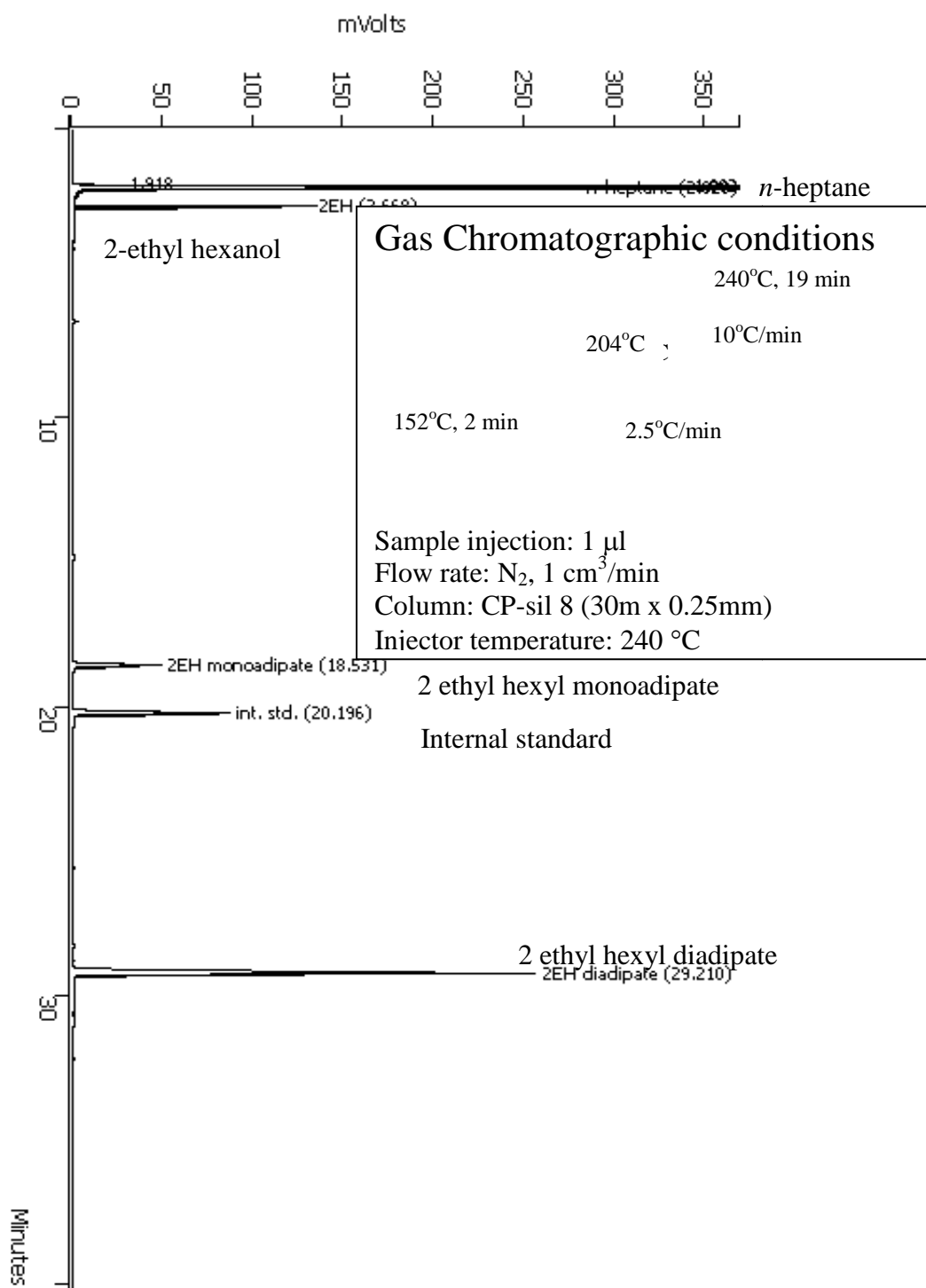


Figure A-11 GC chromatogram of 2-ethyl hexyl adipates product from esterification reaction.

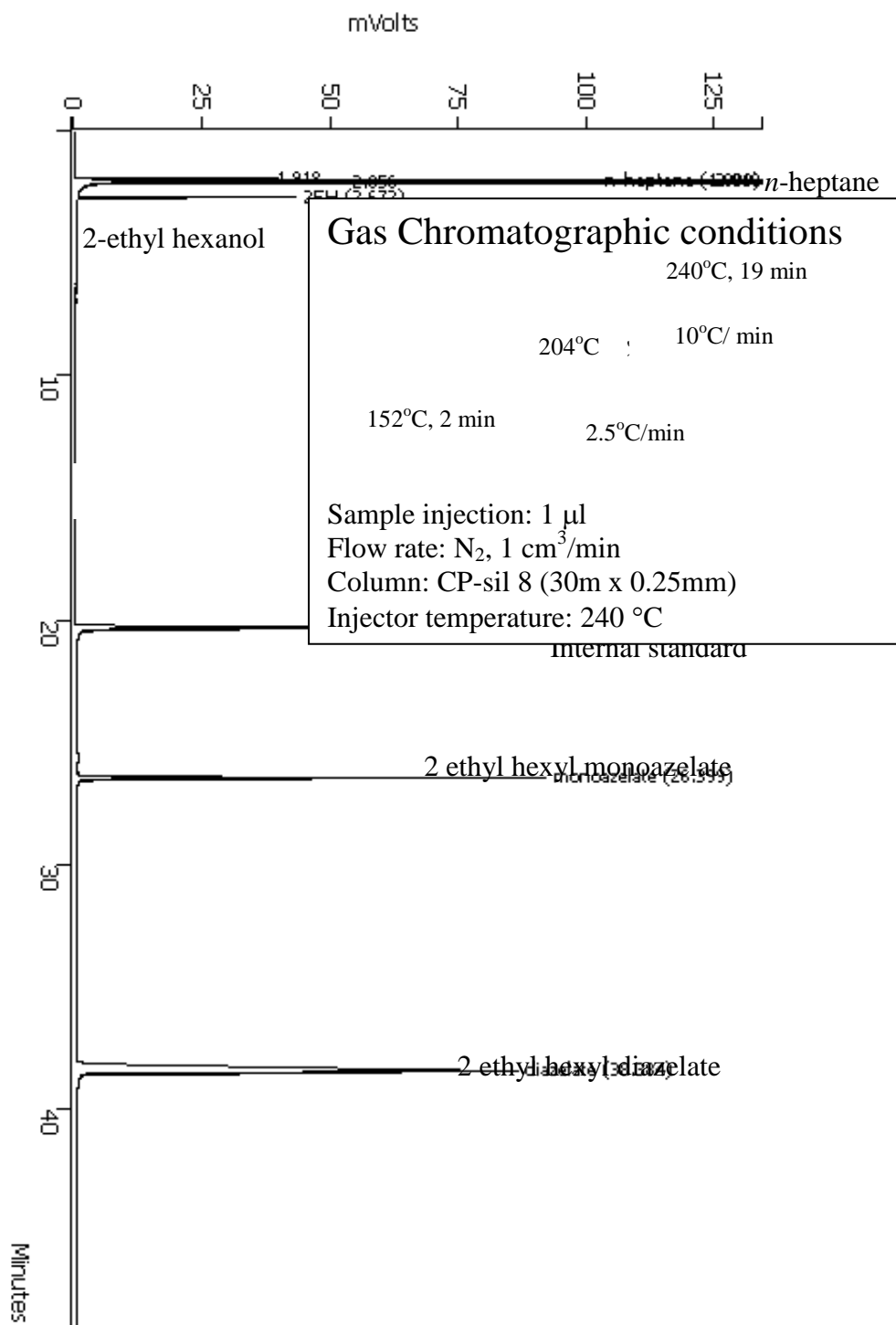


Figure A-12 GC chromatogram of 2-ethyl hexyl azelates product from esterification reaction.

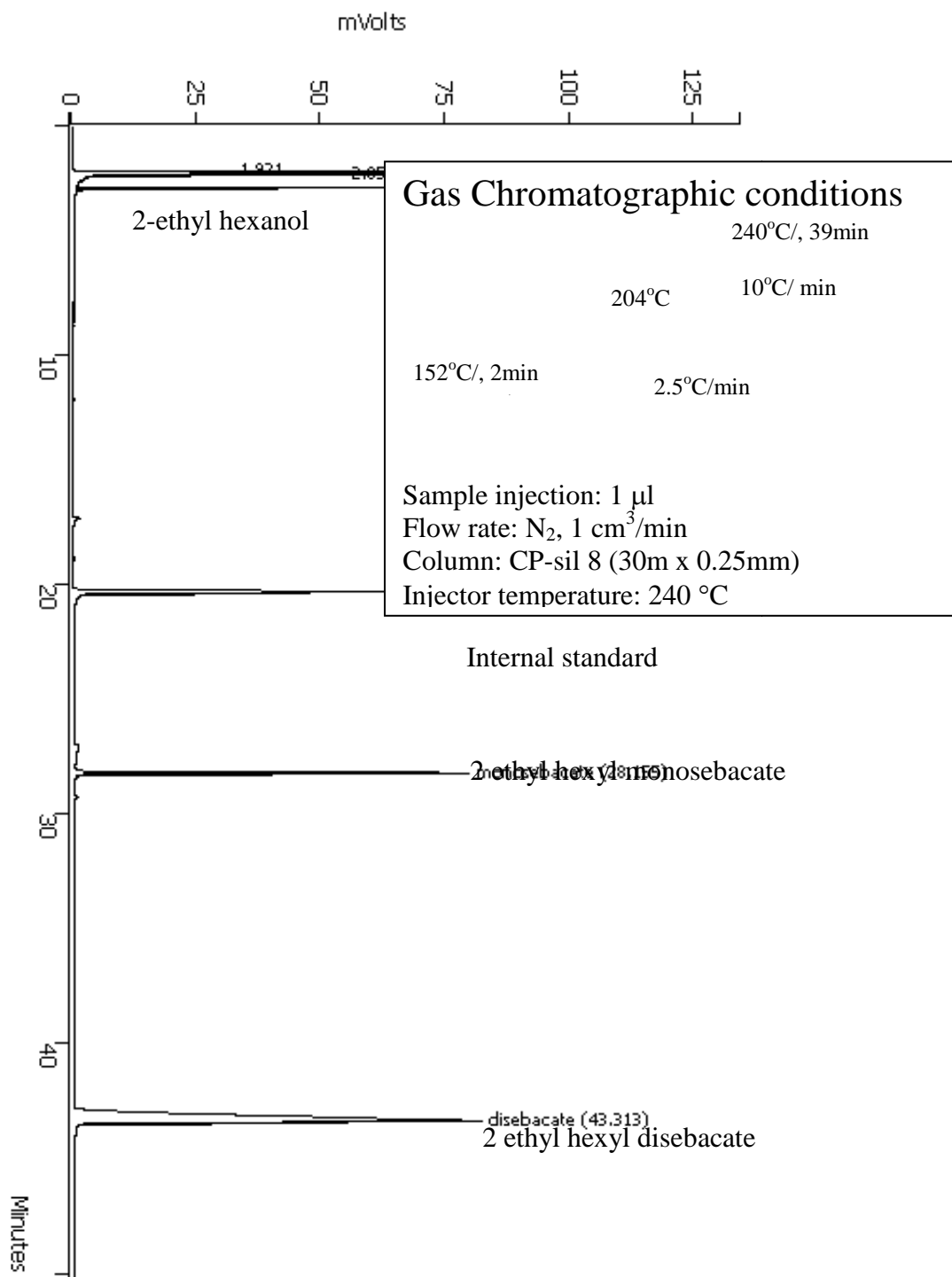


Figure A-13 GC chromatogram of 2-ethyl hexyl sebacates product from esterification reaction.

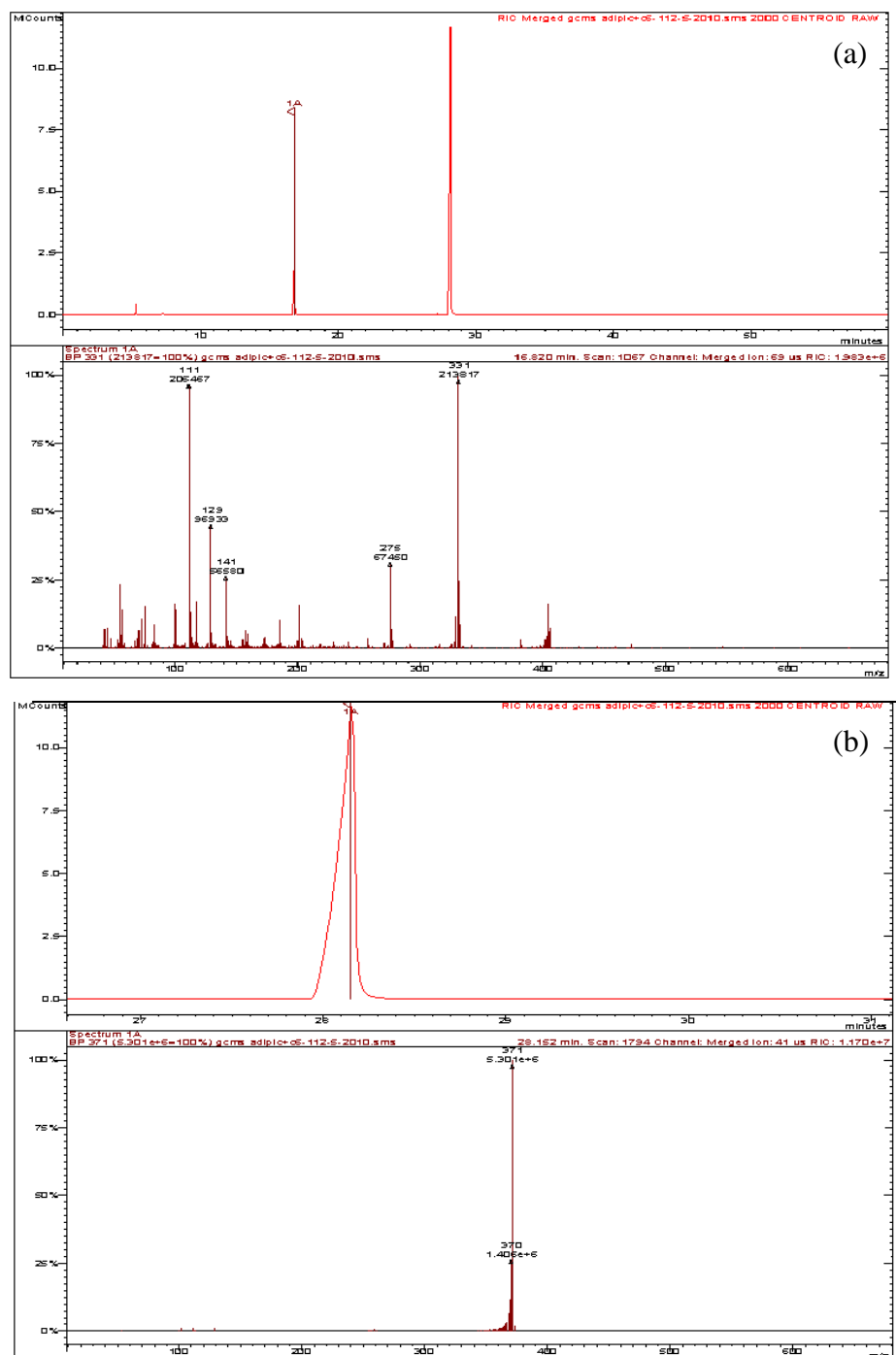


Figure A-14 Mass spectrum of (a) 2-ethyl hexyl monoaddipate and (b) 2-ethyl hexyl diaddipate.

3. Calculation of percent yield and percent selectivity for ester

Gas chromatography analyzer was used to determine products of dicarboxylic acid esterification. Ester products were identified using internal standard method.

The percent yield was calculated based on the results obtained from gas chromatography. Eicosane were used as internal standard.

For example:

A = exact amount of reactant (mol)

B = exact amount of internal standard was added (mol)

C = exact amount of desired product prepared (mol)

D = total volume of the reaction mixture (mL)

E = peak area of the internal standard

F = peak area of the desired product

- The calculation of the percent yield can be described as follows:

The amount of the product from the reaction mixture

$$= \left(\frac{B \times F}{E} \right) = G$$

The amount of the product in reaction mixture (D mL)

$$= G \times D = H$$

The correction factor of the product can be calculated as:

$$= C/H = I$$

Thus, the percentage of product can be calculated as:

$$\% \text{ yield of product} = \left(\frac{H \times I}{A} \right) \times 100$$

VITAE

Mr. Prasert Ruangyotsakul was born on December 1, 1986 in Bangkok, Thailand. He obtained a Bachelor Degree of Science, major in Chemistry from Chulalongkorn University, Bangkok, Thailand in 2008. Since 2009, he has been a graduate student in Organic Chemistry at Department of Chemistry, Faculty of Science, Chulalongkorn University and completed he Master of Science Degree in 2011.

His present address is 1/66 Pluscity Park Village, Soi Ramkhamhaeng 24, Ramkhamhaeng Road, Bangkok district, Bangkok, Thailand 10240.